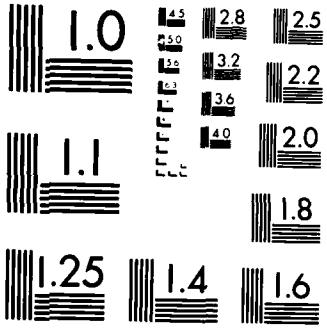

AFGL-TR-84-0260

TWO METHODS OF GLOBAL DATA ASSIMILATION

Isidore Halberstam
Chris Johnson
Donald C. Norquist
Shu-Lin Tung

Systems and Applied Sciences Corporation (SASC)
1577 Springhill Road, Suite 600
Vienna, Virginia 22180

October 1, 1984

Scientific Report No. 4

AIR FORCE GEOPHYSICS LABORATORY
AIR FORCE SYSTEMS COMMAND
UNITED STATES AIR FORCE
HANSCOM AFB, MASSACHUSETTS 01731

This technical report has been reviewed and is approved for publication.

ALLAN J. BUSSEY
Contract Manager

FOR THE COMMANDER

ROBERT A. McCLATCHEY, Director
Atmospheric Sciences Division

This report has been reviewed by the ESD Public Affairs Office (PA) and is releasable to the National Technical Information Service (NTIS).

Qualified requestors may obtain additional copies from the Defense Technical Information Center. All others should apply to the National Technical Information Service.

If your address has changed, or if you wish to be removed from the mailing list, or if the addressee is no longer employed by your organization, please notify AFGL/DAA, Hanscom AFB, MA 01731. This will assist us in maintaining a current mailing list.

REPORT DOCUMENTATION PAGE

1a. REPORT SECURITY CLASSIFICATION: UNCLASSIFIED	1b. RESTRICTIVE MARKINGS:
2a. SECURITY CLASSIFICATION AUTHORITY:	3. DISTRIBUTION/AVAILABILITY OF REPORT: Approved for public release; distribution unlimited
2b. DECLASSIFICATION/DOWNGRADING SCHEDULE:	
4. PERFORMING ORGANIZATION REPORT NUMBER(S):	5. MONITORING ORGANIZATION REPORT NUMBER(S): AFGL-TR-84-0260
6a. NAME OF PERFORMING ORGANIZATION: Systems and Applied Sciences Corporation (SASC) / 6b. OFFICE SYMBOL (If applicable):	7a. NAME OF MONITORING ORGANIZATION: Air Force Geophysics Laboratory
6c. ADDRESS (City, State and ZIP Code): 1577 Springhill Road, Suite 600, Vienna, VA 22180	7b. ADDRESS (City, State and ZIP Code): Hanscom AFB, MA 01731
8a. NAME OF FUNDING/SPONSORING ORGANIZATION: Air Force Geophysics Laboratory / 8b. OFFICE SYMBOL (If applicable): LYT	9. PROCUREMENT INSTRUMENT IDENTIFICATION NUMBER: Contract No. F19628-82-C-0023
8c. ADDRESS (City, State and ZIP Code): Hanscom AFB, MA 01731	10. SOURCE OF FUNDING NOS.

PROGRAM ELEMENT NO.	PROJECT NO.	TASK NO.	WORK UNIT NO.
62101F	6670	00	AC

11. TITLE (Include Security Classification): Two Methods of Global Data Assimilation

12. PERSONAL AUTHOR(S): Halberstam, Isidore; Johnson, Chris; Norquist, Donald C.; Tung, Shu-Lin

13a. TYPE OF REPORT	13b. TIME COVERED	14. DATE OF REPORT (Yr., Mo., Day)	15. PAGE COUNT
Scientific Rpt. No. 4	FROM _____ TO _____	84/10/01	91

16. SUPPLEMENTARY NOTATION:

17. COSATI CODES		
FIELD	GROUP	SUB. GR.
0401		
0402		

18. SUBJECT TERMS (Continue on reverse if necessary and identify by block number): Optimum Interpolation, Objective Analysis, Normal Modes, Initialization, Data Assimilation,

19. ABSTRACT (Continue on reverse if necessary and identify by block number)

An optimum interpolation (OI) method and a method that fits observations to basis functions are described. The selected basis functions are the normal modes of the linearized primitive equations. In both methods the assimilation system consists of the analysis procedure, a non-linear normal mode initialization, and the AFGL global spectral NWP model.

Both methods were tested using FGGE analyses for 7 Jan 79 00GMT as the starting point. Successive 12 h assimilations were conducted for ten cycles for the OI and five cycles for the fitting procedure.

For the OI method results showed a slight increase in error with time when compared with observations, partly attributable to the 12 h forecast length, which was excessive for the forecast error standard deviation prescribed. The fitting procedure showed significantly stronger error increases with time, due in part to faulty conversion of heights to temperatures with the hydrostatic equation and to possible over-

20. DISTRIBUTION/AVAILABILITY OF ABSTRACT	21. ABSTRACT SECURITY CLASSIFICATION
UNCLASSIFIED/UNLIMITED ☒ SAME AS RPT. ☐ DTIC USERS ☐	UNCLASSIFIED

22a. NAME OF RESPONSIBLE INDIVIDUAL	22b. TELEPHONE NUMBER (Include Area Code)	22c. OFFICE SYMBOL
Allan J. Bussey	(617) 861-2977	LY

DD FORM 1473, 83 APR — EDITION OF 1 JAN 73 IS OBSOLETE.

smoothing by the procedure.

TABLE OF CONTENTS

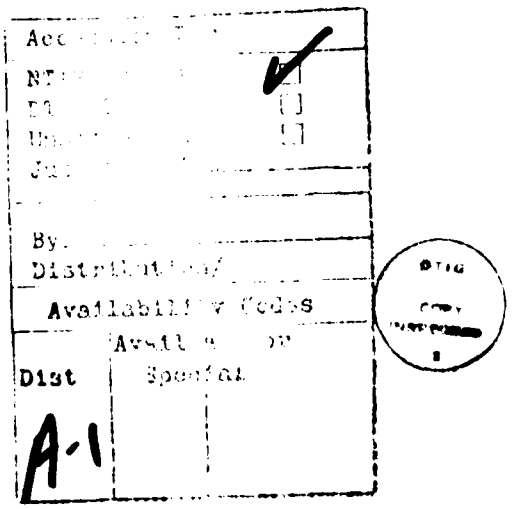

I. INTRODUCTION

This report describes the improvement and testing of two objective analysis methods developed to provide initial conditions for the AFGL Global Spectral Model (GSM). A previous report (Gerlach, 1983[1]) described the construction of the two methods. Subsequent to that report, modifications were made to improve the procedures, and the modified procedures were then used in conjunction with the GSM to generate a series of forecasts in a data assimilation sequence. The first procedure, a multivariate optimum interpolation (OI) procedure, was patterned after the OI scheme of the National Meteorological Center (NMC) as described by Bergman (1979)[2], McPherson et al. (1979)[3], Kistler and Parrish (1982)[4], and Dey and Morone (1983)[5]. The Gerlach report described the design of the procedure in some detail, so only the modifications made since that report will be covered in this paper. The second method, an attempt to fit data to basis functions, was detailed by Halberstam and Tung (1984)[6]. Again, only subsequent modifications and testing will be discussed in the present report.

---

1. Gerlach, A. M., ed., 1983: Objective Analysis and Prediction Techniques - 1983. AFGL-TR-83-0333, Contract F19628-82-C-0023, Systems and Applied Sciences Corporation, ADA142441.

2. Bergman, K. H., 1979: Multivariate analysis of temperatures and winds using optimum interpolation. Mon. Wea. Rev., 107, 1423-1444.

3. McPherson, R. D., K. H. Bergman, R. E. Kistler, G. E. Rasch, and D. S. Gordon, 1979: The NMC operational global data assimilation system. Mon. Wea. Rev., 107, 1445-1461.

4. Kistler, R. E. and D. F. Parrish, 1982: Evolution of the NMC data assimilation system: September 1978-January 1982. Mon. Wea. Rev., 110, 1335-1346.

5. Dey, C. H. and L. L. Morone, 1983: Evolution and performance of the National Meteorological Center Global Data Assimilation System: January-December 1982. Submitted to Mon. Wea. Rev.

6. Halberstam, I. M. and S.-L. Tung, 1984: Objective analysis using Hough vectors evaluated at irregularly spaced locations. Mon. Wea. Rev., 112, 1804-1817.

II. OPTIMUM INTERPOLATION PROCEDURE

A. Recent Modifications of AFGL Statistical Analysis Programs (ASAP)

The optimum interpolation procedure developed for AFGL, designated the AFGL Statistical Analysis Programs (ASAP), involves a terrain surface pressure analysis followed by a separate upper air mass, motion, and moisture field analysis. The surface pressure analysis uses surface observations of pressure and winds to correct the forecast of surface pressure by the GSM on the model's terrain surface. The upper air code performs corrections of height, wind, and specific humidity forecasts on model $\sigma(= p/p_s)$ layers using several types of upper air observations. The following paragraphs discuss the changes made in the two codes since the Gerlach (1983) report.

The only changes in the surface pressure code involve the so-called "buddy check" procedure. Formerly, this procedure was performed after the observations that might affect a particular grid point were located. The observations grouped around that grid point were checked by comparing their observation-minus-forecast residuals with a tolerance that depends on the distance between the observations (see Bergman's Eq. 7.1). This comparison is still made, and the flags still set accordingly, but now this check is performed on all observations before the optimum interpolation procedure begins. The observations are grouped in 5° latitude-longitude boxes, and within each box the buddy check is performed. If an observation is excluded in this process, it is excluded entirely from the interpolation procedure that follows. This eliminates the possibility of an observation being used in the analysis of one grid point and being "flagged out" of the analysis of a neighboring grid point. The assignment of "toss" flags is as it was in the Gerlach (1983) report, but an assignment of a "keep" flag to the higher quality observation (or if both are of equal quality, to both observations) was added for each case where a toss flag was not assigned. After toss and keep flags are assigned for all observations in a particular box, the toss flags are removed from all observations with two or more keep flags before the iterative procedure to remove the observations with the most toss flags begins. In this way, no observation with two or more keep flags is ever eliminated. This follows the practice of NMC as given by Kistler and Parrish (1982).

The question of the necessity of a vertical interpolation of the first guess fields to the new σ pressures as defined by the updated surface pressure remains controversial. Originally, the experimental design for this project called for testing both the inclusion and exclusion of such a vertical interpolation after the surface pressure analysis and before the upper air analysis. Unfortunately, lack of time and a shortage of remaining computer funds made this impractical, so the vertical interpolation was retained for this experiment.

The new buddy check procedure described above for the surface pressure analysis was also included in the upper air analysis. For height, zonal wind, meridional wind, and specific humidity (Z, u, v, q), the residuals are grouped as complete observations (that is, as soundings) on σ layers/levels in 5° latitude-longitude boxes. Then box by box, the Z, u, v, and q residuals are considered separately by layers/levels, with each of the four variables first being subjected to a gross error check. The error limits against which the Z, u, v, and q residuals are checked are defined as four times the forecast error standard deviation values listed in Table 1, interpolated linearly in $\ln p$ to the corresponding σ layer/level pressures. Values in Table 1 for Z, u, v were taken from Dey (1983)[7], and values for q up through 300 mb were compiled from NMC forecast statistics for March 1983 (Morone, personal communication). Values for q above 300 mb were arrived at by assuming that forecast error decreases with decreasing magnitude of q. As before, Z residuals are located at the σ layer interfaces, or levels, while u, v, and q are located in the σ layers. Any residual exceeding the gross error limit is eliminated. Then the toss and keep flags are assigned to the remaining residuals based on failing or passing the tolerance check of pairs of like variables at the layer/level in question. Residuals with more than two keep flags are relieved of their toss flags, and then the iterative procedure to remove residuals with the largest number of toss flags begins. Each succeeding layer/level is checked in this way until all 12 levels are checked; then the next box is examined in the same way.

---

7. Dey, C. H., 1983: The NMC optimum interpolation procedure. Presented at NMC workshop on vector processing and the statistical analysis of meteorological data, Camp Springs, MD.

Table 1. NMC Forecast Error Standard Deviations σ Values (from Dey, 1983[7], and Morone, personal communication)

LATITUDE	90S–10S			10S–10N			10N–30N			30N–50N			50N–90N			90S–90N
Pressure (mb)	Z (m)	u	v	Z	u	v	Z	u	v	Z	u	v	Z	u	v	q(g kg^{-1})
		(m sec^{-1})														
1000	25.4	4.2	4.1	14.7	3.5	3.3	19.4	4.1	3.9	19.7	4.6	4.9	21.6	4.4	4.3	1.8599
850	25.4	3.9	3.7	15.5	3.2	2.8	16.7	3.7	3.4	19.6	4.1	4.3	19.4	3.6	3.6	1.4034
700	26.8	4.2	4.1	19.3	3.6	3.3	18.7	4.1	3.6	19.7	4.2	3.8	20.8	3.6	3.6	0.9348
500	33.5	4.8	4.6	25.4	4.3	3.5	25.6	4.8	4.2	23.2	4.8	4.6	25.8	4.4	4.4	0.3140
400	39.2	5.5	5.7	29.6	4.1	4.0	32.4	5.3	4.9	27.2	5.6	5.3	29.9	5.3	5.0	0.1513
300	47.0	6.6	6.8	40.1	5.8	5.3	42.3	6.5	6.1	34.1	7.1	6.4	36.5	5.7	5.5	0.0604
250	50.6	9.5	7.3	49.4	5.8	5.2	47.3	7.3	6.9	37.4	6.6	6.6	39.2	5.4	5.3	0.0500
200	53.5	7.3	7.0	55.3	7.8	5.8	56.3	7.6	7.6	41.6	6.7	6.2	42.0	4.4	4.3	0.0400
150	57.3	6.5	6.7	61.4	8.2	5.7	67.4	7.3	7.1	46.7	5.9	4.9	48.3	3.7	3.7	0.0300
100	69.8	7.0	6.4	78.0	8.8	7.1	80.1	7.7	6.2	55.2	5.1	4.1	59.4	3.7	3.6	0.0200
70	77.7	6.6	5.5	93.2	7.7	4.8	100.0	5.7	5.3	64.2	7.1	4.9	71.8	5.5	5.1	0.0100
50	90.1	8.3	8.0	108.0	9.9	8.3	101.0	8.7	8.6	78.3	8.2	6.7	88.1	7.6	7.4	0.0050

Another major change made in the height-wind multivariate analysis is the use of the same residuals to calculate a correction for all of Z, u, and v at a particular grid point for a particular σ layer. The proximity of each height (on levels) and wind (on layers) residual with the σ layer grid point to be corrected is calculated using the product of the non-dimensional distance functions μ_{ig}^{tt} and ν_{ig}^{uu} given by

$$\mu_{ig}^{tt} = \exp\left[-k_h \left(\Delta S_{ig}\right)^2\right]$$

$$\nu_{ig}^{uu} = \left[1 + k_p \ln^2(p_i/p_g)\right]^{-1}$$

where i is the index of the observation, g the index of the grid point, $k_h = 1.96 \times 10^{-12}\ m^{-2}$, $k_p = 5.0$, p pressure and ΔS_{ig} the map distance between the observation and the grid point. The N (a variable, currently set at 10) height or wind observations with the largest value of $\mu_{ig}^{tt}\ \nu_{ig}^{uu}$ are then chosen for the calculation of the correction for Z, u, v. Thus, since both wind components are taken together, as many as 2N individual residuals may be used to calculate a correction for each of Z, u, and v at the σ layer grid point. Using the same residuals for correcting all three variables has the two-fold advantage of enhancing the multivariate nature of the analysis while saving computational time since only one correlation matrix is formed for the correction of all three variables.

Next, the actual correlations between the selected residuals and the grid point σ layer Z, u, v are calculated. These form the three right-hand-side vectors which, when combined with a matrix made up of correlations between the selected residuals, make up the three equation sets for the corrections. The systems of equations are solved for the interpolation weights for Z, u, v, respectively, using the Cholesky method for solving a series of linear equations (Stobie, 1984[8]). Once the non-dimensional weights forming the three solution sets are dimensionalized, they are used along with the corresponding residuals to calculate the weighted sum which is the correction to be applied to the first guess values of Z, u, v,

8. Stobie, J., 1984: Cholesky Method for Solving a Series of Linear Equations. TSIN Office Note 84-1, Air Force Global Weather Central, Offutt AFB, NE.

respectively, at that σ layer grid point. The non-dimensionalized weights are used with the respective right-hand-side vectors of residual-grid point correlations to calculate the normalized analysis error (see Bergman's Eq. 2.13).

Since temperature on the σ layers is the mass variable in the prognostic model, the height corrections on the layers have to be converted to temperature corrections on the layers. First, the layer height corrections ΔZ are converted to mean temperature corrections between the 13 layer positions of height (an extra height correction is obtained from the OI height analysis for a layer of thickness $\Delta\sigma_1$ below the terrain surface) using

$$\overline{\Delta T_k} = -g(\Delta Z_{k+1} - \Delta Z_k)/[R \ln(\sigma_{k+1}/\sigma_k)] .$$

The mean temperature corrections are assigned to the "layer-layer" pressures at the 12 intermediate points between the 13 σ layer pressures. The σ values for these intermediate layer-layer positions are defined such that the natural logarithm of the layer-layer sigma is the arithmetic average of the natural logarithm of the sigma values of the surrounding layers. The layer-layer mean temperature corrections are then converted to σ layer temperature corrections using the Flattery algorithm (from the NMC global spectral model preprocessing code) detailed in Appendix A. This algorithm has been used to convert interface temperatures to layer temperatures, and is presented in this way in Appendix A. The application of this technique to the problem of converting layer-layer temperature corrections to layer temperature corrections is carried out analogously, and in our case K = 13, because of the use of the subsurface layer to avoid extrapolation in the Flattery procedure in the lowest model layer. By calculating a correction for the subsurface layer in the upper air OI analysis, the residuals are extrapolated to the pressure corresponding to σ_u using the vertical structure functions in the same way that extrapolations may occur at σ layers above the highest nearby residuals. A similar OI extrapolation to a layer above the highest σ layer was not done due to the sparsity of data and the lesser sensitivity of temperature corrections to corresponding height corrections at those altitudes. This upper level extrapolation by the Flattery routine can occasionally produce temperature corrections in the

top layer that may not be completely realistic, but by extrapolating corrections rather than full temperature values, there is no systematic warming of the upper layer due to the positive lapse rate at this altitude. Corrections may have positive or negative lapse rates, so in some places the corrections would represent large temperature increases while in other places large temperature decreases.

McPherson et al. (1979) describes the procedure of allowing the estimated prediction error, used to normalize the observation errors (see Bergman's Eq. 2.10d), to evolve over succeeding cycles of a data assimilation. The estimated prediction error for one cycle is obtained from the estimated analysis error of the previous cycle. An unfortunate drawback of such a scheme is that over time, sharp gradients of estimated prediction error develop between regions of high data density and regions of low data density (between continents and oceans, for example). This violates the assumption of horizontal invariance of forecast error standard deviation used to derive structure function relationships used in the OI analysis.

An alternative approach suggested by Lorenc (1981)[9] is to accumulate statistics of estimated analysis error over long periods of forecast-analysis cycles, and use these along with forecast error statistics to generate an estimated prediction error field that may remain constant in time in ensuing runs. If A_{gr} represents an analysis value of variable r at grid point g and P_{gr} represents a corresponding prediction value, and if E^a_{gr} is the estimated analysis error calculated from $E^a_{gr} = E^p_{gr}(\epsilon^a_{gr})^{1/2}$ where E^p_{gr} is the estimated prediction error actually used at the grid point and ϵ^a_{gr} is the non-dimensional analysis error (defined by the right-hand-side of Bergman's Eq. 2.13), then a new value of E^p_{gr} can be calculated using

$$(E^{p'}_{gr})^2 = \overline{(A_{gr} - P_{gr})^2} + \overline{(E^a_{gr})^2} \quad .$$

The overbars represent averages over many forecast-analysis cycles, enough to include seasonal and year-to-year variations in the forecasts.

---

9. Lorenc, A. C., 1981: A global three-dimensional multivariate statistical interpolation scheme. Mon. Wea. Rev., 109, 701-721.

these observation σ layer temperatures are used to calculate observation σ level heights using the hydrostatic equation. This check was removed for the calculations of the GSM, INIT, and ANAL curves on Figs. 1 (a-c). Thus, a bad height observation resulted in erroneous σ layer temperature, which introduced an error of equal magnitude in height at each level above when the hydrostatic equation was used to get observation σ level heights. The check of derived observation σ layer temperatures was put in to avoid this vertical propagation of error in calculating residuals for the analysis, and should have been left in for the RMS error calculations. In the other five cases, the error grew with height without any sign of poor quality data in the sounding--apparently, a legitimate bad fit of observation with field value.

In contrast to RMS errors for height, similar curves for vector wind error and surface pressure (Figs. 1 (d-g)) do appear to show an increase of error with time. For the winds, the rate of increase of error seems to increase with altitude, as is seen by comparing the general slopes of the three ASAP-based curves in Figs. 1 (d-f). One likely explanation for this drift away from the observations is that the values used for estimated prediction error (in this case, the values from Table 1) may have been too small for a 12h forecast. Thus, the normalized observation error ϵ^{o}_{ir} would have been too large, so that observations would have had insufficient influence in the correction. Since the values in Table 1 are based on comparing 6h forecasts with observations, they should have been augmented to some degree to serve as 12h forecast error values. Since a 12h forecast is two sequential 6h forecasts with no correction performed in between, one way to augment the values in Table 1 would be to use forecast error growth rates to estimate how large the error should be after six more hours. Such values were not available for this experiment, although estimates could be derived from Table 1 of McPherson et al. (1979). Future runs to experiment with the proper specification of estimated prediction error should be undertaken to eliminate the drift away from observations if a 12h cycle is maintained. Changing to a 6h cycle may very well eliminate the drift, since the actual forecast error in each cycle would be less. In the long run, prediction error statistics could be generated to determine the values that should be used for estimated prediction error for this particular forecast model and analysis scheme.

field was being used to determine which observations would be used in the comparisons. For these RMS errors, only conventional upper air observations (Type 1 observations in the FGGE II-B data set, consisting of rawinsondes, pilot balloons, dropsondes, etc.) were used.

In all cases, the analysis error (ANAL) curve lies below the forecast error (GSM) curve, showing that the analysis is indeed effective in bringing the forecast closer to the observations, as would be expected. The slow component error (INIT) curve lies somewhere in between the two in all cases except for $\vec{V}(\sigma_8)$, where for the most part it lies slightly below the ANAL curve. In all but this case, the initialization removes the fast modes from the analysis, but in so doing partially negates the effect of the analysis in bringing the forecast field closer to the observations, as is expected. Evidently, in the case of the upper level winds, the analysis has a smaller effect on the forecast field than the initialization has in restoring mass-motion balance.

The RMS errors for neight in Figs. 1 (a-c) for the three ASAP fields show a high degree of irregularity with time, but do not seem to reveal a trend toward increasing error. At all three levels, the RMS error takes a jump at 1/11/79 00Z, but the experiment was not carried out long enough to see if this was part of a discernible trend. Given the lower RMS errors on either side of the values for 1/11/79 00Z and 12Z, it appears that this was due to bad fits to data at a few data points rather than a larger error overall. This was confirmed by examining the observation-minus-GSM values for 1/11/79 00Z. Height differences were excessive at about 12 observation sites for $Z(\hat{\sigma}_9)$, while the observation-minus-F3A differences at those same locations were normal. When these 12 observations were removed from the RMS calculation, the RMS error for GSM $[Z(\hat{\sigma}_9)]$ at 1/11/79 00Z dropped back to a level comparable to values for earlier times. Thus, for height at least, most of the irregularity in the curves can be ascribed to bad fits at just a few locations where the F3A fit with observations was normal. In seven of the 12 cases, the bad fit was traced to a bad height observation value at levels below the affected level. In the calculation of observation-minus-field values for the OI analysis and the F3A, a check is made of the observation value temperatures as they are calculated for the σ layers. If the difference between an "observation" value and the field value of temperature is greater than 20°K, it is excluded before

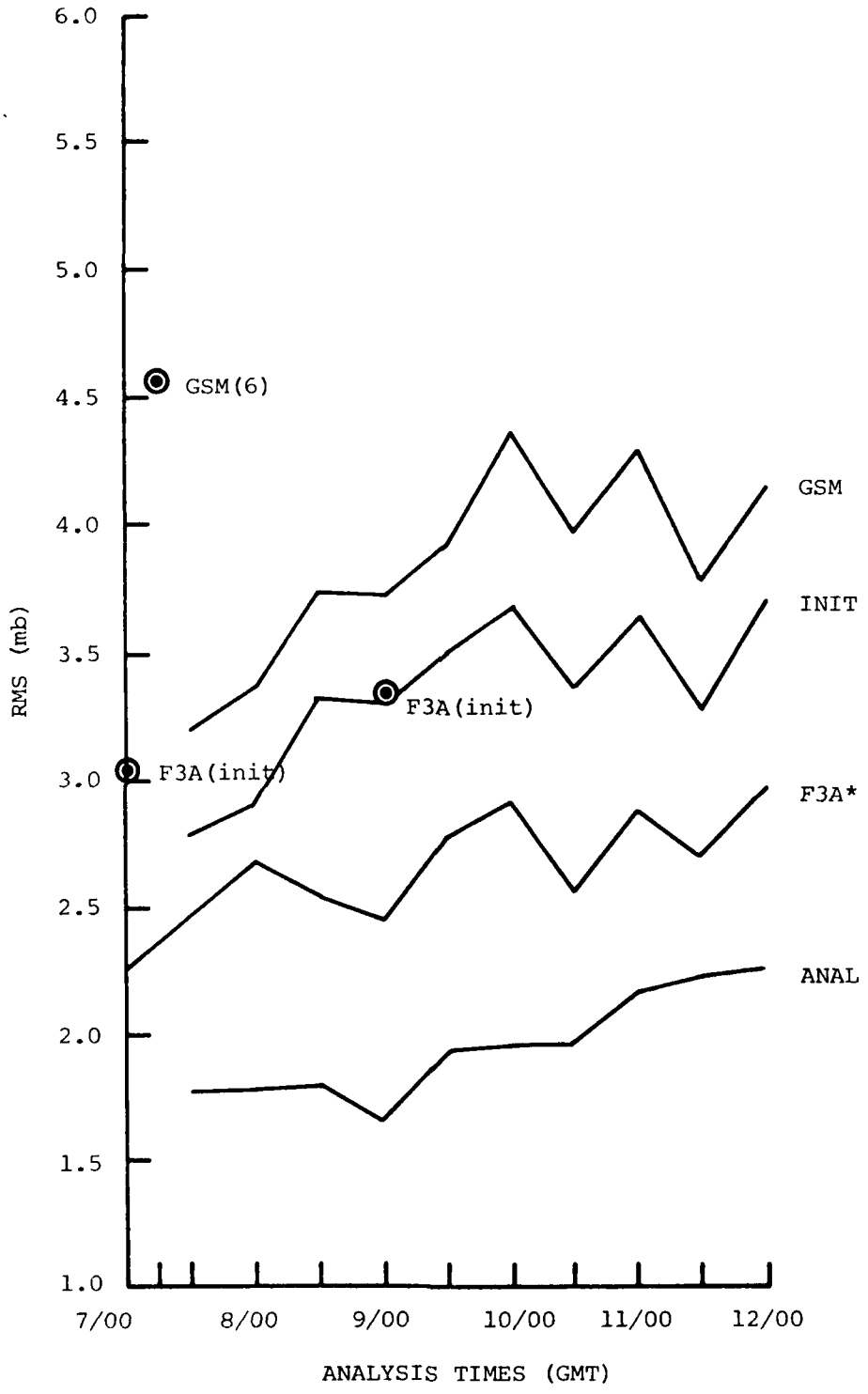

Fig. 1(g). Same as Fig. 1(a) except p_{sfc} ($^*p_{sfc}$ for F3A Derived Using GETPS)

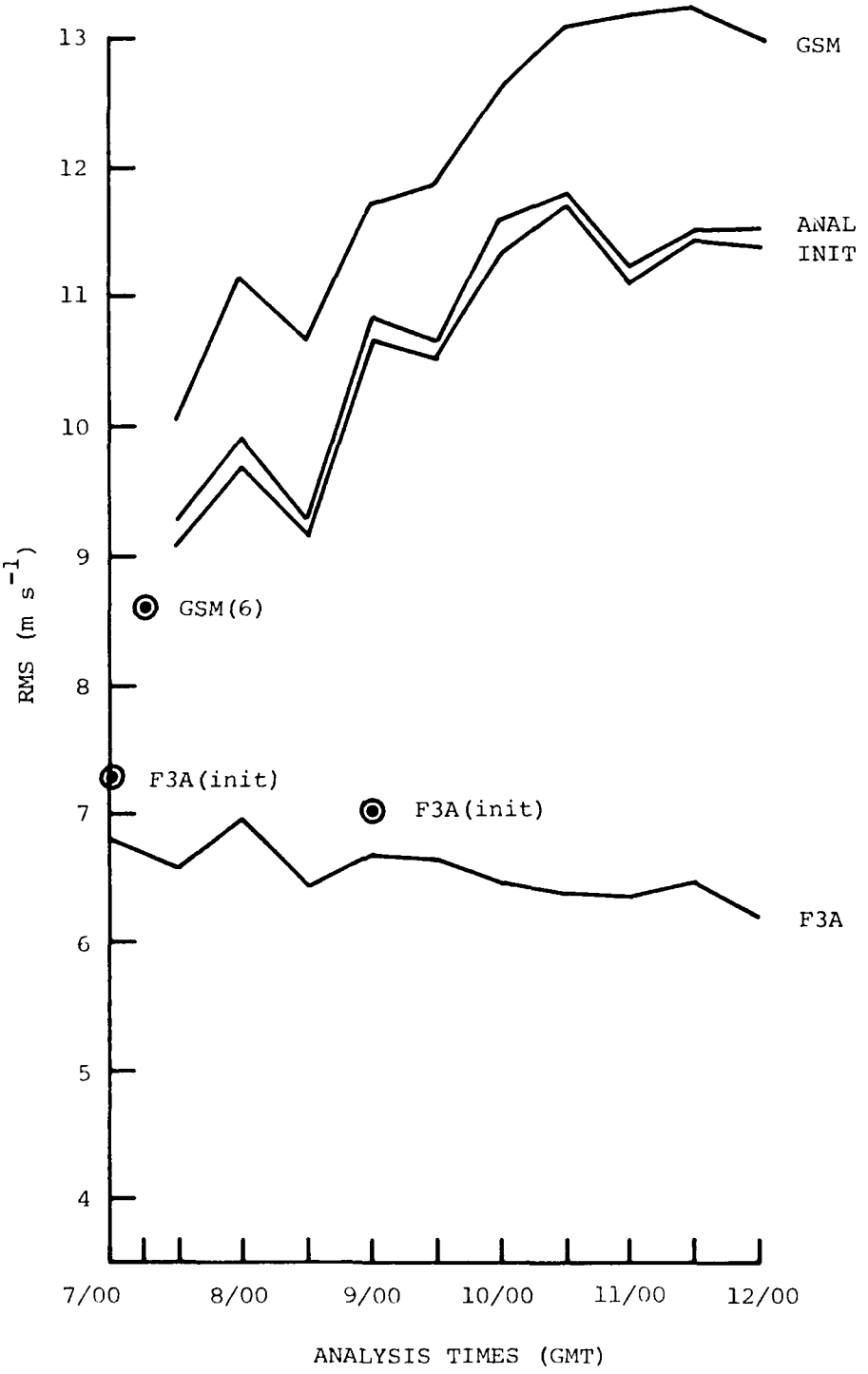

Fig. 1(f). Same as Fig. 1(a) except $\vec{V}$ at Layer 8 (~225 mb)

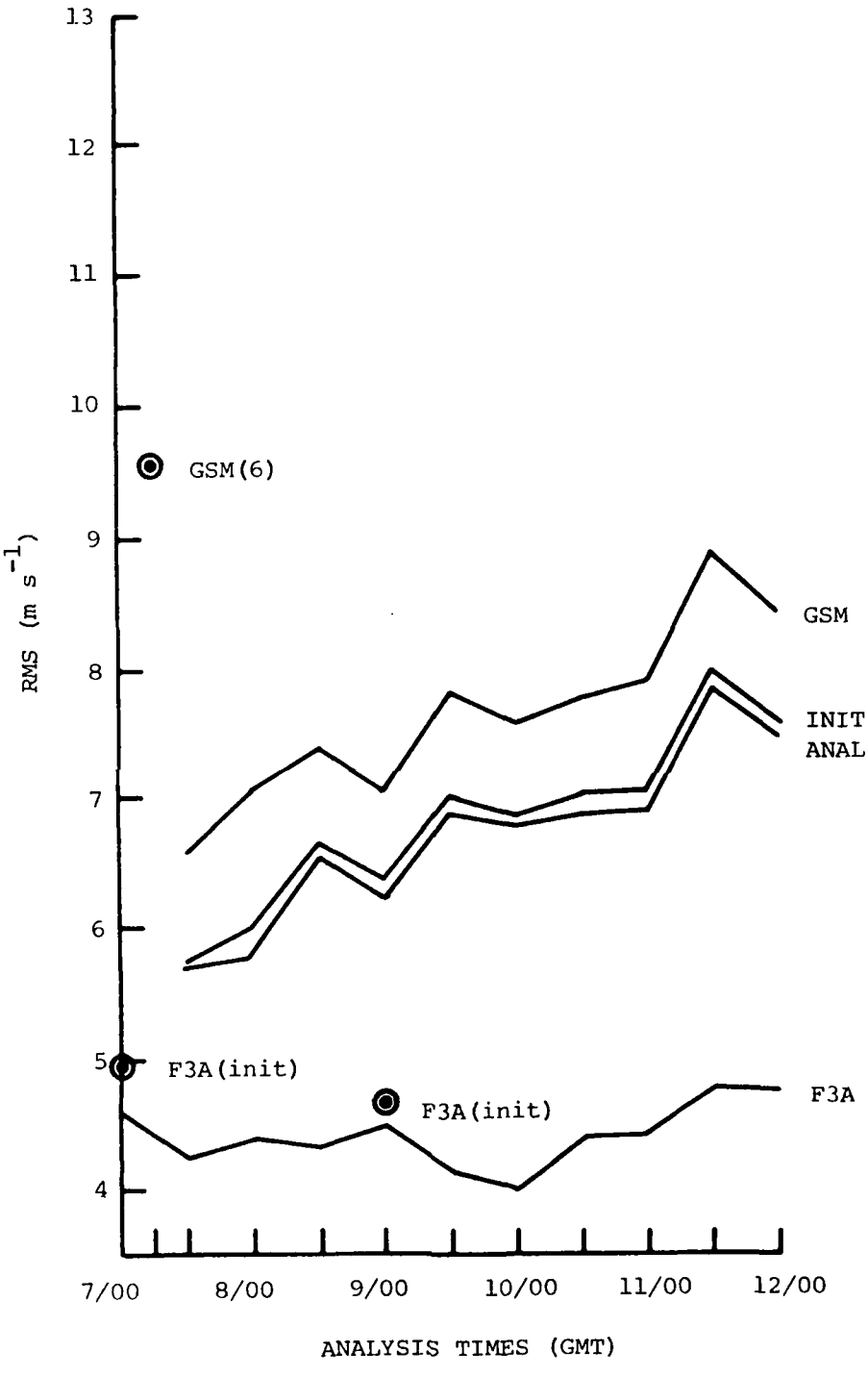

Fig. 1(e). Same as Fig. 1(a) except $\vec{V}$ at Layer 4 (~575 mb)

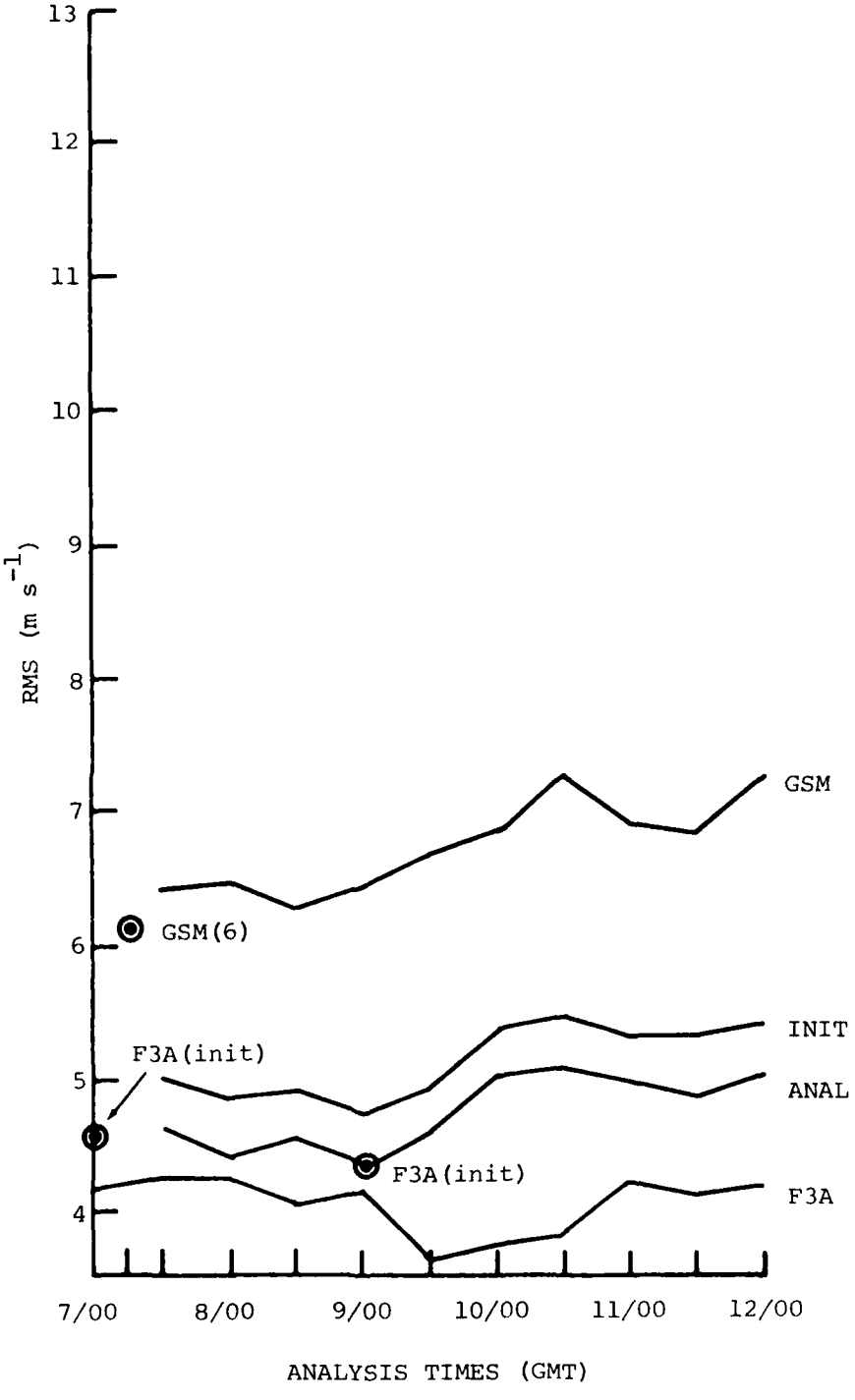

Fig. 1(d). Same as Fig. 1(a) except $\vec{V}$ at Layer 2 (~860 mb)

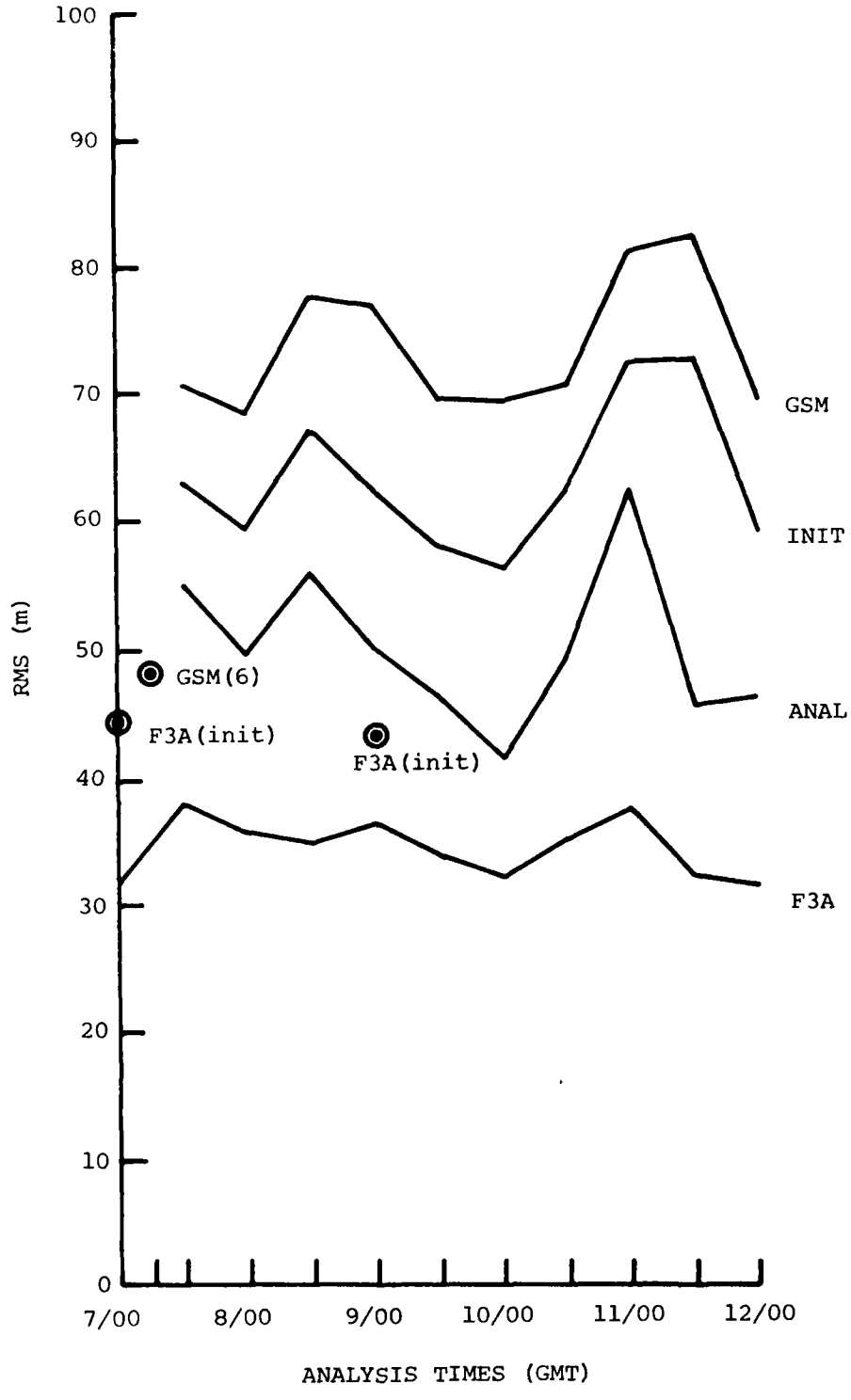

Fig. 1(c). Same as Fig. 1(a) except Z at Level 9 (~200mb)

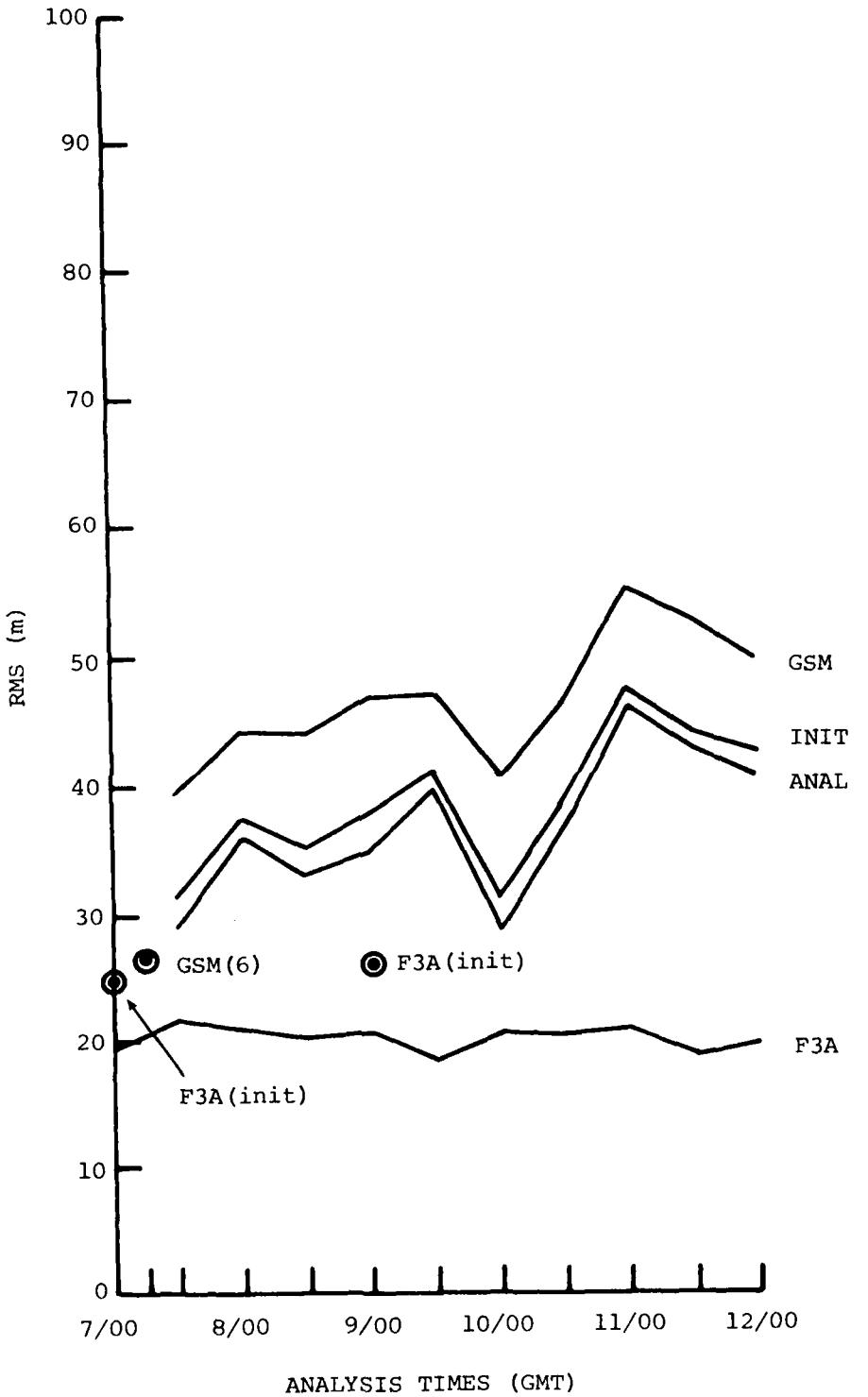

Fig. 1(b). Same as Fig. 1(a) except Z at Level 5 (~500mb)

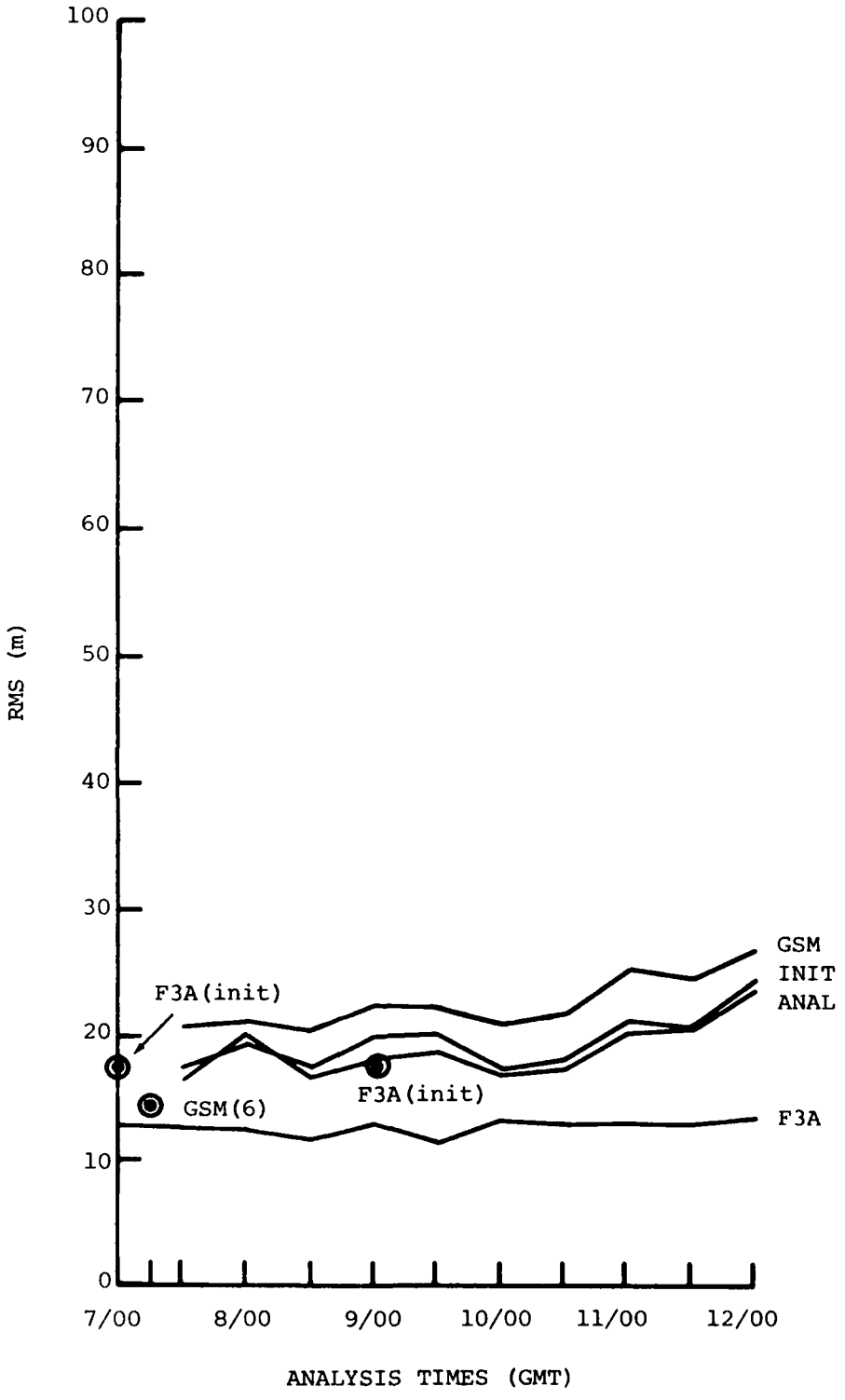

Fig. 1(a). RMS Error between Four Indicated Fields and Conventional Upper Air Observations for Z at Level 3 (~800mb) Using F3A as Basis for Observation Selection

of the forecast (G-GI) with the fast component in the analysis suggests that only a small portion of the analysis fast component can be attributed to the forecast (background) field. Since any fast component information introduced in the mass-motion imbalances in the analysis is removed in the initialization, only the slow component portion of the information supplied to the forecast field by the analysis is of interest. Therefore, it is of importance to know the magnitude of the slow component introduced in the analysis (I-GI), where I, the initialized analysis, is the slow component of the analysis, and GI is the slow component of the forecast field corrected by the analysis. For each variable, a comparison of (A-I) - (G-GI) with (I-GI) shows the relative magnitude of the fast component contributed by the analysis to the slow component contributed by the analysis. The smaller this ratio (in parentheses for average of first eight cases at end of I-GI row), the better the analysis is in contributing useful information to the initial conditions for the next forecast. In the first eight cases of this experiment, it appears that on the average the analysis fast mode to slow mode ratio is lower for heights at the low levels and lower for winds at the higher levels. This would seem to indicate that the initialization procedure adjusts the winds more than the heights to achieve balance at low elevations, but modifies the heights more than the winds to obtain mass-motion balance at the higher levels. By comparison, surface pressure values received much less slow mode information from the analysis in proportion to fast mode information than did upper heights and winds.

That the analysis procedure is effective in pulling the forecasts closer to the observations is evident from Figs. 1 (a-g). The RMS errors upon which these graphs are based were calculated by comparing the FGGE III-A (F3A), the forecast (GSM), initialized analysis (INIT), and the analysis (ANAL) fields with observations. The first step in each case was to calculate the observation-minus-field differences using F3A, then invoke the gross error check and buddy check in the same way that they are used in the analyses. The observations that survived these two checks formed the basis for the calculations of observation-minus-field differences for GSM, INIT, and ANAL. Thus, residuals for these three fields were calculated at the same observation locations and sigma layers/levels for which the F3A had valid values. By using the F3A in this way, it was believed that the comparisons of the other three fields would be more valid since a neutral

		7/12Z	8/0Z	8/12Z	9/0Z	9/12Z	10/0Z	10/12Z	11/0Z	11/12Z	12/0Z	AVE	$\frac{(A-I)-(G-GI)}{I-GI}$
$\rightarrow$ $V(\sigma_4)$	G-A	2.49	2.52	2.82	2.86	2.67	2.96	3.00	3.01	2.97	2.90	2.82	
	A-I	1.61	1.58	1.73	1.74	1.63	1.89	1.87	1.77	1.81	1.81	1.74	
	G-I	2.09	2.11	2.32	2.46	2.27	2.45	2.46	2.49	2.42	2.40	2.35	
	G-GI	0.12	0.10	0.09	0.10	0.09	0.09	0.11	0.10	0.10	--	0.10	
	I-GI	2.08	2.11	2.32	2.46	2.27	2.45	2.45	2.49	--	--	2.33	(0.70)
$\rightarrow$ $V(\sigma_8)$	G-A	4.56	4.22	4.64	4.71	4.50	5.14	5.11	4.52	4.84	5.05	4.73	
	A-I	2.45	2.26	2.58	2.58	2.51	2.69	2.69	2.60	2.67	2.90	2.59	
	G-I	3.70	3.37	3.65	3.79	3.56	4.12	4.06	3.62	3.84	3.88	3.76	
	G-GI	0.51	0.42	0.38	0.42	0.42	0.42	0.43	0.41	0.43	--	0.43	
	I-GI	3.67	3.33	3.64	3.77	3.55	4.10	4.04	3.60	--	--	3.71	(0.58)
P_{sfc} (mb)	G-A	4.44	4.21	3.93	4.50	4.59	5.36	4.59	5.51	4.23	4.75	4.61	
	A-I	3.87	3.66	3.47	3.98	4.02	4.50	4.10	4.74	3.72	4.26	4.03	
	G-I	1.64	1.56	1.50	1.51	1.64	1.87	1.54	1.75	1.72	1.68	1.64	
	G-GI	0.24	0.21	0.20	0.21	0.19	0.19	0.21	0.22	0.21	--	0.21	
	I-GI	1.64	1.58	1.52	1.53	1.67	1.86	1.55	1.75	--	--	1.64	(2.33)

Table 2. Root Mean Square Differences Between (1) GSM Forecast Field and Subsequent Analysis (G-A), (2) Analyzed Field and Initialized Analysis (A-I), (3) GSM Forecast and Initialized Analysis (G-I), (4) GSM Forecast and Initialized Forecast (G-GI), and (5) Initialized Analysis and Initialized Forecast (I-GI) (Averages for G-GI and I-GI are Based on First 9 and 8 Cases Respectively)

		7/12Z	8/0Z	8/12Z	9/0Z	9/12Z	10/0Z	10/12Z	11/0Z	11/12Z	12/0Z	AVE	$\frac{(A-I)-(G-GI)}{I-GI}$
$Z(\hat{\sigma}_3)$	G-A	11.27	10.34	10.63	10.32	11.53	11.63	11.14	11.75	11.26	11.81	11.17	
(m)	A-I	2.21	2.18	2.03	2.27	2.39	2.58	2.36	2.67	2.21	2.57	2.35	
	G-I	10.87	10.00	10.24	9.90	10.94	11.30	10.61	11.65	10.78	11.19	10.75	
	G-GI	0.17	0.16	0.15	0.16	0.15	0.14	0.16	0.16	0.15	--	0.16	
	I-GI	10.87	9.99	10.22	9.89	10.94	11.30	10.60	11.62	--	--	10.68	(0.21)
$Z(\hat{\sigma}_5)$	G-A	19.82	19.30	19.76	20.01	20.15	19.27	19.64	21.77	19.84	22.13	20.17	
	A-I	8.43	8.54	8.35	8.87	9.59	9.67	9.09	9.73	9.09	10.57	9.19	
	G-I	16.26	16.15	16.15	16.22	15.73	16.21	15.63	17.97	15.89	17.02	16.32	
	G-GI	1.45	1.26	1.29	1.34	1.25	1.24	1.33	1.27	1.28	--	1.30	
	I-GI	16.24	16.02	16.03	16.14	15.66	16.17	15.56	17.85	--	--	16.21	(0.49)
$Z(\hat{\sigma}_9)$	G-A	30.39	28.90	30.07	31.37	30.72	30.77	31.27	30.42	31.68	33.96	30.96	
	A-I	22.50	22.43	23.37	24.31	26.04	24.45	23.84	23.57	24.85	27.28	24.26	
	G-I	19.61	18.22	20.77	20.06	18.69	20.42	21.71	19.70	20.51	19.49	19.92	
	G-GI	4.03	3.26	3.30	3.54	3.06	3.19	3.65	3.10	3.09	--	3.36	
	I-GI	19.32	18.07	20.46	19.72	18.43	20.14	21.27	19.33	--	--	19.59	(1.07)
→													
$V(\sigma_2)$	G-A	2.51	2.59	2.74	2.77	2.76	2.80	2.89	2.82	2.91	2.91	2.77	
($m\ s^{-1}$)	A-I	1.61	1.60	1.70	1.71	1.62	1.82	1.84	1.76	1.78	1.80	1.72	
	G-I	2.40	2.39	2.53	2.59	2.57	2.64	2.69	2.65	2.70	2.72	2.59	
	G-GI	0.28	0.24	0.22	0.24	0.24	0.24	0.25	0.24	0.25	--	0.24	
	I-GI	2.38	2.38	2.52	2.57	2.56	2.63	2.68	2.64	--	--	2.55	(0.58)

of 1/7/79 00Z was chosen, and a FGGE III-A analysis for that date and time was interpolated from mandatory levels to 12 sigma levels and truncated to the rhomboidal 30 spectral representation following the procedure given by Gerlach (1983). These spectral values of relative vorticity, divergence, temperature, and specific humidity at the 12 sigma layers as well as terrain surface pressure were subjected to the two iteration, four vertical mode NMI. Resulting initialized fields were then used as initial conditions for a 12h forecast using the GSM. This forecast acted as the first guess in the implementation of the ASAP OI analysis codes, using FGGE II-B observations for 1/7/79 12Z. The analyzed fields were then initialized using the NMI; a 12h forecast was then run, followed by an analysis for 1/8/79 00Z. This pattern was repeated for a total of ten forecast-analysis-initialization cycles, ending with an initialization of the analysis valid for 1/12/79 00Z. The following paragraphs describe the results of the data assimilation experiment. The codes were run on the Air Force Weapons Laboratory Cray computer, taking about 35 minutes of computer time per cycle, of which about 30 minutes were due to the analysis.

Table 2 is a display of the root mean square (RMS) differences between the respective pairs of the three fields generated in each assimilation cycle. For vector winds, the RMS difference is the magnitude of the difference, defined by

$$\vec{V}_{RMS} = \left\{ \frac{1}{N} \sum_{i=1}^{n} [(u_{a_i} - u_{b_i})^2 + (v_{a_i} - v_{b_i})^2] \right\}^{1/2} .$$

The difference G-A represents the change imposed on the forecast field by the analysis, A-I is the fast component of the analysis (due primarily to mass-motion imbalances) since the initialized analysis contains only the slow mode of the analysis, and G-I is the overall change due to the analysis and initialized field. The fourth RMS difference shown, G-GI, is the fast component of the forecast field since the initialized forecast contains only the slow component of the forecast field. The G-GI RMS values are shown only for the first eight cases because these calculations were performed later, and at that time fields for the last two cases were not retrievable because of computer hardware problems. A comparison of the fast component

Since no such statistics are available yet for the AFGL data assimilation system, values of forecast error standard deviation from Table 1 are used for estimated prediction error E^p_{gr}. These values are first linearly interpolated latitudinally to the analysis grid latitudes assuming that the values given in the table correspond to latitudes of 90°S, 0°, 20°N, 40°N, and 90°N, respectively, for each of five columns in the table for Z, u, and v. Then in the analysis for each grid point, the resulting values are interpolated linearly in ℓn p to the σ layer grid points for each layer. These E^p_{gr} values are used as an estimate of f_{ir} for each residual i of type r used in the correction of the grid point g in Bergman's Eq. 2.10d. That is, no attempt is made to further interpolate estimated prediction error to the observation site to provide the denominator for Eq. 2.10d--the grid point value for that variable is used. The numerator of Eq. 2.10d, the estimated observation error E^o_{ir}, is interpolated vertically (linearly in ℓn p to the pressure of the observation) or extracted directly from Dey and Morone's (1983) Table 3. Thus the normalized observation error for the observation i of type r is given by $\epsilon^o_{ir} = E^o_{ir}/E^p_{gr}$.

After the normalized analysis error ϵ^a_{gr} is calculated using Bergman's Eq. 2.13, the dimensionalized analysis error is obtained using $E^a_{gr} = E^p_{gr}(\epsilon^a_{gr})^{1/2}$ for each variable r at grid point g. The E^a_{gr} values for Z, u, v, q, along with the corrections calculated in the analysis and applied to the forecast value P_{gr} to form the analyzed value A_{gr}, are the two terms whose squares are averaged over many cycles to form updated values for $E^{p'}_{gr}$. For this reason, the E^a_{gr} values and corrections are stored from each analysis.

B. Global Data Assimilation Experiment Using ASAP Analysis

A global data assimilation experiment was conducted using the ASAP analysis codes in conjunction with the GSM and the normal mode initialization (NMI). Observations and the starting analysis for this experiment were extracted from the First Global Atmospheric Research Program (GARP) Global Experiment (FGGE) data tapes[10]. A starting date and time

---

10. Obtained from Department of the Air Force, OL-A, USAF Environmental Technical Applications Center (MAC), Federal Building, Asheville, NC 28801.

In all of the graphs except the p_{sfc} plot, where the F3A field used was that obtained from the height and temperature analyses using the GETPS procedure (see Gerlach, 1983, Appendix B), the F3A error was substantially less than the error associated with ANAL. This would imply that the FGGE analysis achieved a better fit with the observations than did the ASAP analysis. A large part of the difference in error level between F3A and ANAL could be explained purely on the basis of length of forecast in the cycles between corrections. In order to obtain an estimate of the forecast error difference between a 6h and 12h forecast using the GSM, a 6h forecast was run starting with the same initialized FGGE III-A field at 1/7/79 00Z. The 6h forecast was compared directly with observations without the buddy and gross checks. The number of radiosondes available at that time was about one-third the number available at the 12h interval observation times. Values of error are plotted on Figs. 2 (a-g) for the 6h GSM forecast. In all cases for height, the difference between GSM(6) and F3A at 1/7/79 00Z is less than half of the difference between GSM (12h) at 1/7/79 12Z and F3A at 1/7/79 00Z. While the claim could not be made that an analysis of the 6h forecast would pull the error down to the level of the F3A error, the net error would be substantially less just by performing more frequent corrections.

Another explanation for the difference between the levels of RMS error for the ANAL and F3A is that by using F3A as a basis for selecting the observations for performing this error analysis, preference is being given to observations that fit best with the F3A field. A different subset of the observations would survive the gross and buddy checks if the ANAL were used as a basis. To test this possibility, the ANAL field was used as a basis for selecting observations for the RMS error calculations, and F3A was evaluated using that set of observations. The results are plotted in Figs. 2 (a-g). For Z, the F3A and ANAL error levels reversed, indicating an approximately equal fit with observations between the two analyses. The results for $\vec{V}$ and p_{sfc} remained virtually the same. For winds, this would imply that the FGGE assimilation fit the observations better at all times regardless of the subset of observations used as a basis for the RMS error calculations. In the case of p_{sfc}, the FGGE III-A analysis of surface pressure was not used as a basis of comparison--the GETPS-derived values were used since this is the field used in the GSM. Naturally, this

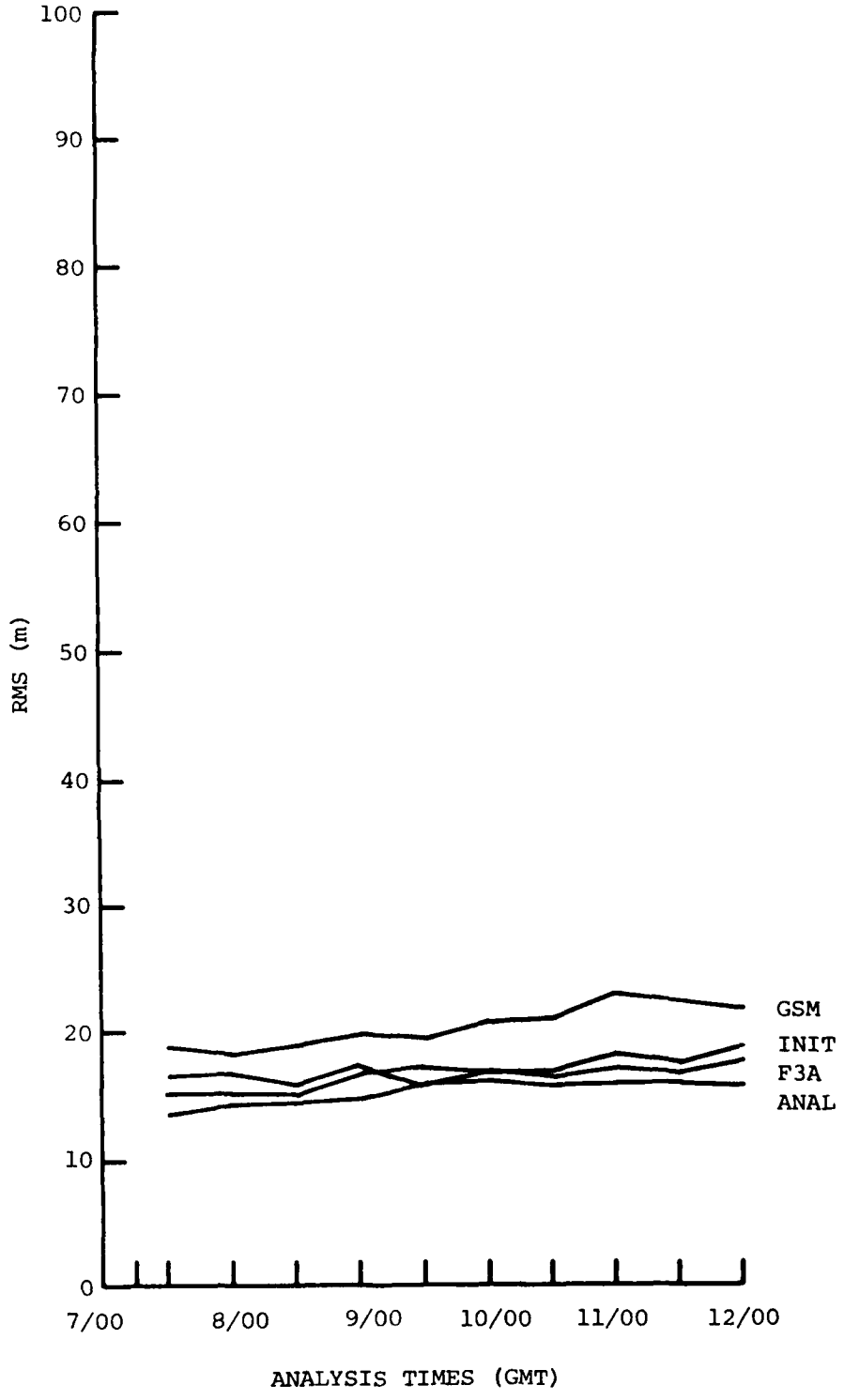

Fig. 2(a). RMS Error between Four Indicated Fields and Conventional Upper Air Observations for Z at Level 3 (~800 mb) Using ANAL as Basis for Observation Selection

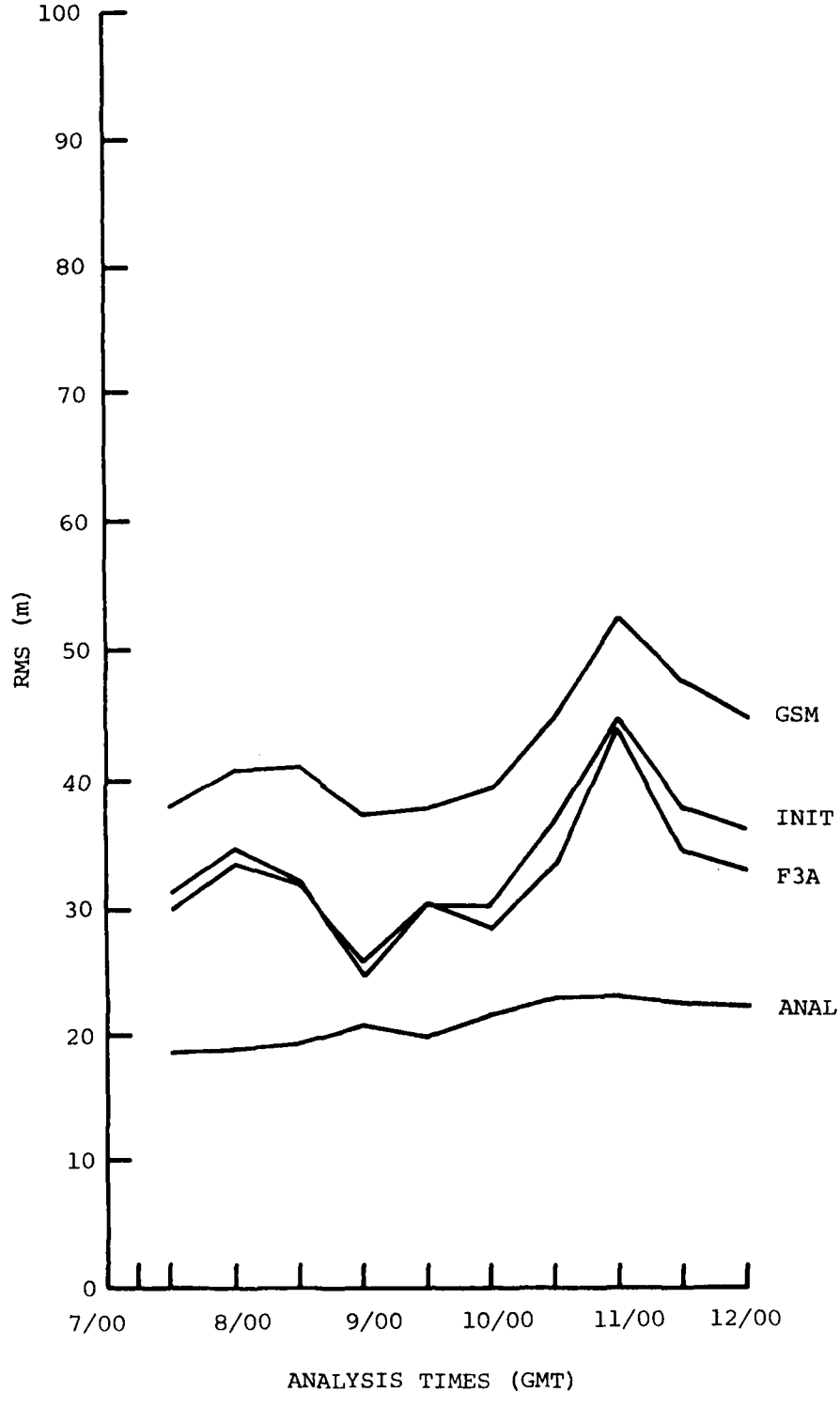

Fig. 2(b). Same as Fig. 2(a) except Z at Level 5 (~500 mb)

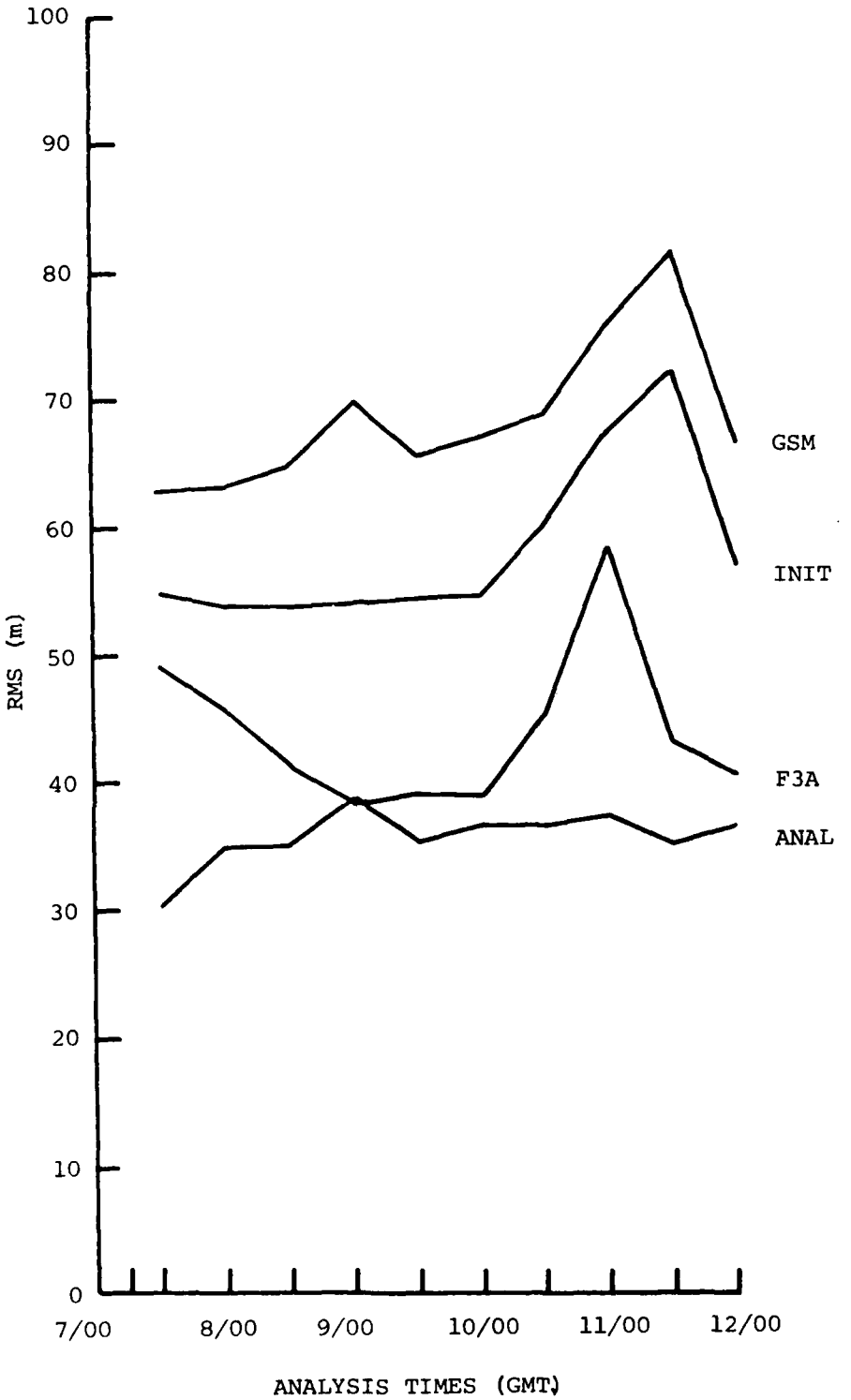

Fig. 2(c). Same as Fig. 2(a) except Z at Level 9 (~200 mb)

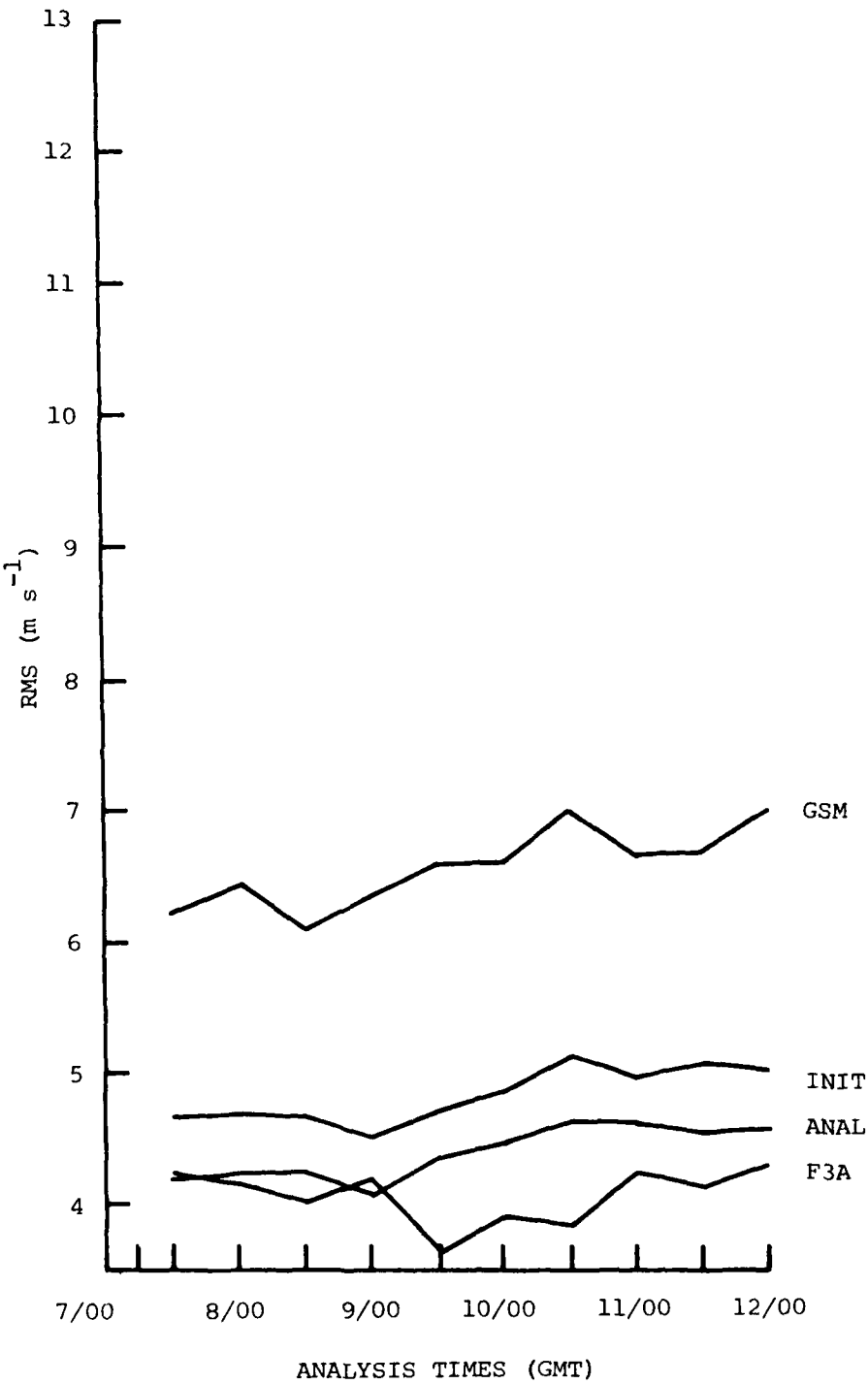

Fig. 2(d). Same as Fig. 2(a) except $\vec{V}$ at Layer 2 (~860 mb)

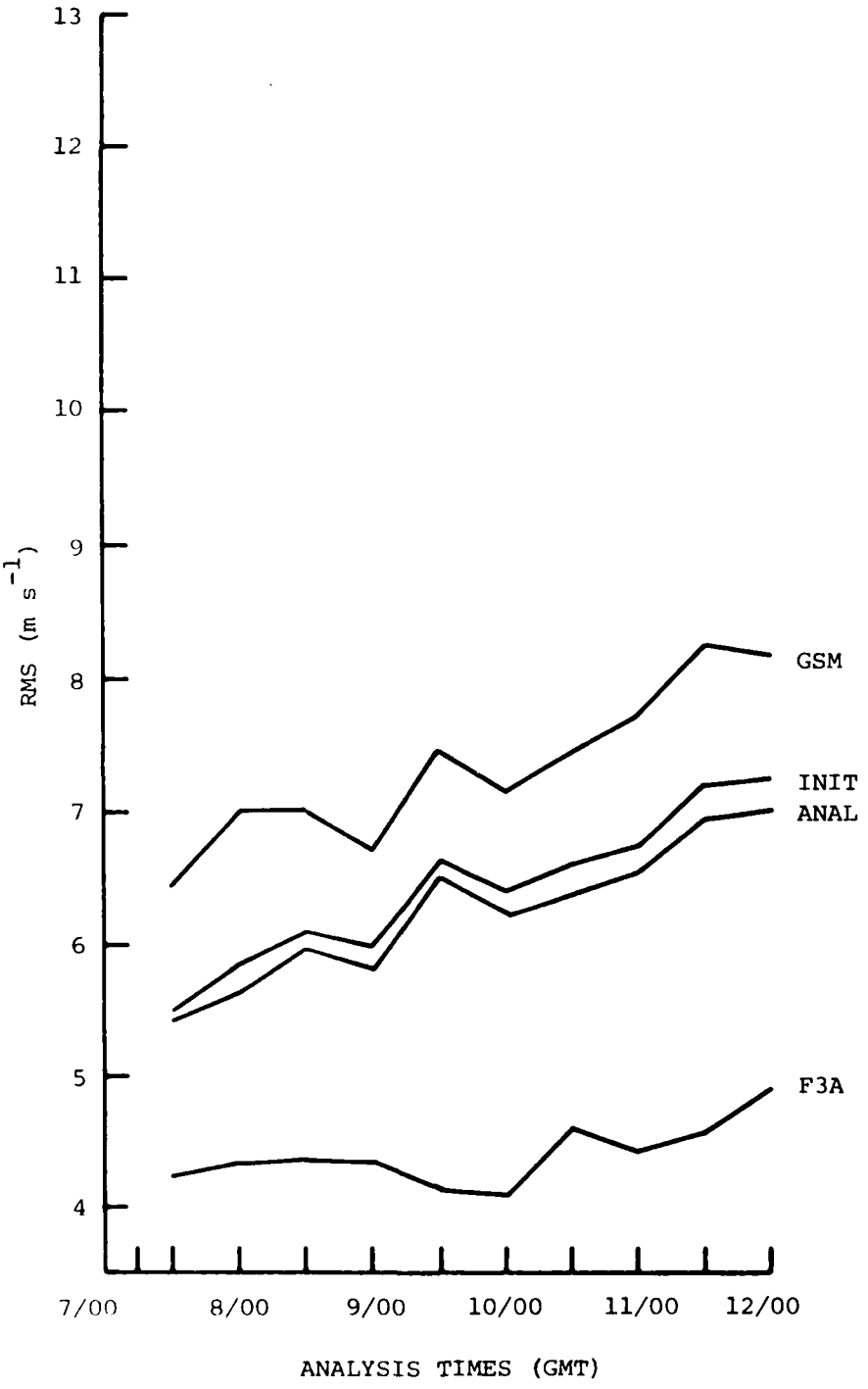

Fig. 2(c). Same as Fig. 2(a) except $\vec{V}$ at Layer 4 (~575 mb)

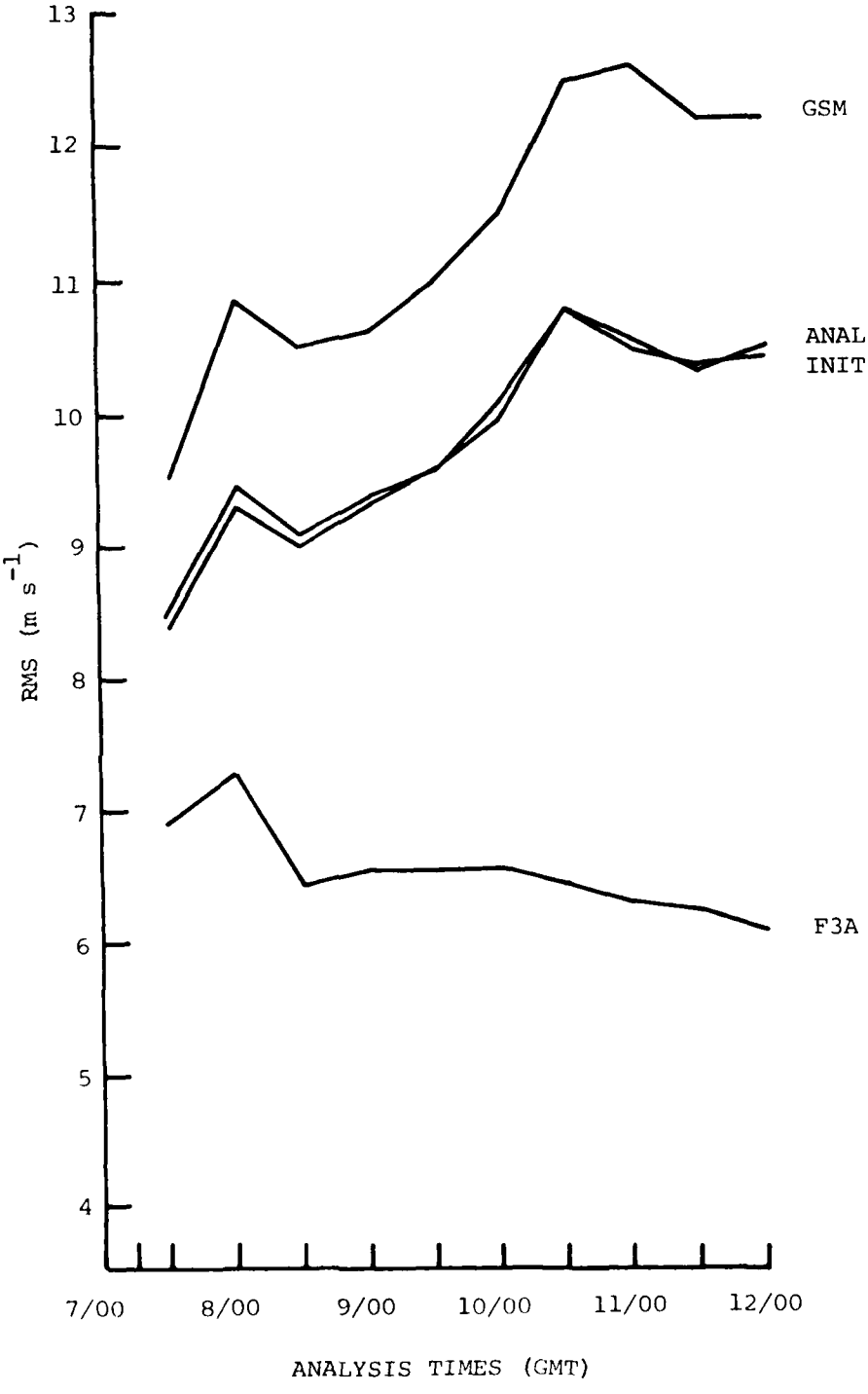

Fig. 2(f). Same as Fig. 2(a) except $\vec{V}$ at Layer 8 (~225 mb)

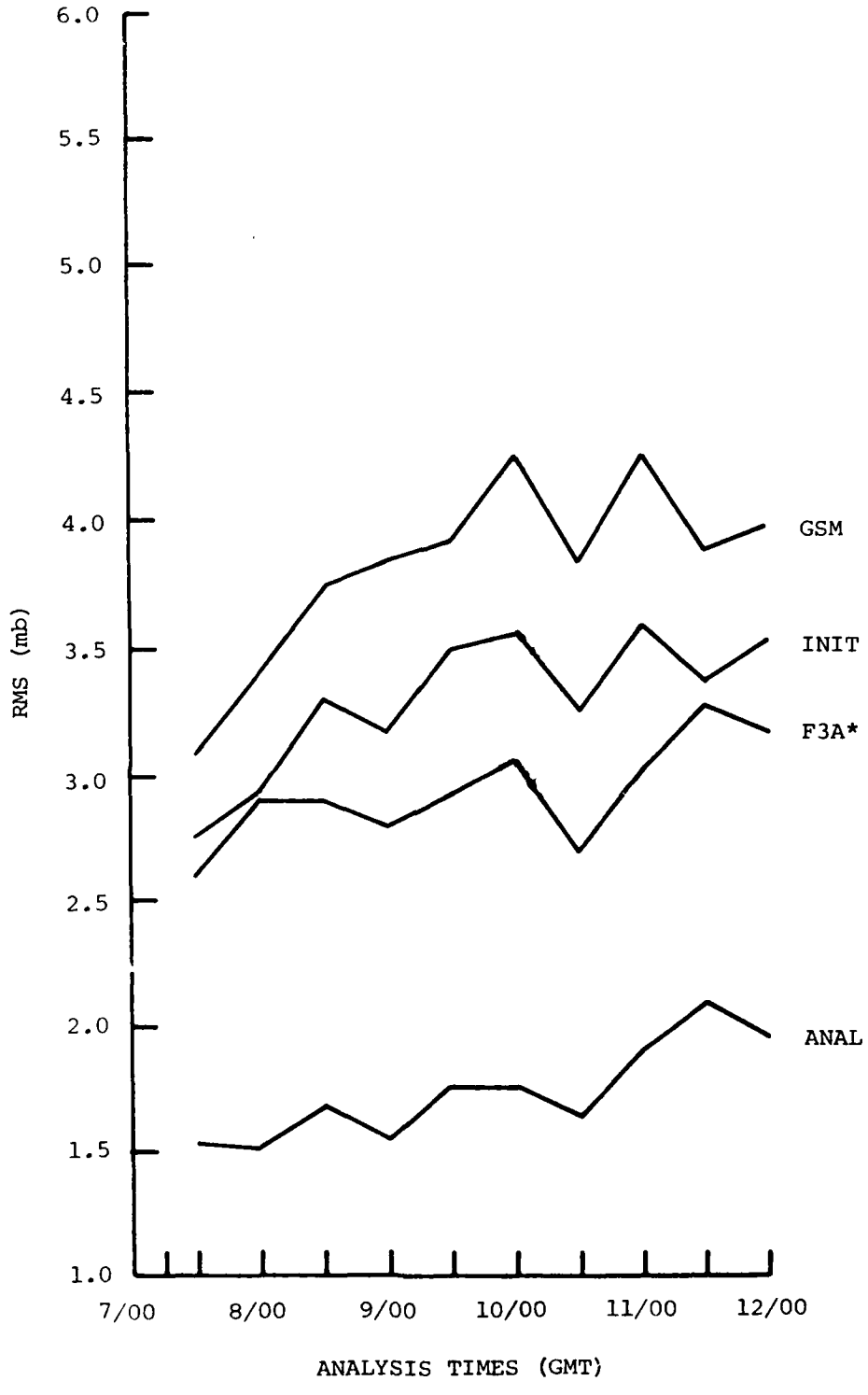

Fig. 2(g). Same as Fig. 2(a) except p_{sfc} ($*p_{sfc}$ for F3A Derived Using GETPS)

field would not fit as well with observations as would an actual analysis such as the ANAL. Finally, the large difference in error level between ANAL and INIT for p_{sfc} indicates that the analyzed field did not maintain a mass-motion balance well in correcting the pressure forecast. The correction imposed by the analysis was modified by the initialization in order to restore balance to the analyzed surface pressure field.

A third set of RMS error graphs (Figs. 3 (a-g)) shows the results of using the observations common to both F3A and ANAL basis sets for heights, winds, and specific humidity. Here, the fits to the observations for F3A for heights are only slightly better than those for ANAL, whereas the relationships between the curves for winds show very little change. While F3A and ANAL cases are not shown, very little relative change occurred in q between the three bases. This series of graphs demonstrates that the comparison of two or more analysis methods as to how they fit observations can depend very much on what set of observations is chosen in the comparison and on what variables are being compared. The results of the comparison of the fields with observations averaged over the ten cases are shown in Table 3. Notice that the number of observations in the bases decreases from the F3A basis to the combined F3A, ANAL basis. The latter set presumably contains only those observations that are agreeable to both F3A and ANAL fields; thus the RMS curves in Figs. 3 (a-f) are much smoother than for the other two bases.

In addition to a comparison of a sequence of analyses from ASAP and FGGE III-A, 48h forecasts based on the respective analyses for 1/9/79 00Z were conducted. The resulting forecast fields, designated ASAP48 and F3A48, respectively, were compared to 1/11/79 00Z observations using the F3A analysis, ASAP analysis, and combined sets for 1/11/79 00Z as a basis for selecting observations to be used in the RMS error calculations. Results are displayed in Table 4, along with comparable values for the initial conditions for both forecasts [INIT0900, initialized ASAP analysis, and F3A (init.), initialized FGGE III-A analysis]. The purpose of this experiment was to see if any anomalies were created by the ASAP analysis that would cause a longer forecast to show a radical departure from reality; that is, to see if a longer forecast based on ASAP would be stable. Although it would have been desirable to conduct several such forecasts for several different dates and times, fiscal constraints ruled

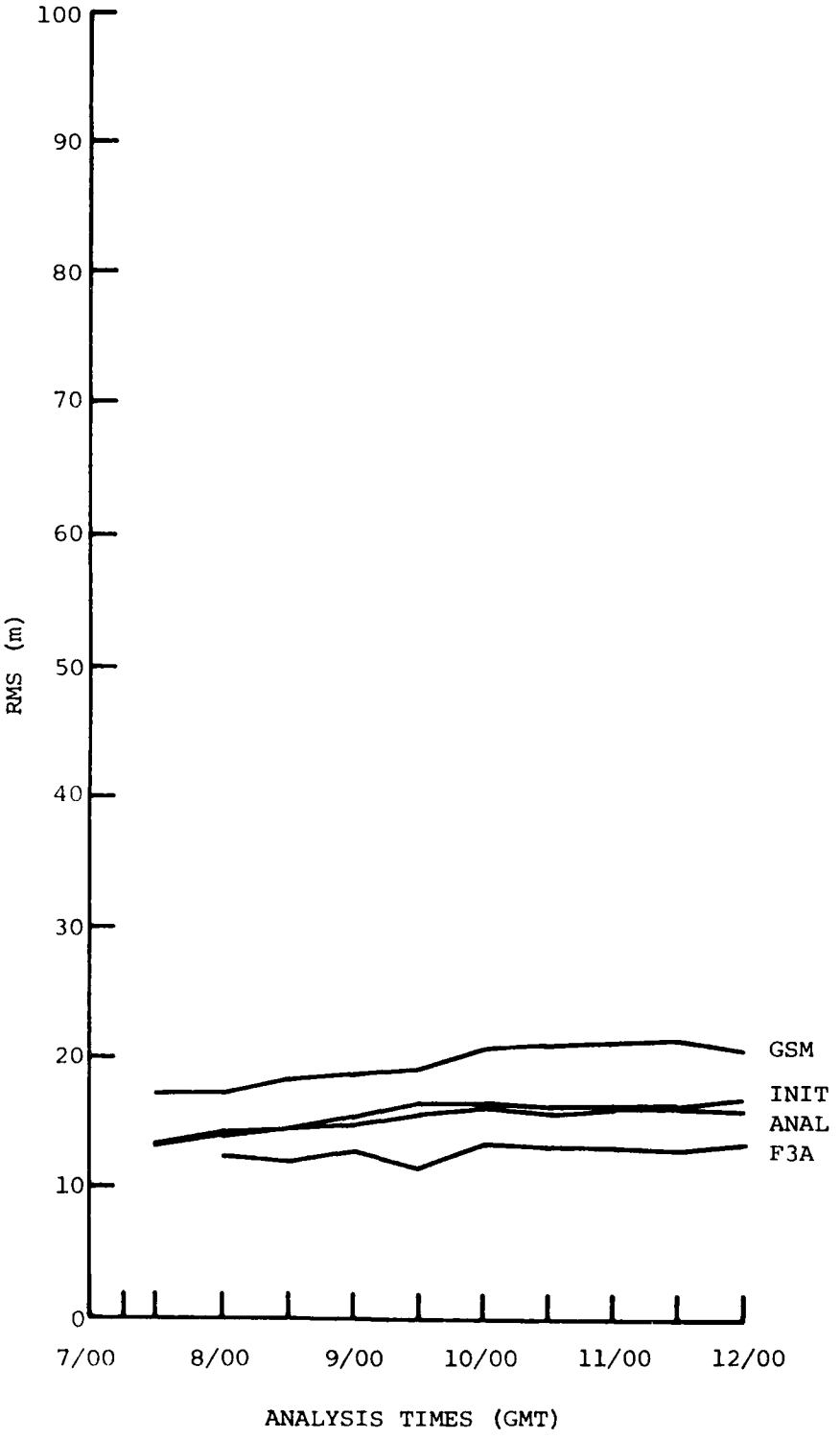

Fig. 3(a). RMS Error between Four Indicated Fields and Conventional Upper Air Observations for Z at Level 3 (~800 mb) Using Observations Common to Both F3A and ANAL Basis Observations

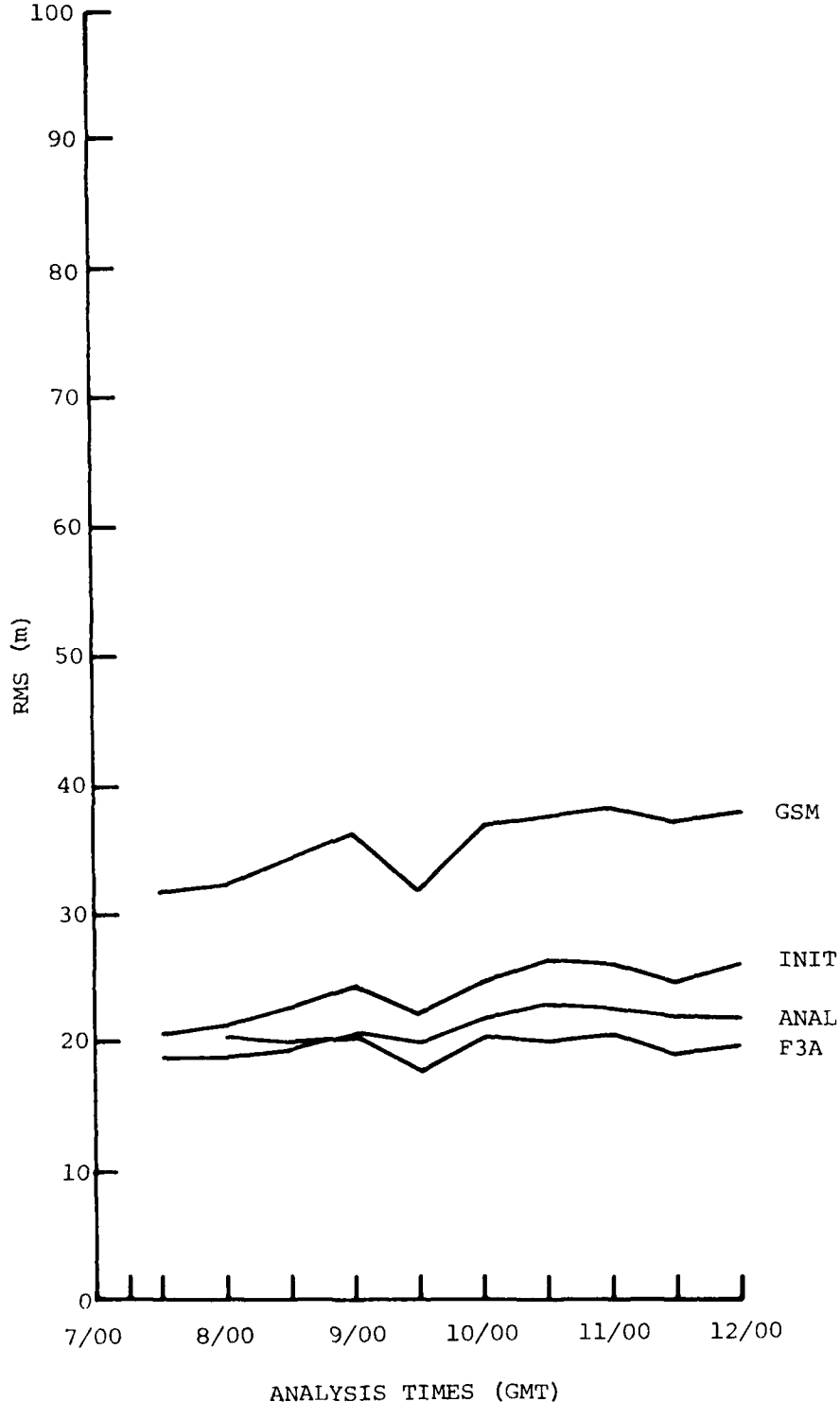

Fig. 3(b). Same as Fig. 3(a) except Z at Level 5 (~500 mb)

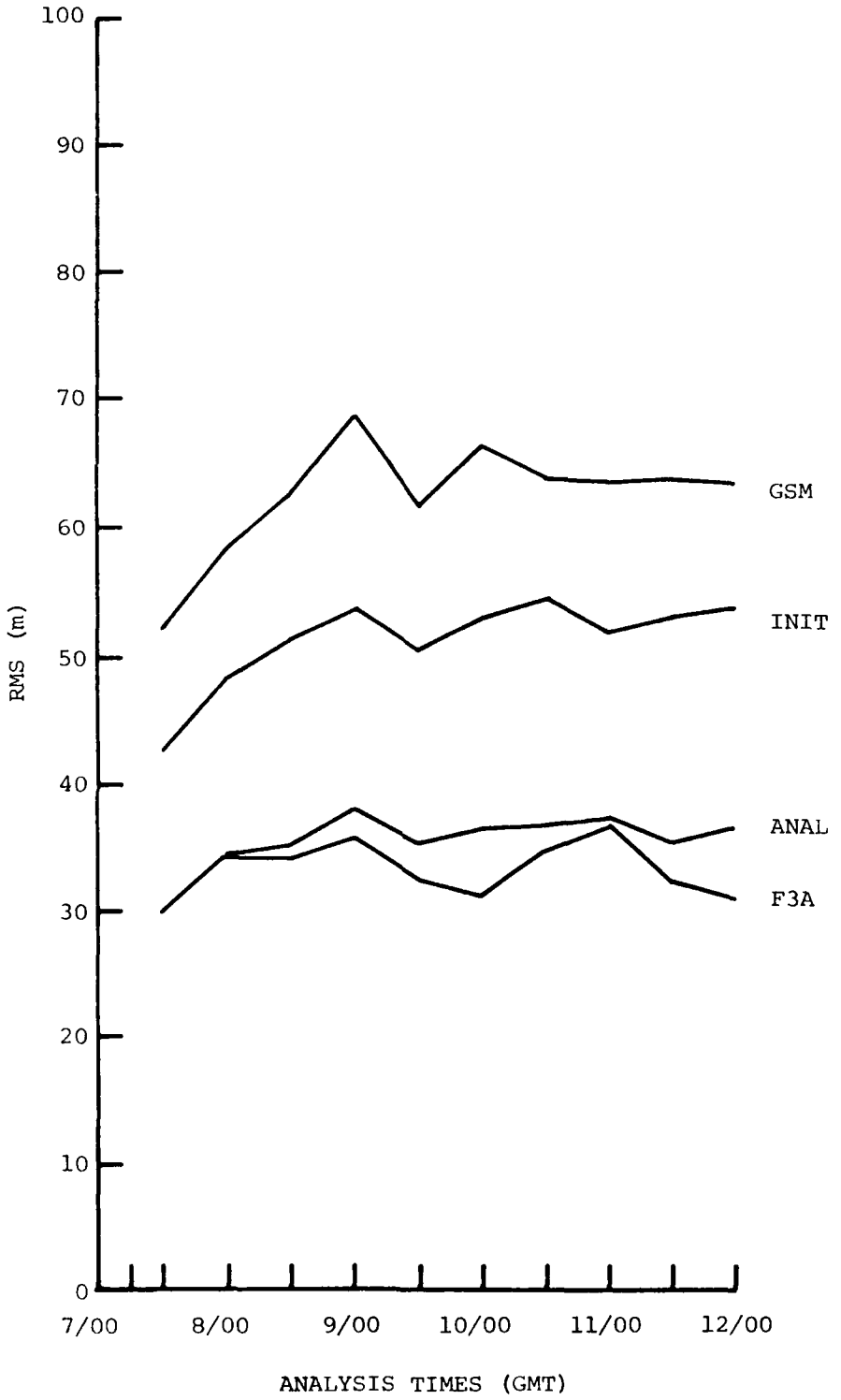

Fig. 3(c). Same as Fig. 3(a) except Z at Level 9 (~200 mb)

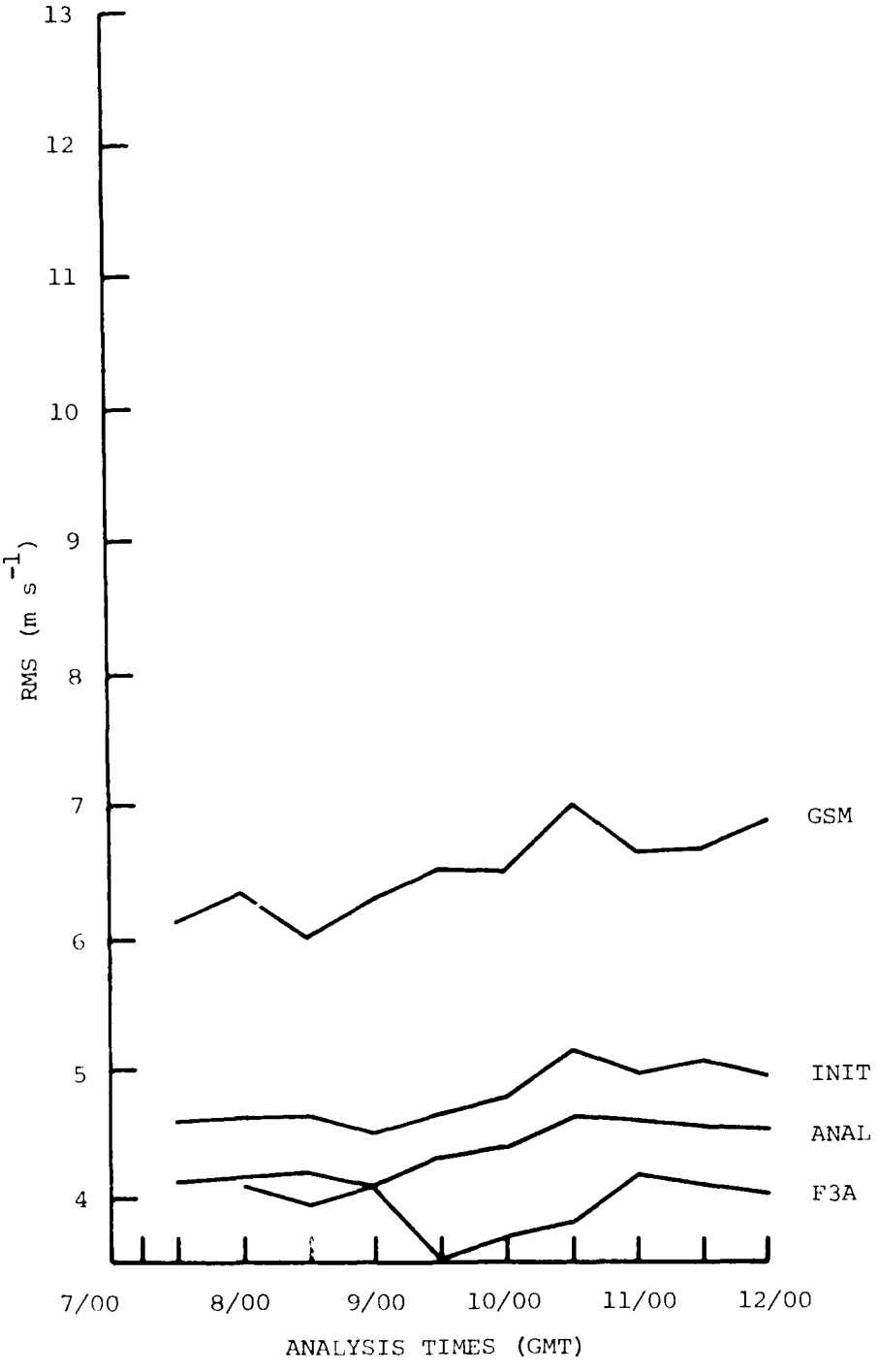

Fig. 3(d). Same as Fig. 3(a) except $\vec{V}$ at Layer 2 (~860 mb)

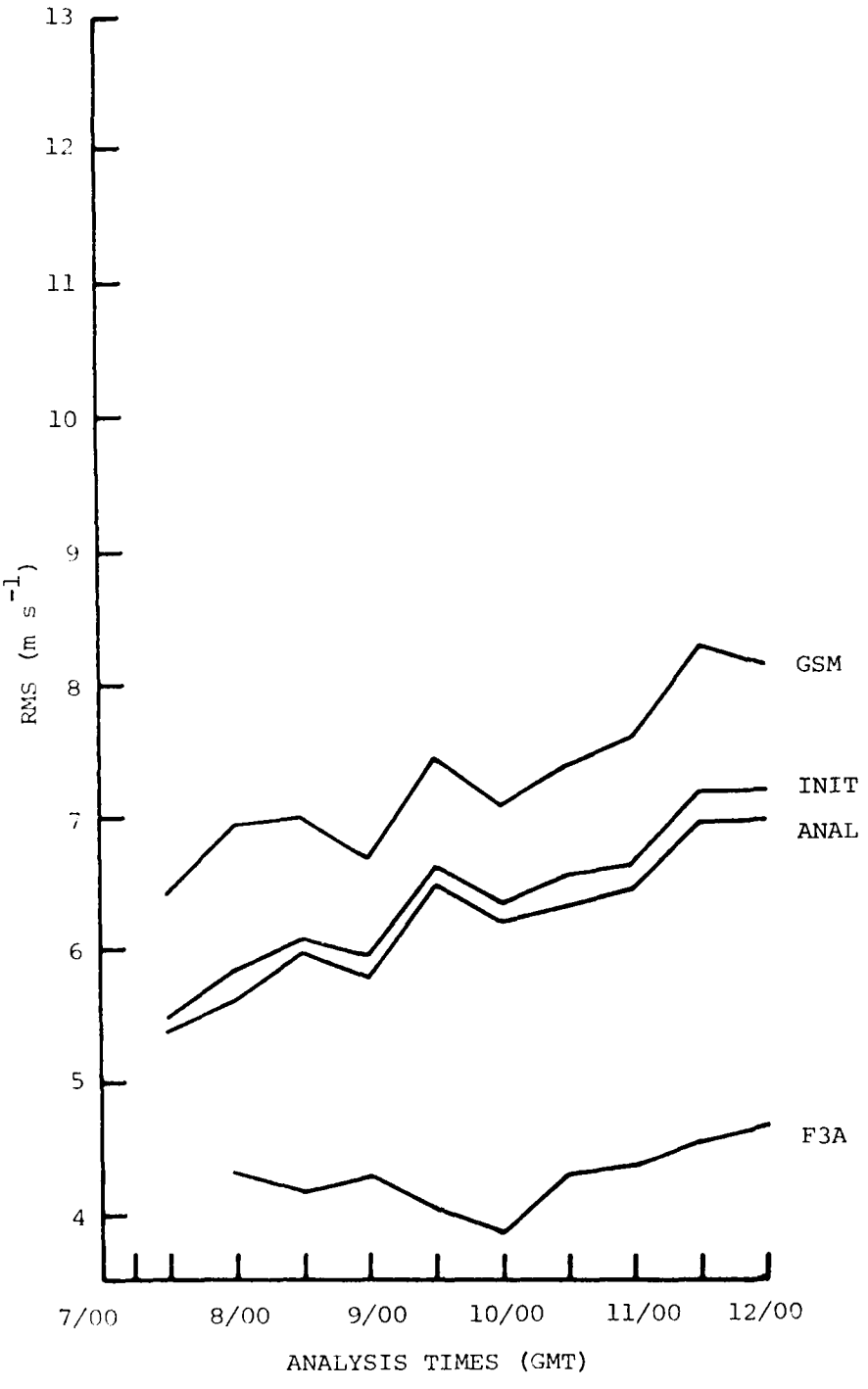

Fig. 3(e). Same as Fig. 3(a) except $\vec{V}$ at Layer 4 (~575 mb)

C. The Iterative and Non-Iterative Cycles

Once the coefficients $b_{n,r}$ are determined, it is possible to apply them to evaluating the variables at grid locations. At this point, the procedure differs little from other analyses. To perform an initialization, the variables must be expressed in terms of divergence, vorticity, temperature, surface pressure, and moisture. Velocities expanded at grid points can be rewritten in terms of divergence and vorticity. The compound function P can be separated into a surface pressure and height component, while moisture is provided independently from the FGGE III-A analyses. Heights can be transformed into temperatures using a hydrostatic relationship, but the procedure is by no means straightforward. In the NMC initialization procedure, Sela's (1980)[16] matrix equation relating temperatures to heights is inverted to solve for temperatures from heights. Yang (1982)[17] has pointed out, however, that this procedure is faulty because the matrix inversion results in unrealistic temperature profiles. NMC is not affected much by this shortcoming because during the course of initialization, the compound function P changes very little, and it is only the change that is computed by the faulty matrix inversion. But in this study, the actual height values are transformed back to temperatures before initialization, and this presents problems. As in Section II of this report, the Flattery least-squares fit, as detailed in Appendix A, is invoked to determine temperatures from heights at the layers. This method had its drawbacks, as well, mentioned in the earlier section of this report. These faults can become quite serious as will be explained later.

Once all the required variables are defined properly at all layers, the initialization procedure can be performed. Although the analysis employs eight vertical modes, the initialization limits the modes to four. This is to prevent divergence of the Machenhauer non-linear iteration scheme. Once the initialization routine has balanced the mass and motion field, there are

16. Sela, J. G., 1980: Spectral modeling at the National Meteorological Center. Mon. Wea. Rev., 108, 1279-1292.

17. Yang, C.H.; 1982: On the solution of the hydrostatic relation in the spectral model of the National Meteorological Center. Mon. Wea. Rev., 110, 1100-1102.

coefficient in the expansion. The second coefficient is found by removing the contribution of the first part and repeating the process; i.e.,

$$b_{2,r} = (F_r - b_{1,r}\Theta_{1,r}) \cdot \Theta_{2,r} (\Theta_{2,r} \cdot \Theta_{2,r})^{-1}.$$

In general

$$b_{k,r} = \left[F_r - \sum_{s=1}^{k-1} b_{s,r}\Theta_{s,r} \right] \cdot \Theta_{k,r} (\Theta_{k,r} \cdot \Theta_{k,r})^{-1} \qquad (3)$$

If the $\Theta_{n,r}$ were truly orthogonal to one another, Eq. (3) would reduce to the simple equation governing the evaluation of coefficients of orthogonal expansions. The departure from orthogonality will determine both the accuracy and validity of Eq. (3) as a means of determining the coefficients $b_{n,r}$.

As mentioned by HT, the problem of ordering of the vectors $\Theta_{n,r}$ is not trivial. It is possible, as we attempted to do in this study, to order the vectors by their contribution to the data vector, i.e., by the magnitude of $F_r \cdot \Theta_{k,r}$. This procedure effectively doubled the analysis time on AFWL's Cray computer, and the resulting improvement was minor. Because we are dealing with residuals, rather than absolute data, it was not possible to predict which vector would have the greatest impact. In fact, the vector Θ_0^0, which is a constant and would result in the mean of each variable, would certainly have been the greatest contributor to a field of variables such as heights or temperatures. In dealing with residuals, however, there is no guarantee that the mean is necessarily greater than any of the other amplitudes of the expansion. It may even be possible that vectors from internal modes with smaller effective depths would result in larger amplitudes than the external mode or some of the larger internal modes. But to order all I(L+1)(M+1) vectors would prove to be computationally impractical. It is thus necessary to separate vertical modes and to deal with only the (L+1)(M+1) vectors corresponding to each vertical mode. It was found that in general $F_r \cdot \Theta_{k,r} >> \Theta_{s,r} \cdot \Theta_{k,r}$ for any value of s and k as long as $s \neq k$. But this inequality depends greatly upon the geographical distribution of data and cannot be generalized for all cases.

In theory, I could be as large as the number of σ levels in the model, in this case, 12. In practice, however, only the first eight vertical modes were retained in the expansion. In case of observations with missing levels, the residuals at those levels were set to zero.

After the horizontally dependent coefficients were determined for each vertical mode, they were expanded in horizontal nmf by the method described by HT. This meant evaluating the nmf at each observation point where the residuals were defined. As with HT, this included the corners of grid boxes that lacked observations, which were assigned residuals of zero. Unlike HT, however, this study included single observations of either heights or velocities, which were fit to either $\hat{U}$, $\hat{V}$, or $\hat{\underline{P}}$ in the hope that the final analysis would create a balance between the heights and velocities even in regions where one or the other was missing. The projected residuals are then fit sequentially to the nmf for each mode, and each successive contribution subtracted from the original projected data vector. In other words, if $\mathbf{F}_r$ represents a vector containing the coefficients $\{a(\phi_i, \lambda_j)\}$ for a particular vertical mode r at all latitudes and longitudes where residuals of height and velocity are found, and we are also given a set of vectors

$$\{\Theta^m_{\ell,r}\} = \begin{pmatrix} \hat{U}^m_{\ell,r}(\phi) \\ \hat{V}^m_{\ell,r}(\phi) \\ \hat{\underline{P}}^m_{\ell,r}(\phi) \end{pmatrix} \begin{cases} \cos m\lambda \\ \sin m\lambda \end{cases}$$

for $m = 0,\ldots,M$ zonal wavenumbers and $\ell = 0,\ldots,L$ frequencies evaluated at the respective latitudes and longitudes where the corresponding u, v, and $\underline{P}$ residuals occur, then we can fit the vector $\mathbf{F}_r$ to the set $\{\Theta^m_{\ell,r}\}$ in a sequential manner. We first order the set $\{\Theta^m_{\ell,r}\}$ in some logical fashion, allowing us to substitute one index, say n, for the ℓ and m. The index n will then range from 1 to (L+1)(M+1). The first coefficient is determined by ignoring the nonorthogonality of the vectors in the set defined over the observation sites and allowing

$b_{1,r} = (\mathbf{F}_r \cdot \Theta_{1,r})(\Theta_{1,r} \cdot \Theta_{1,r})^{-1}$, where $b_{1,r}$ is now the first

where $\zeta^m_{n,\ell}$, $D^m_{n,\ell}$, $\underline{P}^m_{n,\ell}$ are normalized spectral coefficients of vorticity, divergence, and the compound variable, respectively, for zonal wavenumber m, meridional wavenumber n, and frequency index ℓ, P^m_n is the Legendre function, $\hat{U}^m_\ell$, $\hat{V}^m_\ell$, and $\underline{\hat{P}}^m_\ell$ are the normal mode functions (nmf) for the zonal component of velocity, the meridional component, and the compound variable, respectively. $\epsilon^m_n \equiv (n^2 - m^2)^{1/2} (4n^2 - 1)^{-1/2}$, ϕ is latitude, and $i \equiv \sqrt{-1}$. At the poles, $\hat{U}^m_\ell$ and $\hat{V}^m_\ell$ will be zero, except for m = 1, when $P^1_n(\cos\phi)^{-1}$ approaches $\pm [n(n+1)(2n+1)]^{1/2}/2\sqrt{2}$ as ϕ approaches $\pm \pi/2$. For m = 0, the Rossby waves have to be derived separately under the constraints that $\hat{V}^0_\ell = 0$ and the normalization requirement that $\sum_n |\zeta^0_{n,\ell}|^2 + |\underline{P}^0_{n,\ell}|^2 = 1$. A set of solutions is then obtained by means of Kasahara's (1978)[15] procedure of arbitrarily allowing one coefficient to equal 1 and computing the others. This leads to a sequence of vectors which can then be orthonormalized with a Gramm-Schmidt procedure, and the resulting coefficients are combined to produce $\hat{U}^0_\ell$ and $\underline{\hat{P}}^0_\ell$ for the Rossby modes.

In order to avoid considerable computational efforts in finding the values of the nmf for every observation point, we calculated and stored their value for each degree of latitude and interpolated whenever necessary. For high wavenumbers this may engender some error, especially near the equator, but hardly ever greater than 1 percent, which is acceptable for this study. A suggestion will be offered later as to how to reduce this error.

To simplify the three-dimensional aspect of the analysis problem, all observations were interpolated to model σ layers by means of an OI method described in Section II (pp. 9-10). The first guess field was then formed by spectral expansion of the forecast at the observation sites and the residuals computed. The resulting field of residuals was then projected on the model vertical modes $\{Z_i(\sigma)\}$, i=1,...,I. Because the vertical modes are orthonormal with respect to the model σ structure, the computation of the projections was fairly straightforward so that any variable $A(\phi,\lambda,\sigma)$, where λ is longitude, defined at a particular location ϕ_i, λ_j, σ_k, was represented as

$$A_{ijk} = \sum_{r=1}^{I} a_r(\phi_i, \lambda_j)\, Z_r(\sigma_k) \quad . \tag{2}$$

15. Kasahara, A., 1978: Further studies on a spectral model of the global barotropic primitive equations with Hough harmonic expansions. J. Atmos. Sci., 35, 2043-2051.

optimum interpolation (OI) but was hindered by the computational requirements for his recommendations.

By employing the normal mode functions directly in the analysis process, we hope to merge some of the features of initialization with objective analysis. In this study, the normal mode functions were the same as those generated by Ballish (1980)[13] for NMC's spectral model. These functions are determined by linearizing the tendency equations for vorticity, divergence, heights, and surface pressure. The resulting solutions supply eigenvalues corresponding to effective heights in the atmosphere and eigenvectors of spectral coefficients for vorticity, divergence, and a compound variable combining surface pressure and geopotential. The eigenvectors are separated by zonal wavenumber and frequency. The frequencies can be classified as Rossby, or rotational, waves, eastward-propagating gravity waves, or westward-propagating waves. For this study, as well as for NMC's purposes, gravity waves with a period of 48 h or more are kept along with all Rossby frequencies. All others are discarded. As with the Hough functions described by Kasahara (1976)[14], the coefficients can be used to create meridional normal mode functions for velocity and the compound variable. The expansions are of the following form:

$$\text{a.}\quad \hat{U}^m_\ell(\phi) = -\sum_n \left[\left\{ \zeta^m_{n,\ell} \left[n\,\epsilon^m_{n+1} P^m_{n+1} - (n+1)\,\epsilon^m_n P^m_{n-1} \right] + m\,D^m_{n,\ell} P^m_n \right\} (\cos\phi)^{-1} n^{-1/2} (n+1)^{-1/2} \right] \qquad (1)$$

$$\text{b.}\quad -i\,\hat{V}^m_\ell(\phi) = -\sum_n \left[\left\{ D^m_{n,\ell} \left[n\,\epsilon^m_{n+1} P^m_{n+1} - (n+1)\,\epsilon^m_n P^m_{n-1} \right] + m\,\zeta^m_{n,\ell} P^m_n \right\} (\cos\phi)^{-1} n^{-1/2} (n+1)^{-1/2} \right]$$

$$\text{c.}\quad \hat{P}^m_\ell(\phi) = \sum_n \underline{P}^m_{n,\ell} P^m_n$$

13. Ballish, B.A., 1980: Initialization, Theory, and Application to the NMC Spectral Model. PhD Thesis, University of Maryland, 151 pp.

14. Kasahara, A., 1976: Normal modes of ultra long waves in the atmosphere. Mon. Wea. Rev., 104, 669-690.

global model rather than Hough functions, which are normal modes of the Laplace tidal equations. The data were projected onto eight of a possible 12 vertical modes, then projected along the horizontal normal modes. There were two sets of experiments. In the first set, an initialization was performed after the analysis and forecasts generated from the initialized field. In the second set, the initialized field replaced the forecast field as the first guess, and a second analysis was produced based on the observed data and the initialized field. This procedure was repeated once more before a final initialized field was readied for the forecast model. This iterative procedure was designed to create a field which would reflect both the data and the large scale motion of the atmosphere. In mathematical terminology, the iteration was meant to converge on the intersection between the "slow" and "data" manifolds.

B. The Fitting Functions

During the course of preparation for a numerical weather forecast, data are moved from their observation locations usually to a fixed grid and are balanced for the forecast model by initialization. The interpolation of data to a fixed grid is a process referred to by meteorologists as an "analysis." The balancing of the resulting fields is termed "initialization," indicating that the field of variables is adjusted to serve as initial conditions for the model. In recent years, the initialization process has centered about model normal modes, which are the solutions to the linearized model equations. To balance the tendencies of the variables, the non-linear terms are also included in some fashion. The entire process is labeled "non-linear normal mode initialization" (NLNMI). It is very possible that the analysis procedure may work at cross odds to the initialization requirements unless the two are somehow combined. Interpolation to specific grid points alters the nature of the data being interpolated. When initialization is performed, the data are again modified, raising doubts as to the fidelity of the final product to the observations. It would be advantageous to combine the processes of analysis and initialization so that the final product does not depart radically from the original observations. In fact, Phillips (1982)[12] believed such an integration was possible in the case of

12. Phillips, N.A., 1982: On the completeness of multi-variate optimum interpolation for large-scale meteorological analysis. Mon. Wea. Rev., 110, 1319-1334.

III. ANALYSIS WITH DISCRETE NORMAL MODE FUNCTIONS

A. Introduction

A prescription for combining objective analysis with normal mode initialization was offered by Halberstam and Tung (1984)[6] (HT, hereafter) who demonstrated that Hough functions evaluated at observation sites can be fit to height and wind observations to produce an analysis that can be considered "pre-initialized." In order to make the fitting procedure economically feasible, it was necessary to compromise on a least-squares fit. It was shown that when a procedure such as the one outlined by Holmström (1963)[11] was substituted for a least-squares fit, the resulting error is smaller than a least-squares fit in areas of few observations. Holmström's procedure is a sequential computation of the coefficients of the expansion by subtracting from the original observation vector the fit produced by each vector from the set of basis function vectors. As can be anticipated, the geographical distribution of data plays an important role in the size of the analysis error. This makes precise estimation of the error a difficult task. It was shown by HT that the error is related to the non-orthogonality of the vectors; namely, the degree to which the dot products of the vectors depart from zero. Several comparisons were made by HT using a set of Hough functions from the external mode only, with 500 mb radiosonde data from FGGE II-B. Their results showed that although rms differences between analysis and data were quite large, the sequential method did control the errors. An iterative procedure, where the resulting analysis was substituted as the first guess field in the calculation of residuals, resulted in smaller errors between the observations and the final analysis.

In this study several modifications were made; each will be explained in detail. The modifications were geared to a global analysis based on all FGGE II-B data which are not rejected by a checking procedure. This would include satellite-derived heights or single level aircraft data. The basis functions were chosen to be the normal mode functions of the AFGL spectral,

---

11. Holmström, I., 1963: On a method for parametric representation of the state of the atmosphere. Tellus, 15, 127-149.

C. Conclusions

Though hampered by the objectivity problem of using observations whose error levels are not accurately known as a basis for verification, it appears that the OI analysis procedure described in this and two preceding reports works reasonably well in producing global forecasts in conjunction with the NMI and GSM. Although the 10 cycle data assimilation procedure showed some increase of error with time in the sequential forecasts for winds and pressure, this may be due to an underestimate of estimated prediction error for the 12h forecasts used in the assimilation experiment. For further study, a 6h forecast length is recommended, even though fewer conventional observations are available at 06Z and 18Z. In addition, it is recommended that observations with high quality control index values (poor quality) from the FGGE II-B data set not be used with this procedure, since their inclusion (especially in conventional upper air observations) often results in erroneous interpolations to σ layers/ levels when use of a correct observation just above or below the erroneous one would have led to an acceptable interpolated value. Finally, while results for moisture were not discussed in this report because of the simple, univariate nature of the moisture analysis, the results of the moisture analyses in this study will be used as a standard against which an improved OI based global moisture analysis method will be compared in a follow-on study.

methodologies. Fortunately, Dey and Morone (1983) show curves for RMS error against observations for both initial conditions and 6h forecasts for 1 1/2 years of assimilation performances of the NMC Global Data Assimilation System (GDAS). These curves were qualitatively averaged over their duration to obtain the values for the GDAS shown in Table 5. The

Table 5. Qualitative Comparison of ASAP(1) with GDAS(2) RMSE Against Observations.

	GSM	INIT	DIFF
Z (500mb)			
GDAS (500mb)	24 (m)	18	6
ASAP (~500mb)	35.2	23.7	11.5
$\vec{V}$ (250mb)			
GDAS (250mb)	8.6 (m s^{-1})	6.4	2.2
ASAP (~225mb)	11.3	9.7	1.6

(1) Values based on average of 663 radiosondes over the globe for ten cycles: 1/7/79 to 1/12/79 (12h forecasts)

(2) Values based on 102 northern hemisphere radiosondes for 6h forecast cycles: 7/81 - 12/82 (Dey and Morone, 1983)

corresponding ASAP values (based on the ten 12h cycles) averaged over the time period and based on the intersection set of observations (F3A + ANAL basis) were taken from Table 3. The absolute values for both the forecast (GSM, 6h for GDAS, 12h for ASAP) and the corresponding initialized analysis resulting from that forecast field (INIT) are larger for the ASAP system in all cases. But considering only the net change imposed by the analysis-initialization processes on the forecast (the DIFF column) shows that, at least qualitatively, the effectiveness of the ASAP system is competitive with that of the GDAS.

out that possibility. Thus, while it is somewhat risky to draw sweeping conclusions from one comparison, it appears that the ASAP based forecast has RMS errors that are of the same order of magnitude as F3A based forecast RMS errors.

In all cases, the F3A48 forecast verifies better against observations than does the ASAP48 forecast. However, since in most cases the initial conditions also verify more closely in the F3A case, a more accurate measure of forecast performance is the error growth during the course of the 48h forecast in each case. By comparing the difference between F3A48 and F3A (init) with the difference between ASAP48 and ASAP (init), we see that the error growth for heights was less for ASAP only in the Z ($\hat{\sigma}_5$) "F3A only" case, but in all cases for the highest level winds. The two forecasts are about even in error growth in predicting surface pressure. Thus, in this case, the ASAP forecast does not appear to be the victim of any anomalous error that would have resulted in a grossly large verification error at 48 hours.

As in the case with the 12h assimilation cycles, the fit of fields to observations very much depends on the set of observations chosen. This 48h experiment shows that the forecast verifies best in almost all cases against the most restrictive set of observations, the intersection of the F3A and ANAL based sets, which in all cases contains the fewest observations. Once again, the difference between statistics for three different sets of basis observations, especially for Z, indicates that results can depend on which observations are selected for the verification of forecasts and analyses. This results from the fact that the errors associated with observations reduce the objectivity of the verifications, since no accurate objective measure of observation error is known. No two methods of throwing out bad observations, whether manually or automatically, will result in the same set of observations against which the relative "goodness" of two or more forecasts/analyses can be compared. All that can be said in this case is that the RMS errors associated with the two forecasts are of the same order of magnitude.

Finally, as a basis of reference for a newly developed assimilation system, it is of interest to establish at least a qualitative comparison with a well-established, operational assimilation system to see if the level of performance of the system is competitive with established

Table 4. RMS Errors for 48h Forecast Experiment

Variable	Experiment	F3A(init)	ASAP(init)	F3A48	ASAP48	No. Obs.
Z(m)						
	F3A only	17.81	19.94	28.22	33.10	654
$\hat{\sigma}_3$	ASAP only	17.61	16.79	26.45	31.48	642
	F3A + ASAP	12.83	15.24	23.89	28.57	639
	F3A only	25.96	37.75	70.01	78.02	642
$\hat{\sigma}_5$	ASAP only	24.85	25.67	68.65	76.29	636
	F3A + ASAP	21.55	24.26	58.69	66.92	625
	F3A only	43.28	62.43	105.73	126.17	614
$\hat{\sigma}_9$	ASAP only	41.90	54.13	103.31	123.85	616
	F3A + ASAP	40.26	53.59	95.95	116.70	603
$\vec{V}$(m s^{-1})						
	F3A only	4.38	4.75	8.08	9.13	675
σ_2	ASAP only	4.46	4.51	7.98	8.98	665
	F3A + ASAP	4.35	4.49	7.94	8.97	652
	F3A only	4.62	6.37	8.92	9.67	631
σ_4	ASAP only	4.52	5.98	8.94	9.71	603
	F3A + ASAP	4.45	5.94	8.79	9.52	593
	F3A only	7.04	10.67	14.73	14.24	582
σ_8	ASAP only	6.90	9.32	14.31	13.82	565
	F3A + ASAP	6.74	9.27	14.29	13.83	561
	F3A only	3.34	3.30	4.95	6.09	2736
p_{sfc}	ASAP only	3.56	3.17	4.87	6.05	2715
	F3A + ASAP	--	--	--	--	---

Table 3. RMS Differences between Fields and U.A. Observations
(Averaged over 10 12-hour Assimilation Cycles)

	Obs. Allowed by F3A		Obs. Allowed by ANAL		Obs. Allowed by F3A + ANAL	
	RMS	No. Obs.	RMS	No. Obs.	RMS	No. Obs.
$Z_{\hat{\sigma}=3}$ (~800 mb)						
GSM	22.67(m)	690	20.41	683	19.38	679
INIT	19.63		16.84		15.37	
ANAL	18.83		15.27		15.16	
F3A	12.66		16.74		12.43	
$Z_{\hat{\sigma}=5}$ (~500mb)						
GSM	46.63	678	42.52	671	35.20	663
INIT	38.64		33.62		23.71	
ANAL	36.67		21.02		20.69	
F3A	20.14		32.73		19.76	
$Z_{\hat{\sigma}=9}$ (~200mb)						
GSM	73.56	639	68.61	634	62.46*	627
INIT	63.39		58.29		51.12	
ANAL	50.32		35.60		35.41	
F3A	34.78		44.01		33.88	
→						
$V_{\sigma=2}$ (~860mb)						
GSM	6.76(m s^{-1})	740	6.55	724	6.50	709
INIT	5.15		4.82		4.77	
ANAL	4.77		4.39		4.35	
F3A	4.05		4.06		3.93	
→						
$V_{\sigma=4}$ (~575mb)						
GSM	7.65	705	7.34	683	7.31	672
INIT	6.83		6.42		6.39	
ANAL	6.70		6.25		6.21	
F3A	4.39		4.40		4.27	
→						
$V_{\sigma=8}$ (~225mb)						
GSM	12.05	627	11.35	610	11.28	604
INIT	10.61		9.76		9.70	
ANAL	10.76		9.82		9.77	
F3A	6.52		6.54		6.34	

*INIT-ANAL > GSM-INIT

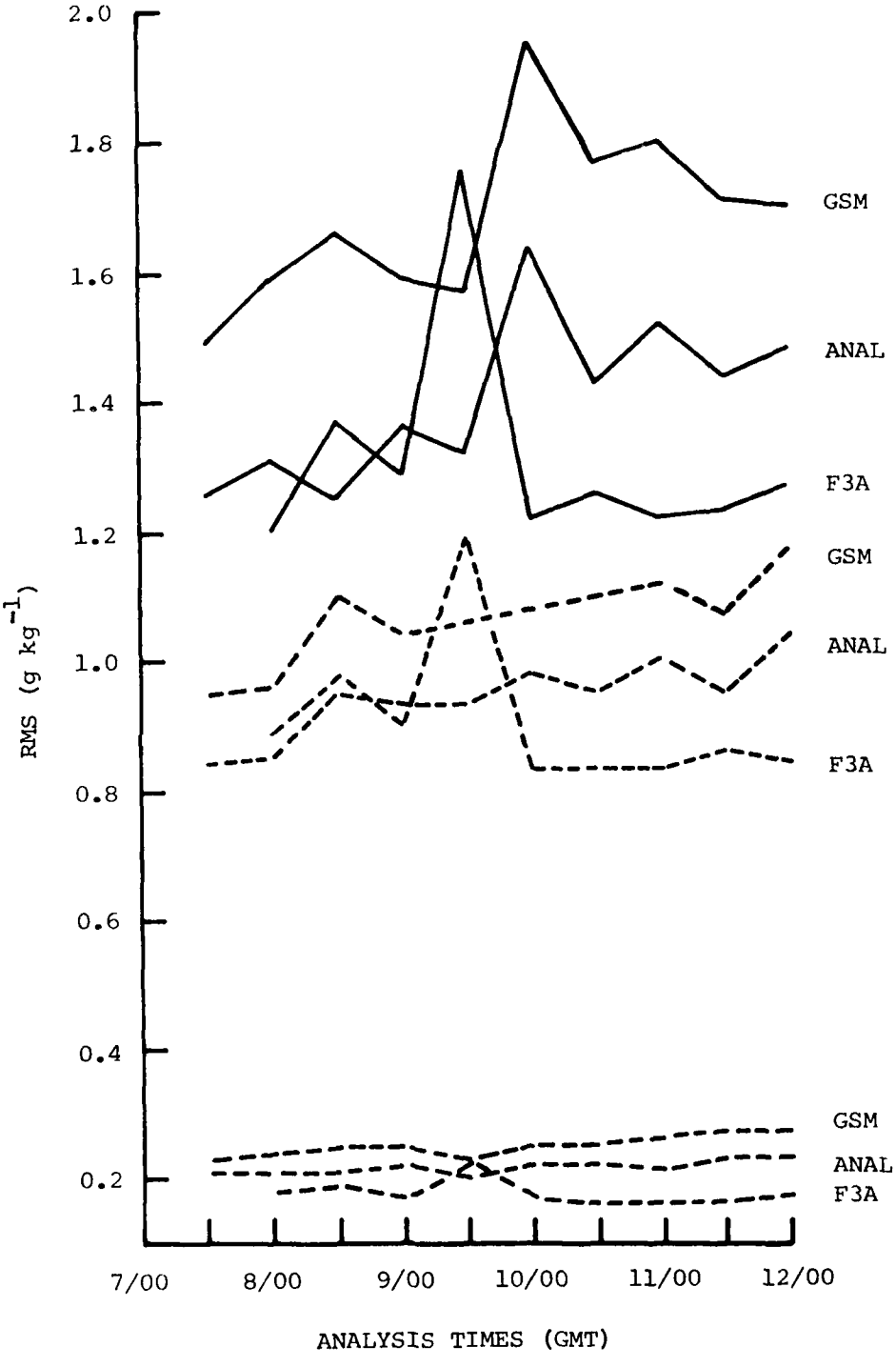

Fig. 3(g). Same as Fig. 3(a) except q at Layer 1 (~960 mb) (top), q at Layer 3 (~725 mb) (middle), and q at Layer 5 (~435 mb) (bottom)

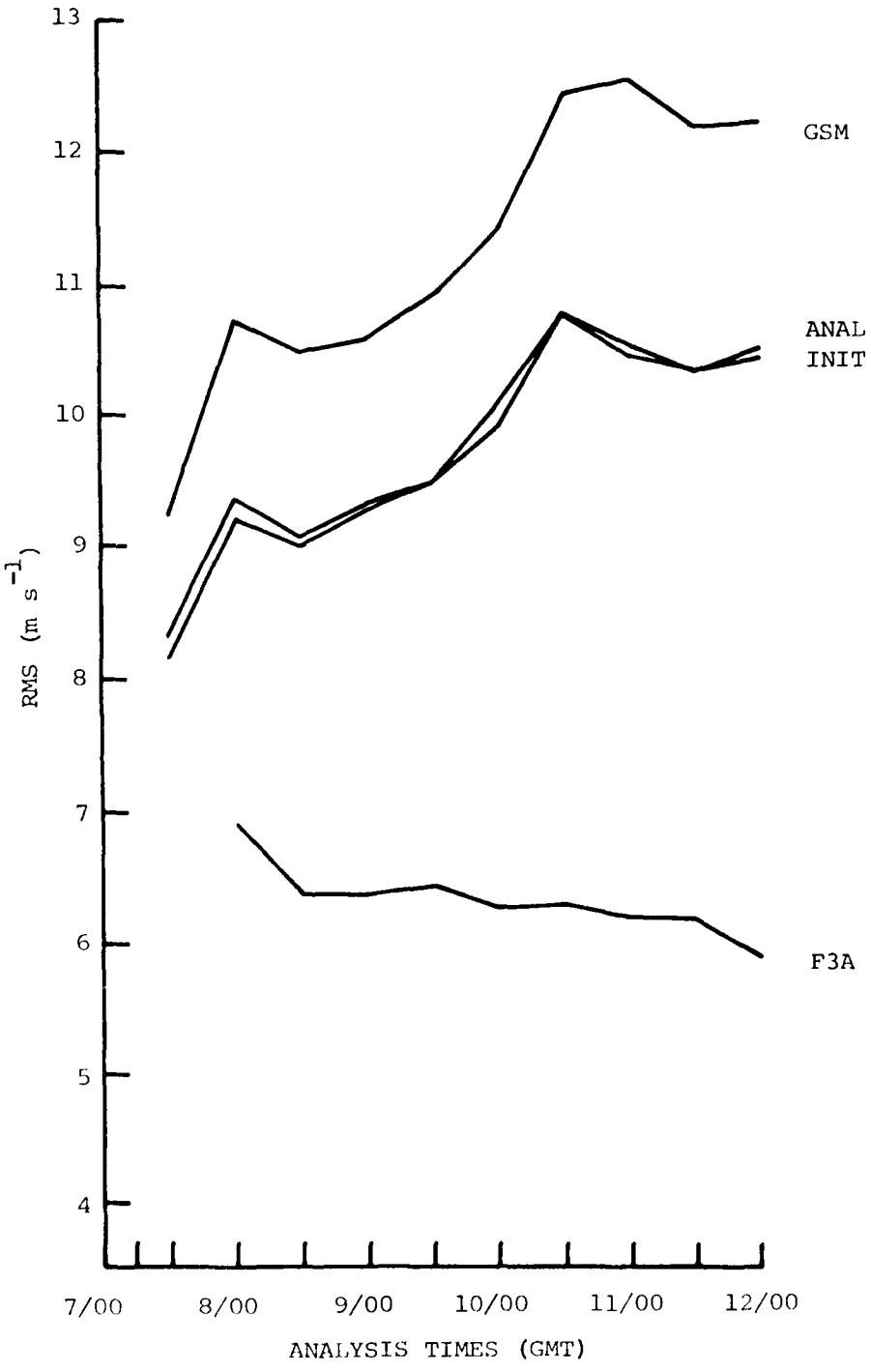

Fig. 3(f). Same as Fig. 3(a) except $\vec{V}$ at Layer 8 (~225 mb)

two possible paths to follow. One can either perform a forecast with the initialized field, thereby ending the cycle, or one can regard the initialized field as a new first guess field and begin the cycle anew. The rationale behind the second path is that by repeated analyses and initializations, one can expect that if convergence occurs, the final fields will be both close to the observations and in a balanced state. Indeed, Williamson and Daley (1983)[18] proposed sequential iterations of OI and initialization for this very reason. In our case, with the model normal modes employed in both the analysis and initialization, one would hope that convergence would be rapid. Because of computational constraints, we were restricted to no more than three iterations per cycle.

To prepare for the iterations, the initialized data in the form of spectral coefficients of divergence, vorticity, temperature, surface pressure, and specific humidity had to be converted into residuals of velocity and the compound function at the observation sites. This involved expanding the spectral coefficients to obtain velocities and heights at the observation sites, subtracting them from the observed data, and then repeating the analysis cycle. When the requisite number of iterations is completed, a forecast is produced immediately after the initialization procedure.

D. Surface Pressure Calculations

Residuals are calculated at the beginning of the cycle by means of the method outlined in Section II of this report. That is, the observed variables are interpolated by means of OI vertical correlation functions to the σ layers of the model. The first guess field is then evaluated at the observation points and subtracted from the observations. However, whereas surface pressure is analyzed separately in Section II of this report, here it is derived from the heights near the surface by a quadratic interpolation. The reason for this is the excessive computer time needed to perform the OI surface pressure analysis, given the vast amount of surface data available. The interpolation also insures that the heights and surface pressure will be

18. Williamson, D. L. and R. Daley, 1983: A unified analysis-initialization technique. Mon. Wea. Rev., 111, 1517-1536.

in dynamic balance, whereas an independent derivation of surface pressure may lead to an inconsistency which would have to be corrected by the initialization.

After the analysis procedure, the residuals of the compound function P are separated into height and surface pressure residuals. The height residuals are then added to the first guess field to form the updated heights. Surface pressure could have been updated the same way (i.e., by adding the analyzed residuals to the first guess surface pressure) but we chose to interpolate the new heights to the surface to form the updated surface pressure field. This is in keeping with NMC's practice where all surface pressures for modeling purposes are prescribed by the upper air height observations.

The σ surfaces are redefined with respect to pressure by the new surface pressure before initialization. As in the ASAP program outlined earlier in this report, the variables carried at the σ layers are interpolated in pressure coordinates to the new σ layers with the assumption that they are linear in $\ln p$ (except for heights, which are redefined as layer temperatures before interpolation). With the variables defined on the new σ layers, initialization can proceed.

E. Run Stream Summary

A review of the programs used in the analysis procedure may be helpful in the understanding of the full cycle. There are 12 individual programs in the current procedure:

1. The global spectral model. The model produces a 12h forecast from a previously analyzed field to serve as the first guess field. Run time: approximately 290 CPU seconds on the Cray.

2. The post-processor. The spectral values of vorticity, divergence, temperature, surface pressure, and moisture are reproduced as velocity, height, surface pressure, and specific humidity on grid space on the σ layers. Run time: 19 CPU seconds.

3. The ASAP residual calculations. OI analysis interpolates observations to σ layers, expands the spectral coefficients of the first guess field at the observation sites, and calculates the residuals of velocities and temperatures. Run time: 345 CPU seconds.

4. Reformation of the residuals. Missing observations are filled by residuals equal to zero so that all levels at an observation site will be filled. Also, grid boxes containing no observations are filled with zeroes at their respective four corners as in HT. Pressure residuals are interpolated from height residuals and residuals of the compound function computed. Run time: 63 CPU seconds.

5. Vertical modes program. At each observation site, the residuals are projected onto eight of the model's vertical modes. Run time: 4 CPU seconds.

6. Analysis program. The projected residuals are analyzed horizontally by sequential fits to the normal mode functions. The results are the coefficients of the normal mode coefficients for all eight vertical modes. Run time: 650 CPU seconds.

7. Evaluation of analysis on grids. The residuals are computed at grid points by expansion of the normal mode functions at the appropriate latitude and longitude. Run time: 68 CPU seconds.

8. Analyzed data on grid. Residuals are added to the first guess values computed at the grid points. The compound function residuals are divided into surface pressure and height residuals. First guess heights are added to each layer and the updated heights interpolated at the surface to produce surface pressure and the new σ structure. The heights are converted to layer temperature by the Flattery method. Run time: 75 CPU seconds.

9. The expansion of grid data. The velocities, temperatures, and surface pressure are converted to spectral coefficients of divergence, vorticity, temperature, and surface pressure. Spectral coefficients of moisture are added from the FGGE III-A analyses, while the fixed spectral coefficients of terrain height are added, as well. Run time: 11 CPU seconds.

10. Initialization. The NMC initialization program is run, resulting in spectral coefficients of vorticity, divergence, temperature, surface pressure, and specific humidity. Run time: 32 CPU seconds. If no iterations are desired, or if the full number of iterations has been completed, the next step is a return to the first program where a new 12h forecast is produced. If the data are to be matched to the initialization by iteration, the following two steps are added:

11. The post-processor. As with program 2, the initialized field is converted to grid point space in terms of velocities and heights for use as the new first guess field. Run time: 8 CPU seconds.

12. Residual recalculation. The observations are now matched with the new first guess field which is expanded at the observation sites. Values of zero are added as before in data void areas and at missing layers. Surface pressure and height residuals are combined as compound variable residuals. Run time: 380 CPU seconds. From here, one returns to program 5 to repeat the cycle.

F. Results

Table 6 compares analyses from the non-iterative experiments with model forecasts and with the analyses after initialization. It is the counterpart to Table 2 of Section II, except that wind components are separated, all 12 levels are included, and only four dates are available. The large errors at the highest levels led us to believe that extrapolation by the Flattery scheme, as indicated in Section II, p. 11, was a principal source of error in the analysis. Indeed, the large error seems to propagate downward over the course of the four analysis periods. In a subsequent experiment where the upper level temperatures were replaced by first guess temperatures rather than extrapolated temperatures, errors at the top were smaller, but errors in lower layers were unaffected for the most part.

There are other important conclusions one may draw from Table 6 when contrasted with Table 2. First, the differences between the forecasts and the analyses are almost always greater here than they are in Table 2. One could view this as proof that our analysis has a greater effect on the first guess field than an OI analysis does. On the other hand, it could be an indication of poorer forecasts resulting from this analysis. Second, the change produced by the initialization is relatively less for this analysis than for the OI analysis, especially for surface pressure and heights of the upper σ levels. This can be understood in light of the OI treatment of surface pressure and the use of nmf for our analysis. In Section II the surface pressure analysis was described in detail as a completely independent analysis, as opposed to our derivation of pressure as an interpolation (extrapolation) from heights at the lower σ layers. This means

Table 6. RMS Differences at Grid Points between Forecast and Analysis (F-A), Forecast and Initialized Field (F-I), and Initialized Field and Analysis (I-A) for Heights (Z) at All 12 Levels and for the Two Components of Velocity (U,V) at All 12 Layers (Surface Pressure (PS) for the Four Analysis Times Also Appears at the Bottom)

			1	2	3	4	5	6	7	8	9	10	11	12
		Z	3.21	9.32	15.84	17.74	22.37	27.72	30 27	31.47	32.31	38.92	86.53	1020.01
	8 00Z	U	2.25	2.12	2.00	2.31	2.70	3.03	3.22	3.37	3.17	2.88	2.44	2.24
		V	3.76	3.51	3.41	4.10	5.21	5.97	6.20	6.17	5.81	5.08	4.62	5.35
		Z	1.53	3.32	8.04	15.48	24.31	29.76	32.61	33.93	33.32	39.74	94.15	1125.43
	8 12Z	U	2.10	2.04	1.93	2.04	2.36	2.75	3.01	3.18	3.25	2.94	2.68	2.74
		V	3.40	2.98	2.72	3.14	3.98	4.55	4.70	4.79	4.62	4.16	3.78	4.51
F-A		Z	1.51	3.72	8.80	15.98	24.24	29.52	32.19	33.67	34.34	42.32	105.49	1246.72
	9 00Z	U	2.19	2.17	2.02	2.16	2.58	3.04	3.28	3.40	3.26	2.97	2.89	3.32
		V	3.25	2.86	2.64	2.96	3.60	4.04	4.35	4.65	4.56	4.24	4.00	4.78
		Z	1.92	5.29	10.98	16.92	23.38	27.13	28.37	28.91	30.42	44.16	118.65	1378.53
	9 12Z	U	2.08	2.01	1.99	2.16	2.52	2.84	3.01	3.07	2.98	2.89	2.90	4.07
		V	3.35	2.94	2.75	3.03	3.64	4.25	4.58	4.72	4.57	4.48	4.48	5.31
		Z	3.26	9.52	16.26	18.45	23.90	30.17	33.19	34.38	35.71	42.97	90.89	1026.46
	8 00Z	U	2.30	2.13	2.04	2.40	2.91	3.25	3.44	3.54	3.20	2.89	2.61	2.63
		V	3.05	2.76	2.60	3.10	3.72	3.90	3.84	3.84	3.79	3.60	3.57	3.26
		Z	1.54	3.31	7.76	14.52	22.58	27.49	30.04	31.26	31.31	39.96	97.41	1130.13
	8 12Z	U	1.97	1.89	1.78	1.97	2.38	2.73	2.94	3.08	3.10	2.81	2.08	2.55
		V	2.62	2.20	2.01	2.28	2.75	2.94	2.88	3.10	3.13	2.93	2.87	2.58
F-I		Z	1.53	3.64	8.27	14.56	21.62	25.95	28.10	29.19	29.78	39.84	106.23	1250.50
	9 00Z	U	2.02	1.95	1.74	1.89	2.38	2.83	3.00	3.02	2.80	2.65	2.60	2.85
		V	2.54	2.17	1.99	2.22	2.53	2.60	2.72	3.06	3.10	2.97	3.00	3.06
		Z	1.90	5.05	10.06	14.60	19.56	22.84	24.53	26.02	28.56	44.33	119.41	1380.42
	9 12Z	U	1.98	1.81	1.76	1.92	2.28	2.58	2.75	2.85	2.73	2.68	2.63	3.12
		V	2.66	2.23	2.07	2.28	2.53	2.72	2.84	3.08	3.15	3.29	3.39	3.31

I-A

			1	2	3	4	5	6	7	8	9	10	11	12
8 00Z	Z	0.65	2.00	4.51	8.84	14.31	18.79	21.75	23.66	24.46	25.46	30.45	79.58
	U	1.41	1.44	1.45	1.45	1.52	1.68	1.82	1.87	1.79	1.65	1.54	1.99
	V	1.87	1.90	1.91	2.00	2.42	3.05	3.48	3.58	3.21	2.61	2.44	3.36
8 12Z	Z	0.58	1.69	3.72	7.26	11.78	15.47	17.85	19.24	19.58	20.15	26.23	75.54
	U	1.22	1.24	1.23	1.20	1.24	1.39	1.54	1.59	1.50	1.37	1.30	1.85
	V	1.76	1.78	1.73	1.70	2.02	2.63	3.07	3.20	2.93	2.60	2.43	3.26
9 00Z	Z	0.57	1.66	3.61	7.03	11.42	15.04	17.44	19.02	19.90	21.31	27.68	83.79
	U	1.32	1.35	1.35	1.32	1.37	1.51	1.63	1.67	1.57	1.50	1.51	2.29
	V	1.75	1.76	1.72	1.70	2.03	2.63	3.07	3.22	3.03	2.87	2.68	3.67
9 12Z	Z	1.58	1.73	3.85	7.54	12.15	15.74	17.92	19.05	19.42	21.15	31.86	104.68
	U	1.26	1.28	1.29	1.29	1.36	1.51	1.62	1.64	1.50	1.39	1.50	2.71
	V	1.72	1.74	1.69	1.68	2.06	2.70	3.12	3.22	2.92	2.81	2.89	4.20

PS

	8 00Z	8 12Z	9 00Z	9 12Z
F-A	4.77	4.95	5.24	5.54
F-I	4.67	4.77	4.91	5.22
I-A	2.97	2.65	2.62	2.69

that the gross atmospheric mass structure as depicted by the upper air analysis will not necessarily be in dynamic balance with the surface analysis of Section II. In an attempt to balance the atmospheric structure, the initialization will quickly change the surface pressure to be in harmony with the upper air mass structure. Indeed, the initialization procedure combines heights and pressures into one variable before adjusting the gravity waves. Because the overall structure of the atmosphere is mostly defined by the first guess, with the OI performing some minor adjustments, the initialization procedure will substantially alter the pressure analysis imposed by the surface OI and substitute a field close to the first guess. With our analysis, changes are made to the large scale structure by expansion in nmf. Thus, when NLNMI takes place, there is no tendency to draw the analysis back to the first guess field.

Figs. 4 and 5 are counterparts to Figs. 1 and 2 from Section II. Shown are the rms errors of forecast, analysis, or initialized field against observations for the five dates of this study (six dates if one includes the final forecast for 1/10/79 00Z) at layers 2, 4, and 8 for the east-west component of velocity and levels 2, 4, and 8 for heights. Vertical axis resolution varies from figure to figure to ease comparisons. Figs. 4 (a-f) are for observations retained after checking with FGGE III-A values as a basis for verification. Figs. 5 (a-f) use the analysis as a basis. Many of the figures indicate that the forecast sometimes is closer to the observations than the analysis or the initialized field for the same time. This is particularly true at the higher levels and more clearly for velocities than heights. At the upper levels, this may be caused by contamination from the highest level due to the Flattery scheme. At lower levels, the error growth is almost as large as if no update occurred at all. For comparison, Table 4 of Section II displays 48h forecast errors verifying at 1/11/79 00Z. Taking into consideration the differences in levels displayed for heights and the vector wind error versus the component wind, one finds that the model forecast errors are fairly close to the error incurred by our assimilation cycle. This would seem to indicate that not enough weight is being given to the observed values. Thus, despite the fact that the analyses do somewhat alter the first guess fields as is evident from the figures, their impact is not sufficient to draw the fields closer to the observations. Although it was thought beneficial to filter the observations through expansion in nmf, it is probable

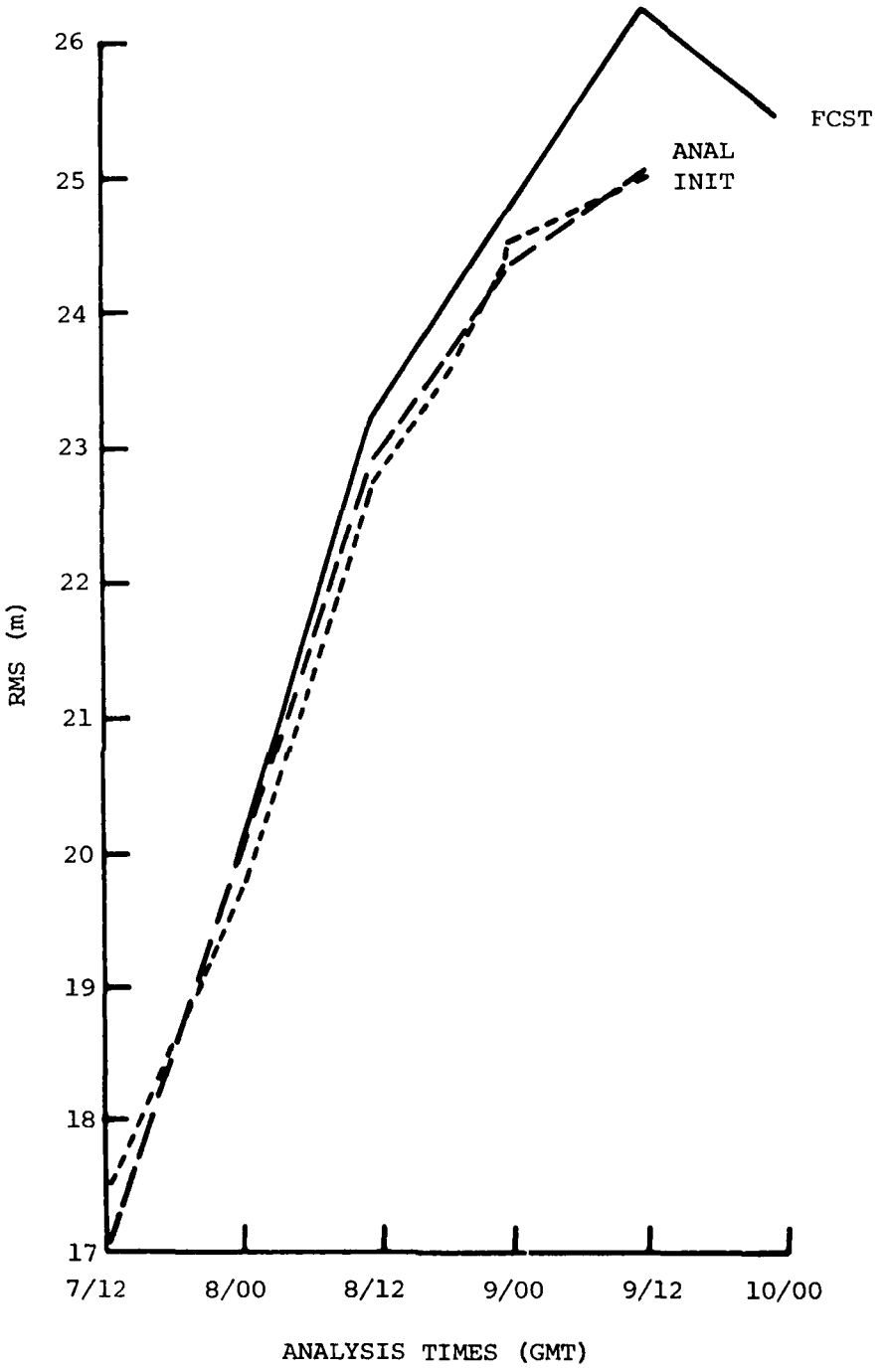

Fig. 4(a). RMS Differences as a Function of Time between the Analysis (long dash), Initialized Data (short dash) or Forecast (solid line) and Observations with FGGE III-A as a Background Criterion for Retention, for Z at Level 2

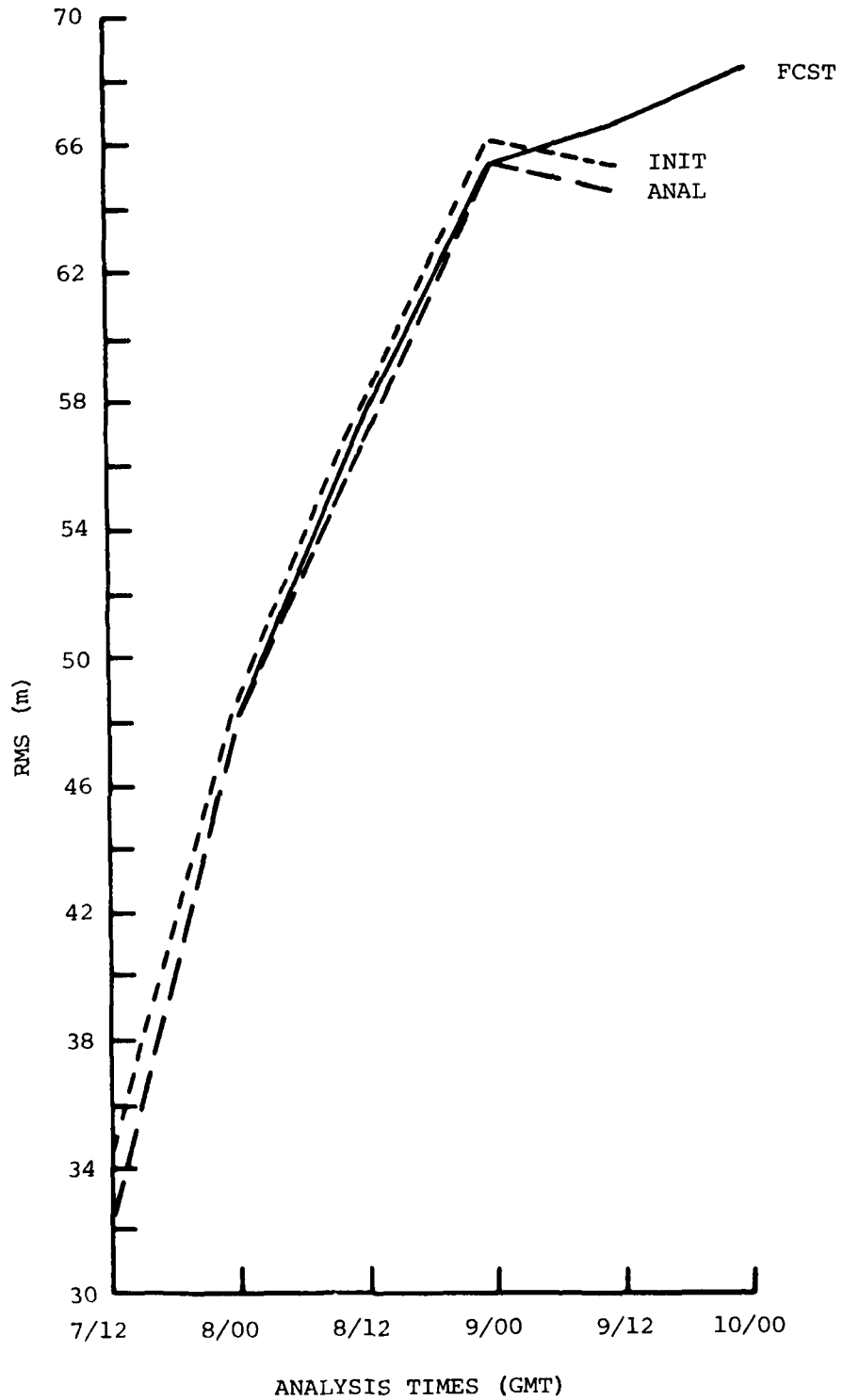

Fig. 4(b). Same as Fig. 4(a) except for Z at Level 4

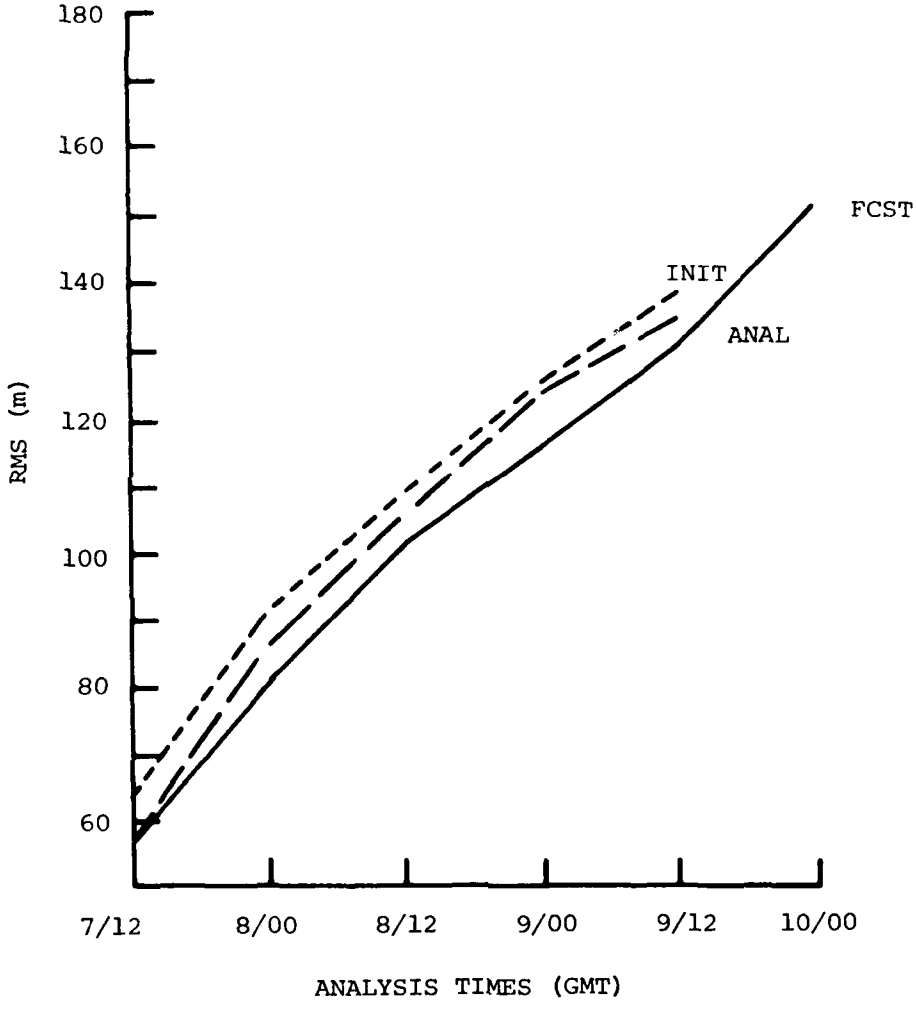

Fig. 4(c). Same as Fig. 4(a) except for Z at Level 8

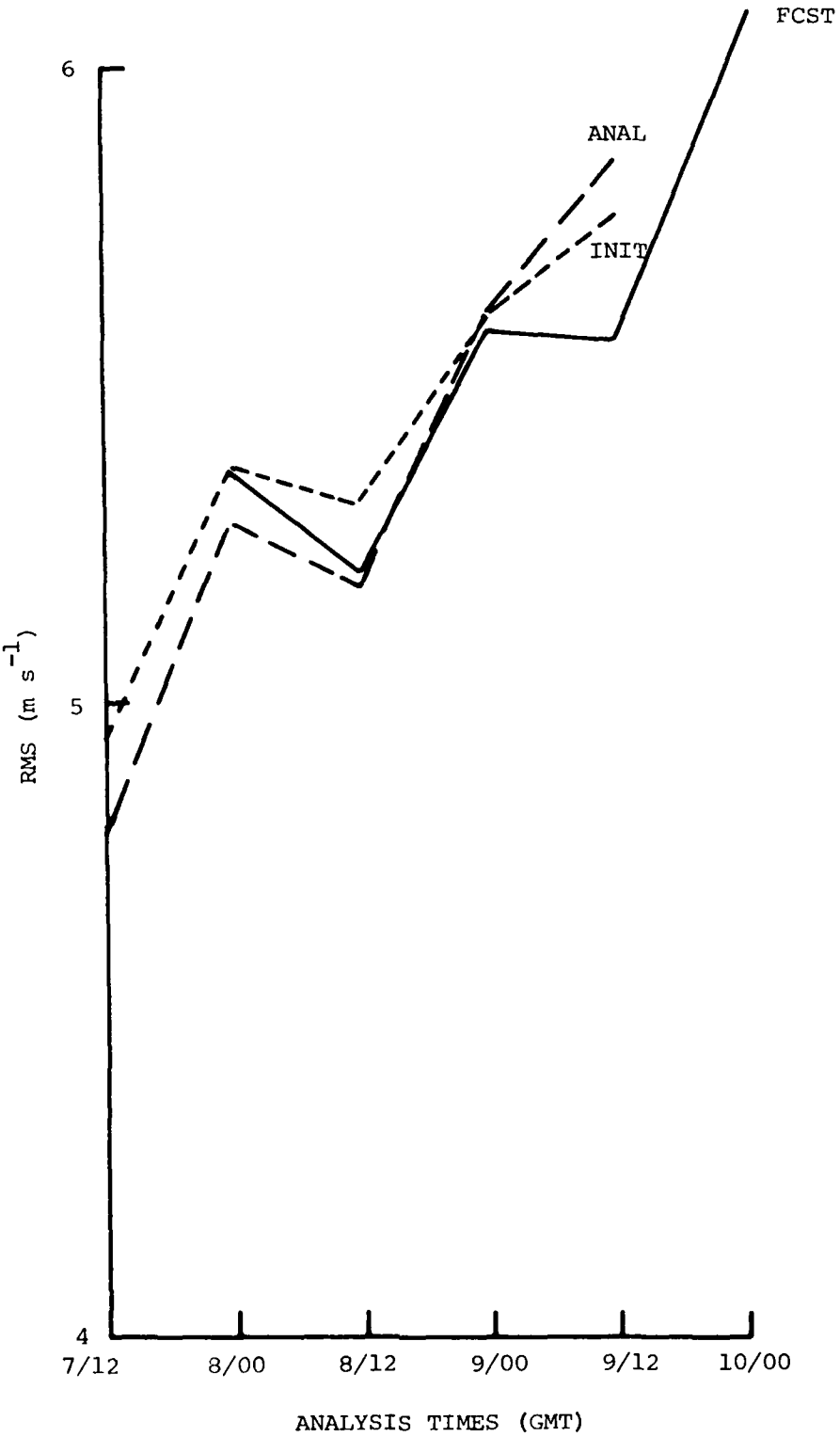

Fig. 4(d). Same as Fig. 4(a) except for the East-West Component of $\vec{V}$ at Layer 2

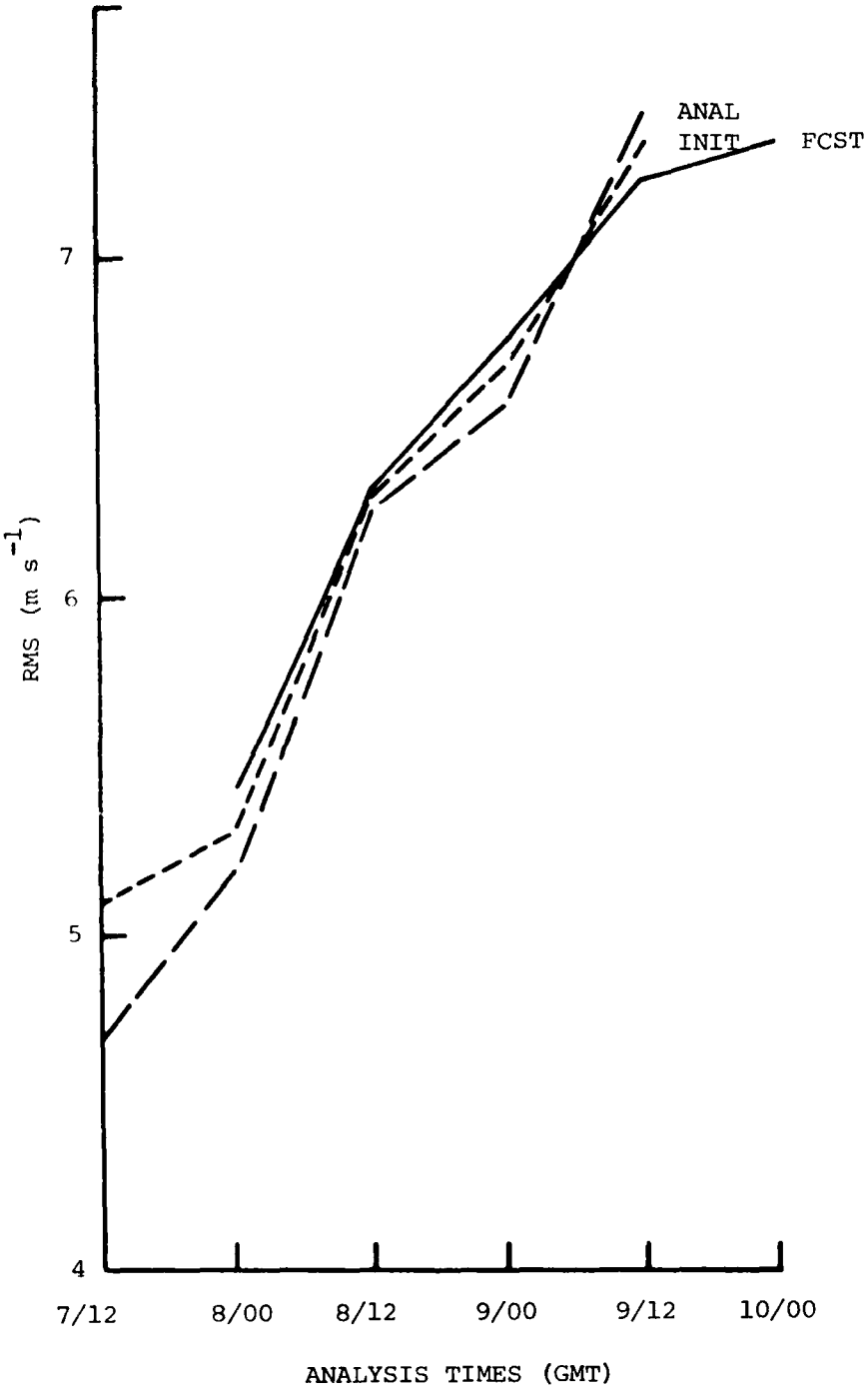

Fig. 4(e). Same as Fig. 4(a) except for the East-West Component of $\vec{V}$ at Layer 4

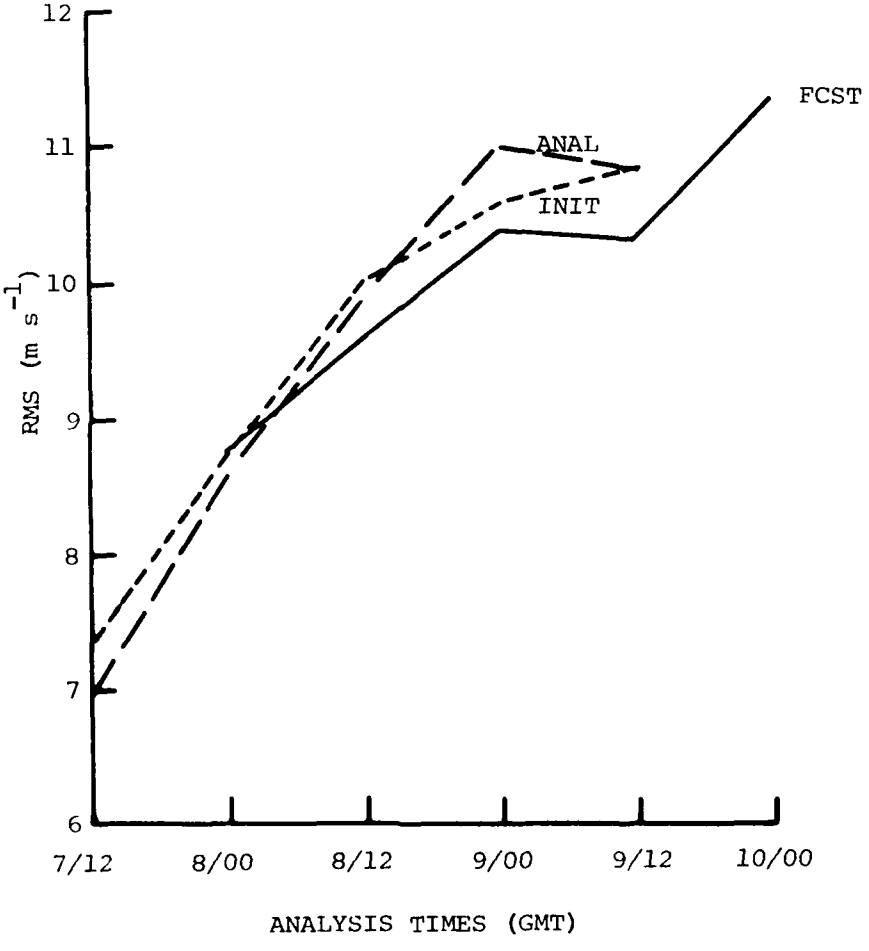

Fig. 4(f). Same as Fig. 4(a) except for the East-West Component of $\vec{V}$ at Layer 8

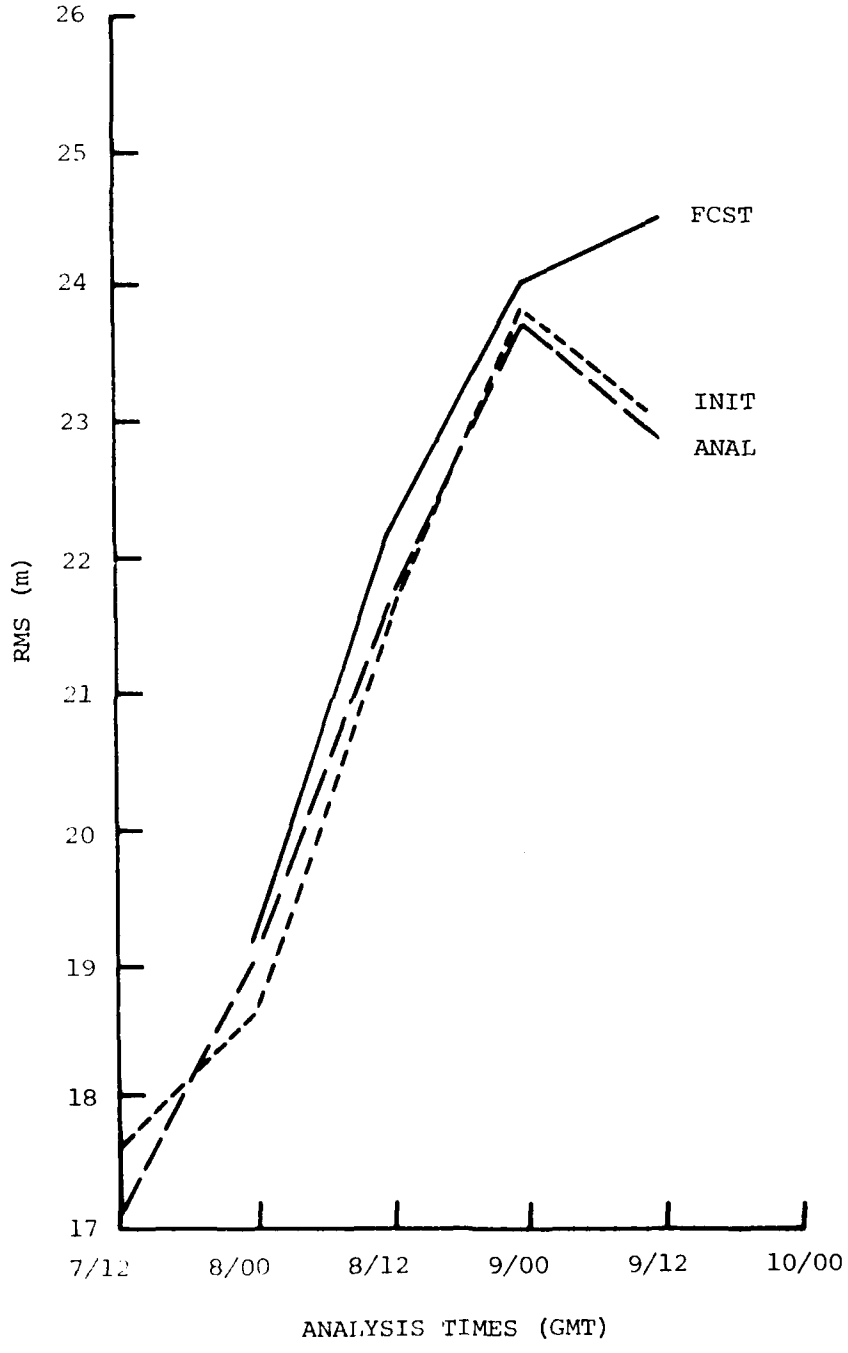

Fig. 5(a). Same as Fig. 4(a) except the Analysis Is Used as the Basis for Retention of Observations

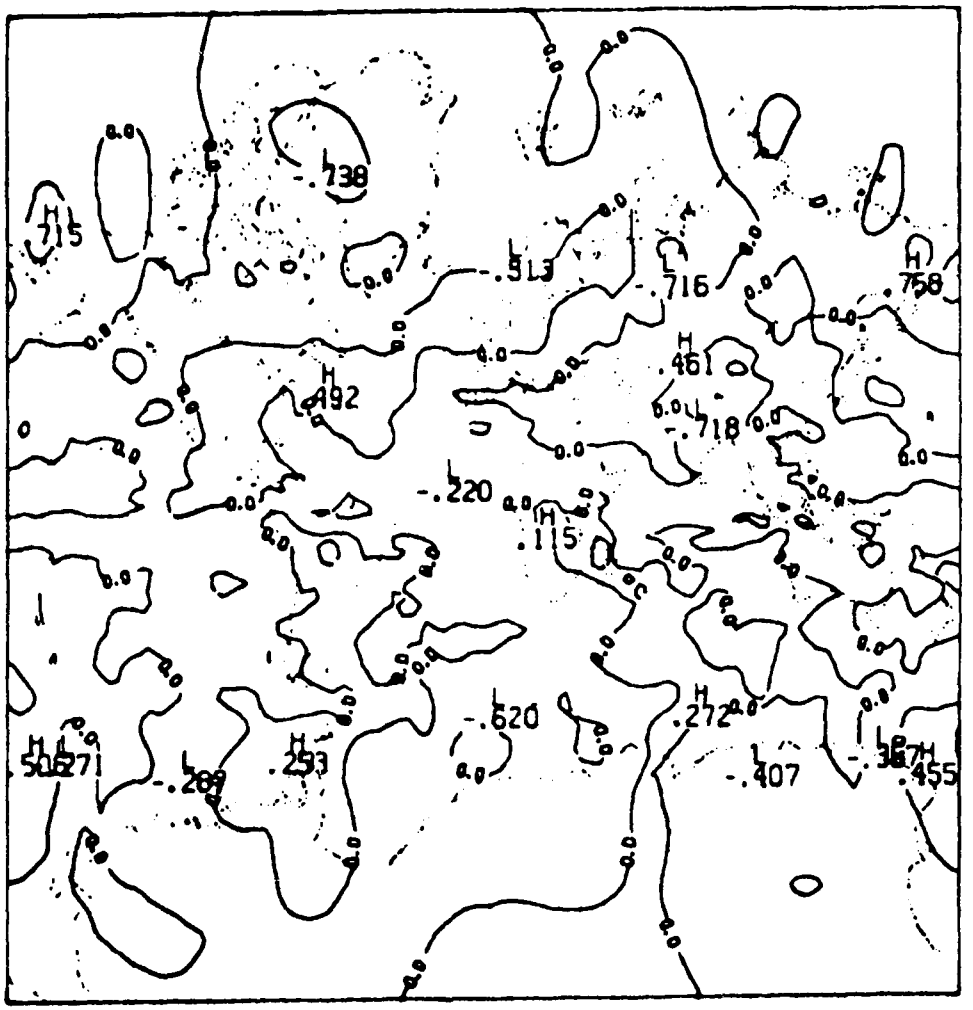

Fig. 7(a). Difference Contours between the Forecast and Analyzed Height Field for 1/8/79 00Z at Level 4 (Contour Interval is 60 m, Labels Are in Hectameters)

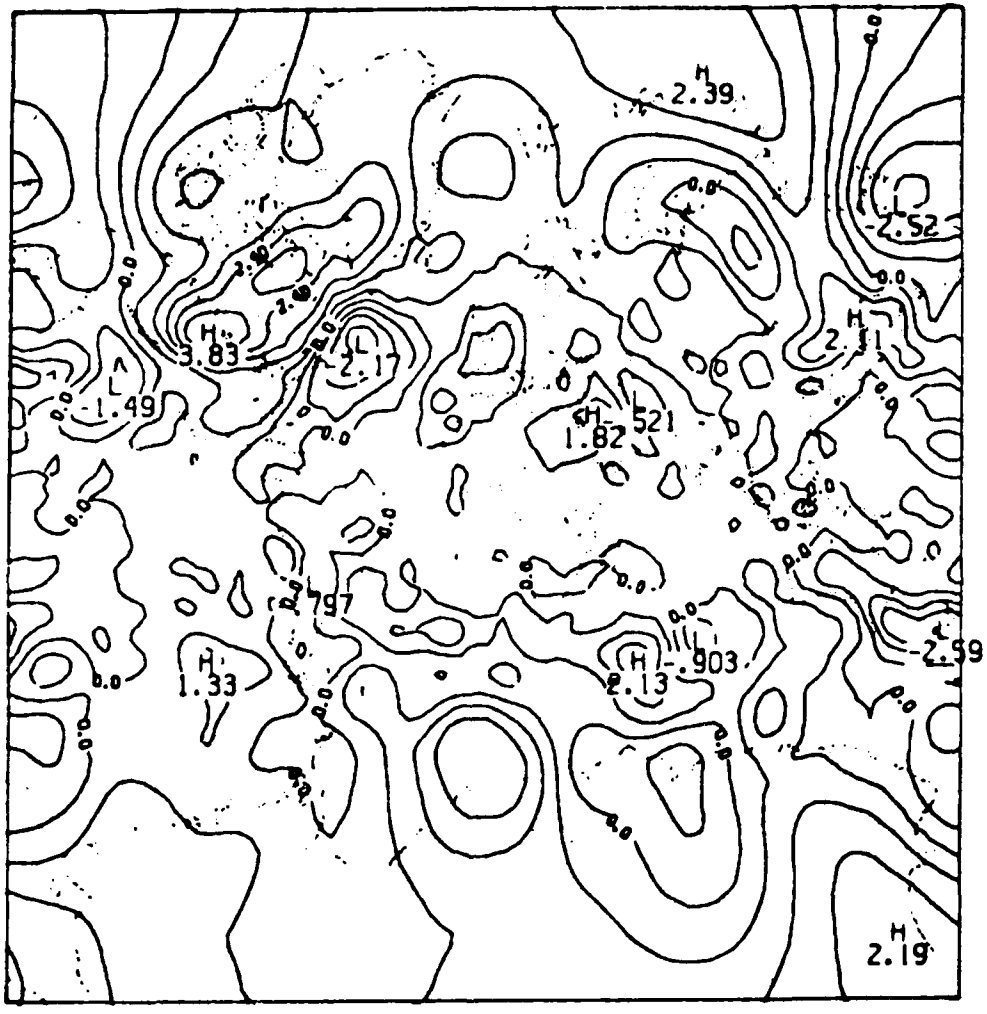

Fig. 6(e). Difference Contours between the Forecast and FGGE III-A Height Field for 1/10/79 00Z at Level 4 (Contour Interval is 60 m, Labels Are in Hectameters)

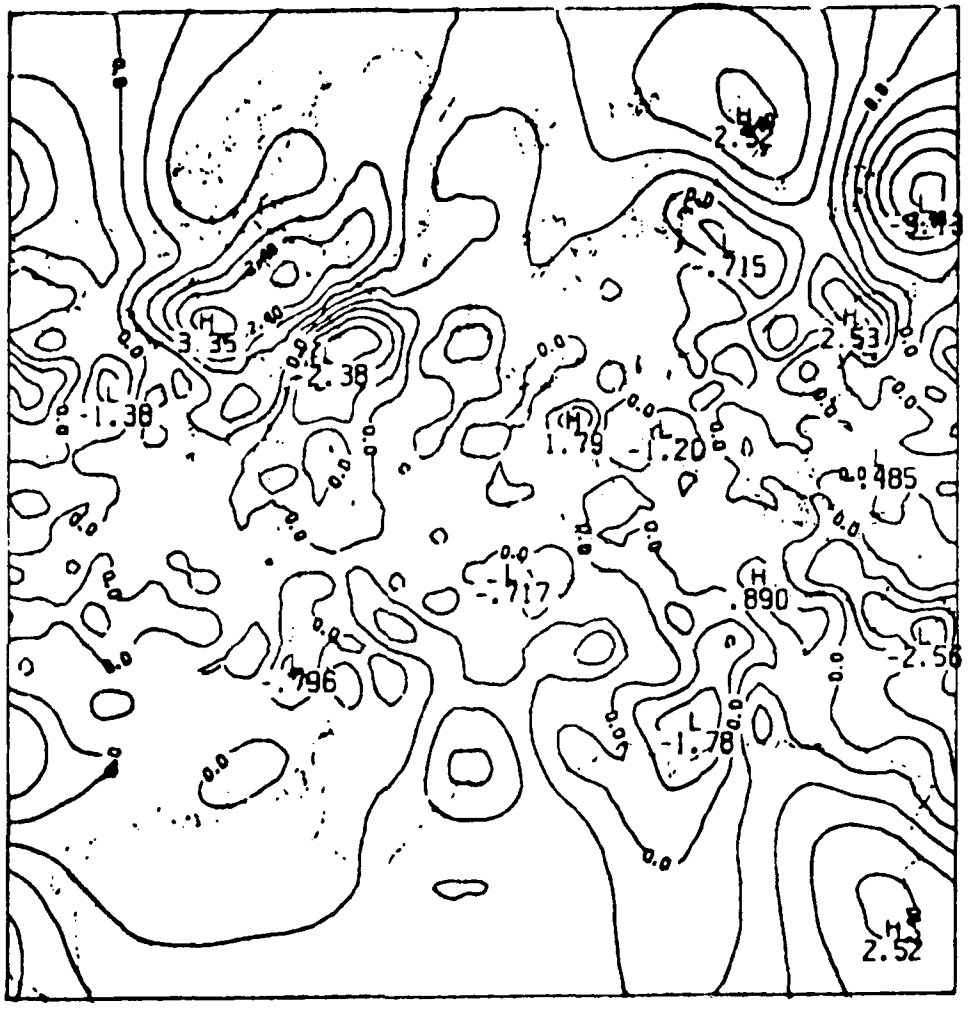

Fig. 6(d). Difference Contours between the Forecast and FGGE III-A Height Field for 1/9/79 12Z (Contour Interval is 60 m, Labels Are in Hectameters)

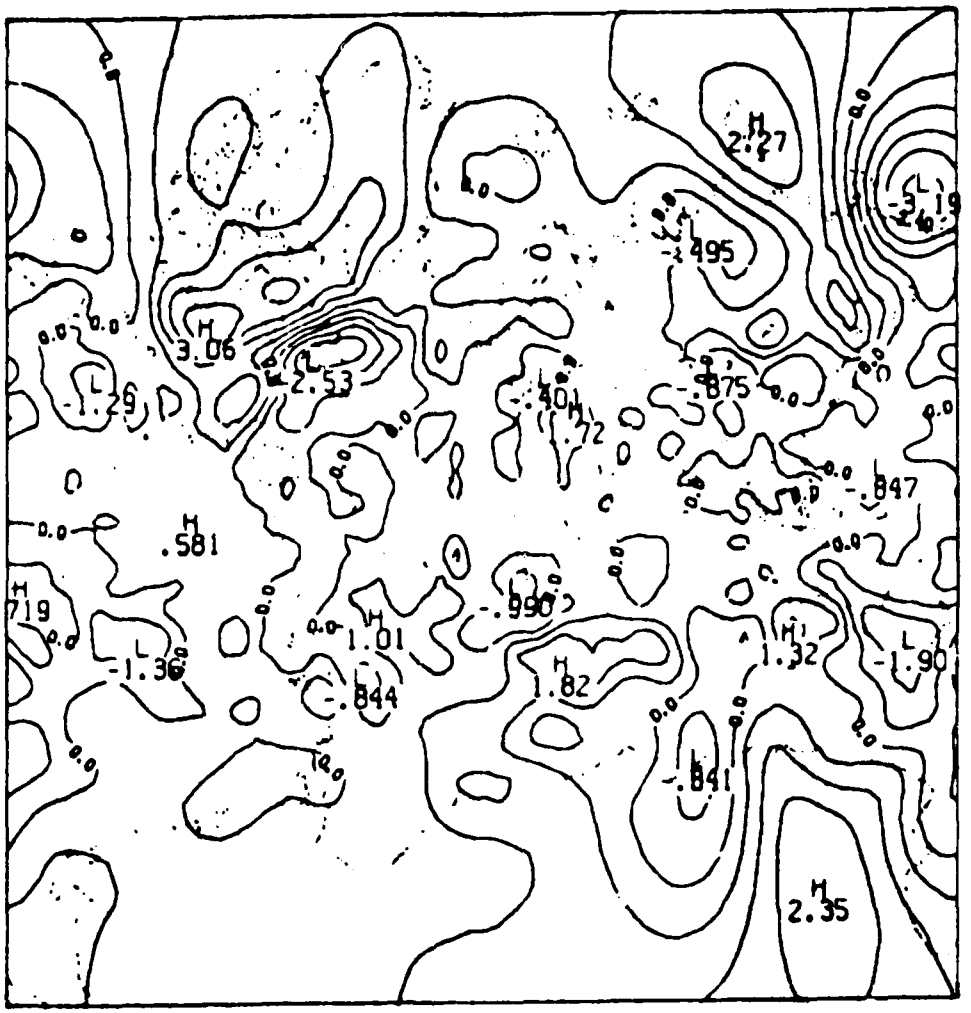

Fig. 6(c). Difference Contours between the Forecast and FGGE III-A Height Field for 1/9/79 00Z at Level 4 (Contour Interval is 60 m, Labels Are in Hectameters)

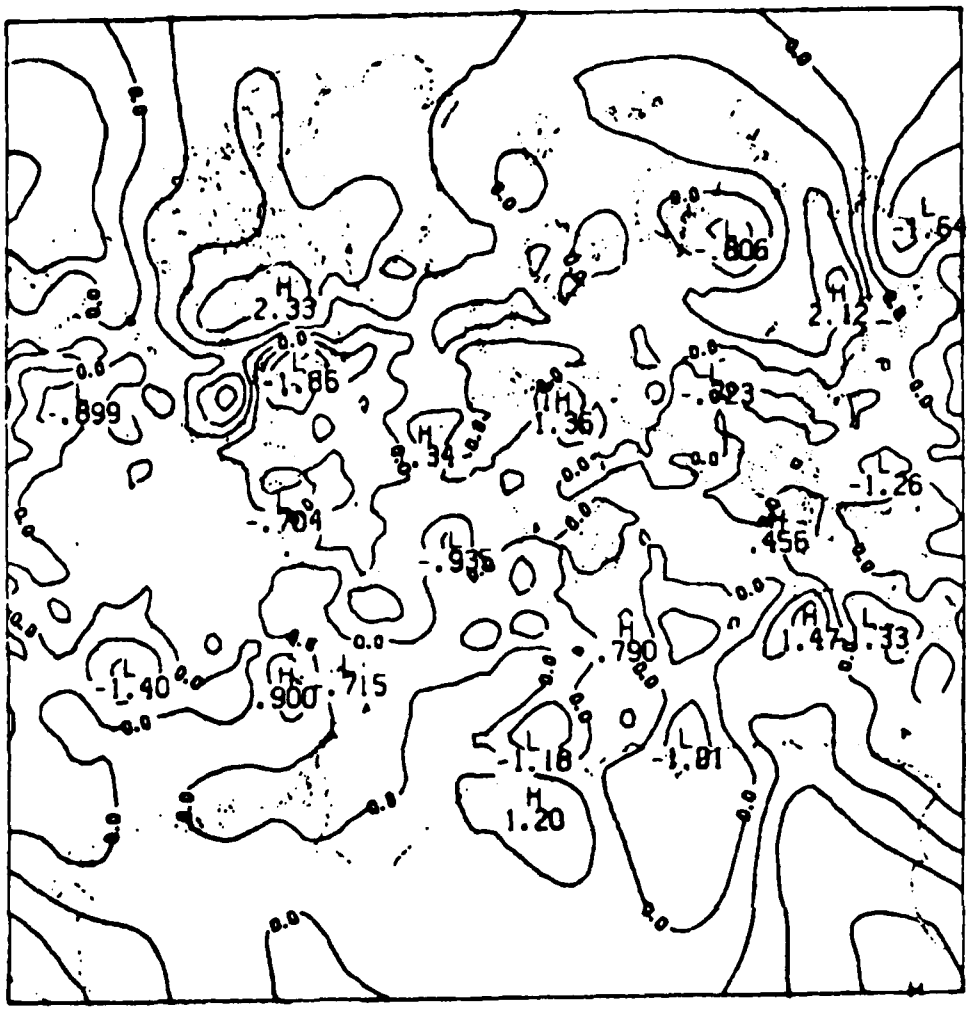

Fig. 6(b). Difference Contours between the Forecast and FGGE III-A Height Field for 1/8/79 12Z at Level 4 (Contour Interval is 60 m, Labels Are in Hectameters)

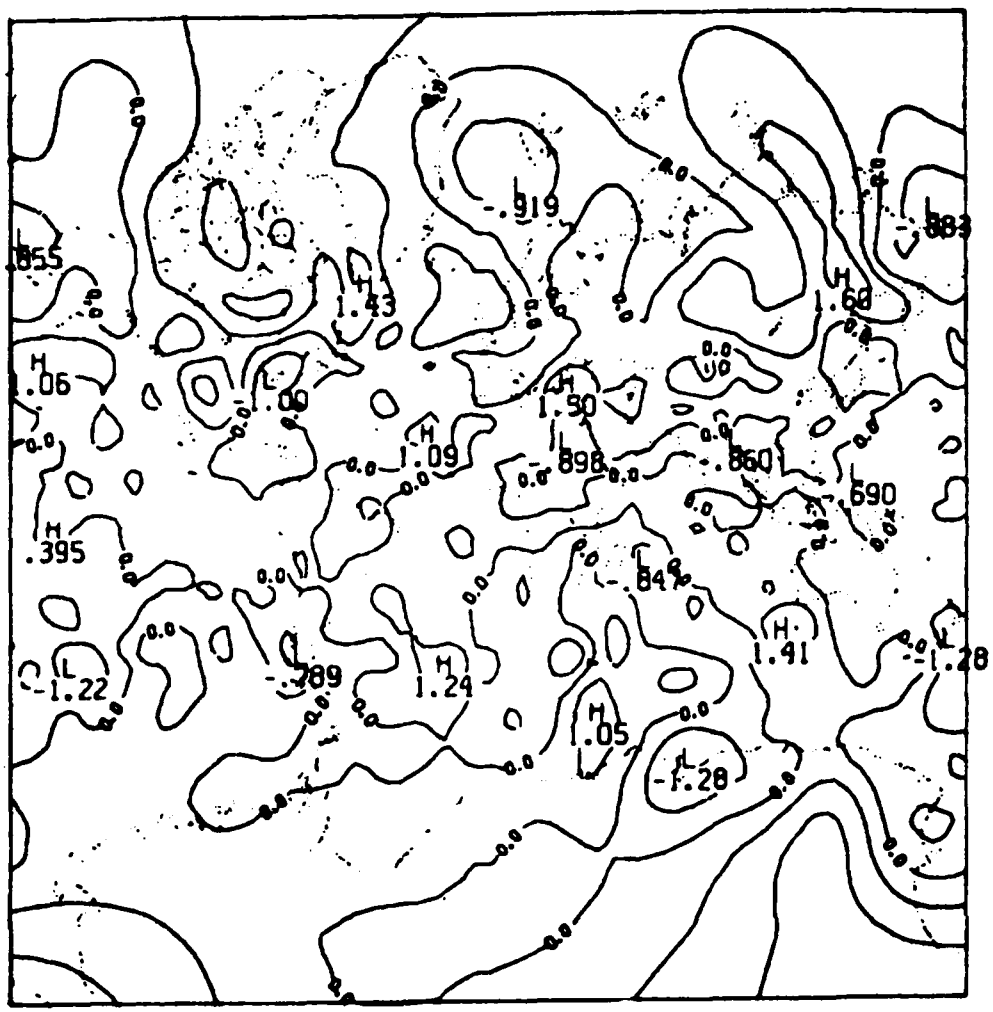

Fig. 6(a). Difference Contours between the Forecast and FGGE III-A Height Field for 1/8/79 00Z at Level 4 (Contour Interval is 60 m, Labels Are in Hectameters)

situation, and the forecast based on the last iteration was far inferior to the forecast based on only one iteration.

There are several possible explanations for the non-convergence of the iterative process. The simplest is that the procedure is by nature divergent. This would result from either the analysis or the initialization furthering the solution from the data or slow manifold rather than bringing it closer. In an earlier test with just the external vertical mode of Hough functions, this did not seem to occur. In fact, the process was seen to converge. In our current procedure, however, the analysis and initialization did not appreciably draw the first guess closer to the observations, as is obvious from Fig. 5, where, in some cases, the analysis and initialization actually widen the gap between the first guess and the observations. When this procedure was repeated, it merely reinforced the departure from observations. It is also possible that the introduction of higher frequencies, just as with the Machenhauer scheme in the initialization procedure, can cause a divergence in the solution. Another obvious source of error is the Flattery scheme and its attendant extrapolation at the top of the atmosphere. But this error was restricted to the uppermost levels, as was discovered when the uppermost temperatures were replaced by first guess temperatures and divergence still occurred. There is still the distinct possibility that a coding error exists, especially in the recalculation of the residuals in program 12 of Subsection E above. A few extra tests are necessary in order to locate the source of the growing errors and to correct them. These have not been possible to date because of budget considerations.

Figs. 6 (a-e) show the contoured differences between the five forecast heights and the FGGE III-A height fields at level 4 for 1/8/79 00Z, 1/8/79 12Z, 1/9/79 00Z, 1/9/79 12Z, and 1/10/79 00Z, respectively. The contour interval is 60 m and the labels are in hectameters. As can be seen there are several areas where departures between the two fields become quite large during the five sequences. Noteworthy are the departures near the US East Coast, the US Rockies, and Eastern Siberia. The differences do not grow continuously and seem to drop off during the last forecast period.

Figs. 7 (a-d) are contours of differences between the forecast heights at level 4 and our analyzed heights at the same level from 1/8/79 00Z through 1/9/79 12Z, respectively. These may be viewed as adjustments made to the first guess field by our analysis, rather than as a verification

Table 7. RMS Differences between Analyzed Heights (m) at 12 Levels or Velocity Components (ms^{-1}) at 12 Layers and Observations for the Second and Third Iterations of the Analysis Procedure, with FGGE III-A Serving as a Background Check for Validation of Observations

		Level											
		1	2	3	4	5	6	7	8	9	10	11	12
2nd	Z	13.13	23.19	39.74	55.78	77.88	93.42	101.86	107.27	113.58	128.57	254.33	219.01
itera-	U	5.52	5.72	5.68	6.16	7.99	9.33	10.36	10.17	9.80	8.14	8.11	12.44
tion	V	5.23	6.40	6.45	8.35	10.69	12.80	13.50	13.59	11.47	9.60	8.25	8.54
3rd	Z	13.41	27.64	50.75	72.51	101.96	122.98	132.67	138.79	145.75	163.04	324.63	285.12
itera	U	6.35	6.33	6.45	7.43	9.88	11.83	13.21	12.85	12.22	10.11	11.13	13.38
tion	V	5.69	6.55	6.60	8.61	10.92	13.13	14.00	14.03	11.98	10.09	9.60	9.27

that too much filtering occurred and the influence of the observations was lost. This may have occurred because: 1. there are too many data void areas where zero residuals were inserted, 2. there were no weights given to the observations over the first guess field, or 3. the sequential calculation of coefficients has a tendency to damp the wave amplitudes resulting in oversmoothing, as mentioned by HT. In fact, the lack of impact may be a result of a combination of all three reasons and further experimentation is required to determine and correct the precise cause of the problem. Indeed, the iterative experiments could have rectified some of the problems but they, too, failed.

The main goal of the iterative scheme is to draw the analysis closer to the observations while maintaining the large scale aspects of the analysis. The iterations are akin to those proposed by Williamson and Daley (1983)[18], who demonstrated the effects of repeating OI analyses and an initialization procedure. The expectation is that by alternating between an OI which maintains geostrophic balance and an initialization which corrects the gravity wave components, an equilibrium will be reached such that the final analysis will be in balance with respect to the model and yet close to the observed data. Our attempt to perform this type of iteration is based on the same reasoning, except that instead of an OI analysis, our analysis scheme, using only the large scale nmf as interpolation media, is substituted. The large scale nmf would keep the Rossby modes and lower frequency gravity modes intact while approximating the data. The initialization procedure would then adjust the higher frequency gravity modes to return the fields to balance on the "slow" manifold. Eventually the iteration would hopefully converge on the ideal intersection of the "data" manifold and the "slow" manifold as depicted by Williamson and Daley (1983). Unfortunately, our iterative cycle did not converge at all. Table 7 compares rms errors of the analyzed fields versus observations for heights and the east-west component of velocity for iterations 2 and 3 with FGGE III-A data as a basis for the checking procedure. The iterations were performed for the 1/8/79 00Z fields and can be compared with the first iteration depicted in Figs. 4 (a-f). As is readily seen, there is a definite divergence of the iterative process with observed values departing from the analyzed values. Subsequent initialization did not do much to improve the

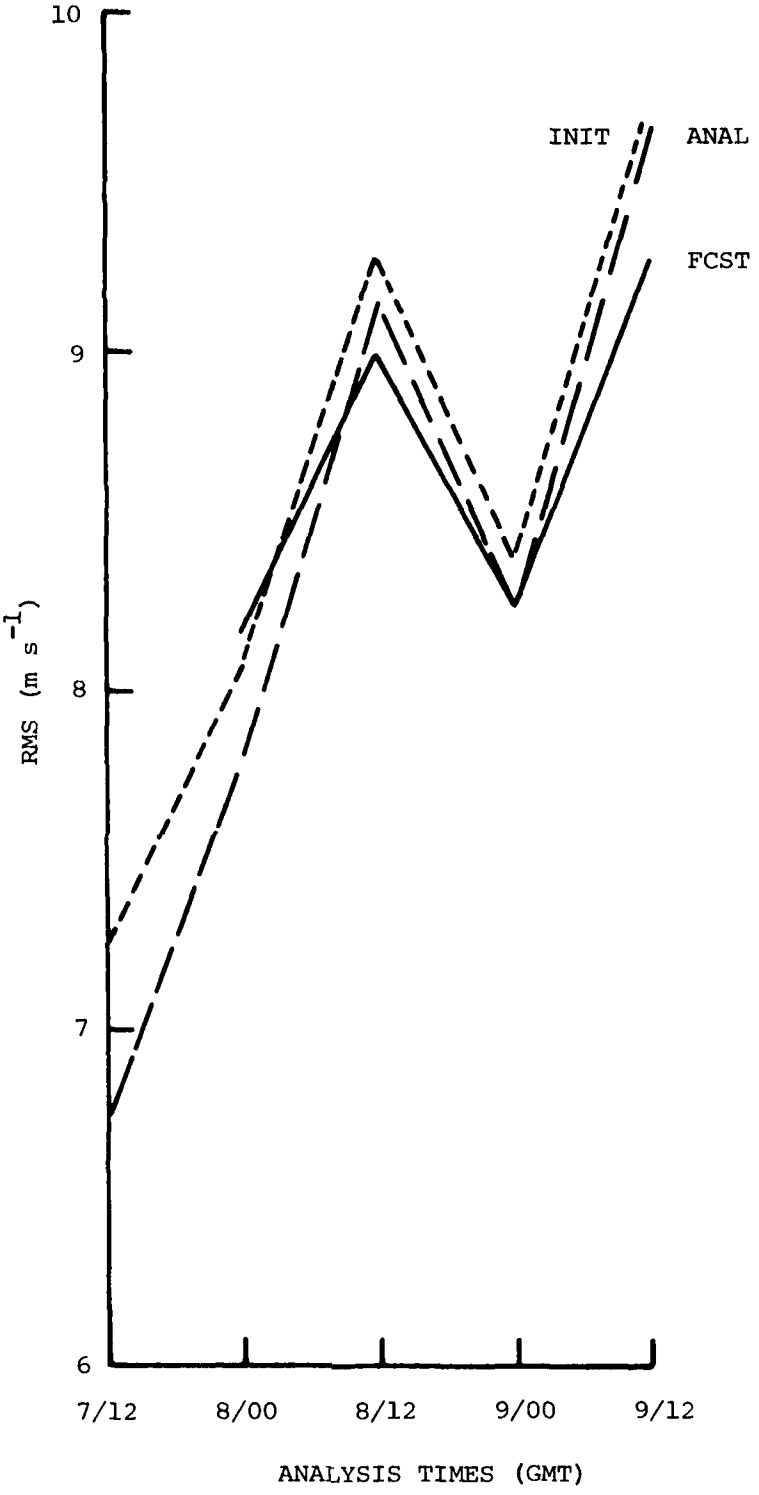

Fig. 5(f). Same as Fig. 4(f) except the Analysis Is Used as the Basis for Retention of Observations

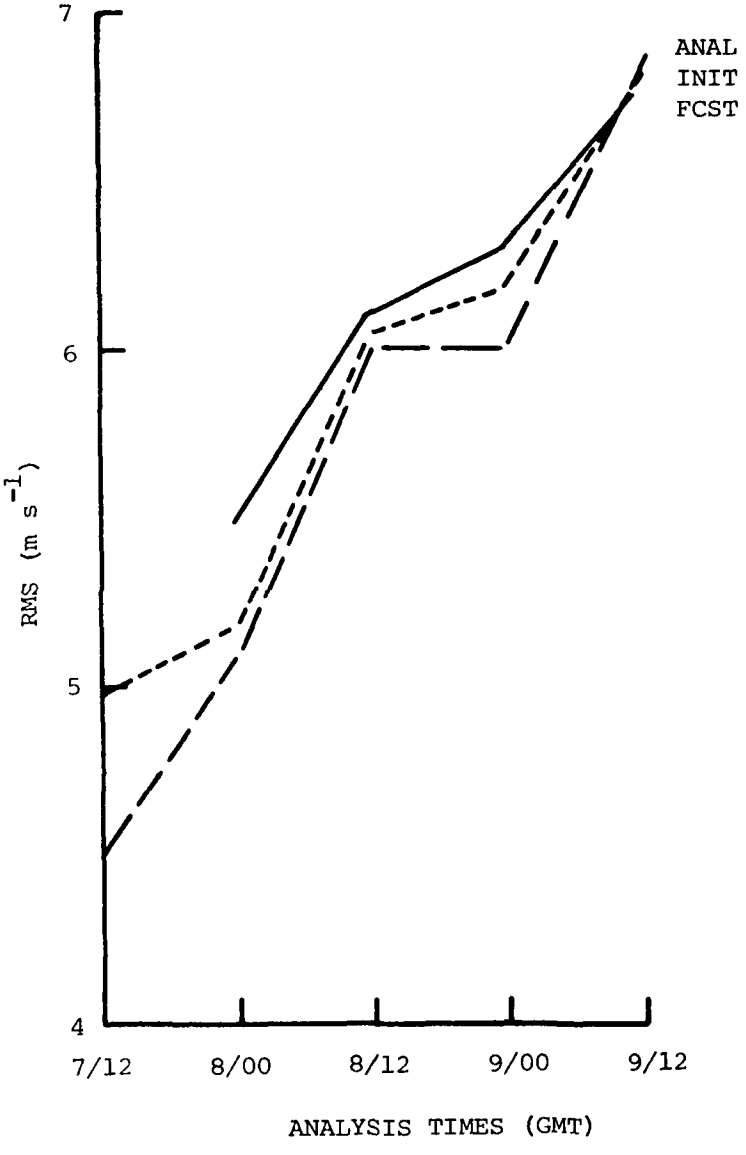

Fig. 5(e). Same as Fig. 4(e) except the Analysis Is Used as the Basis for Retention of Observations

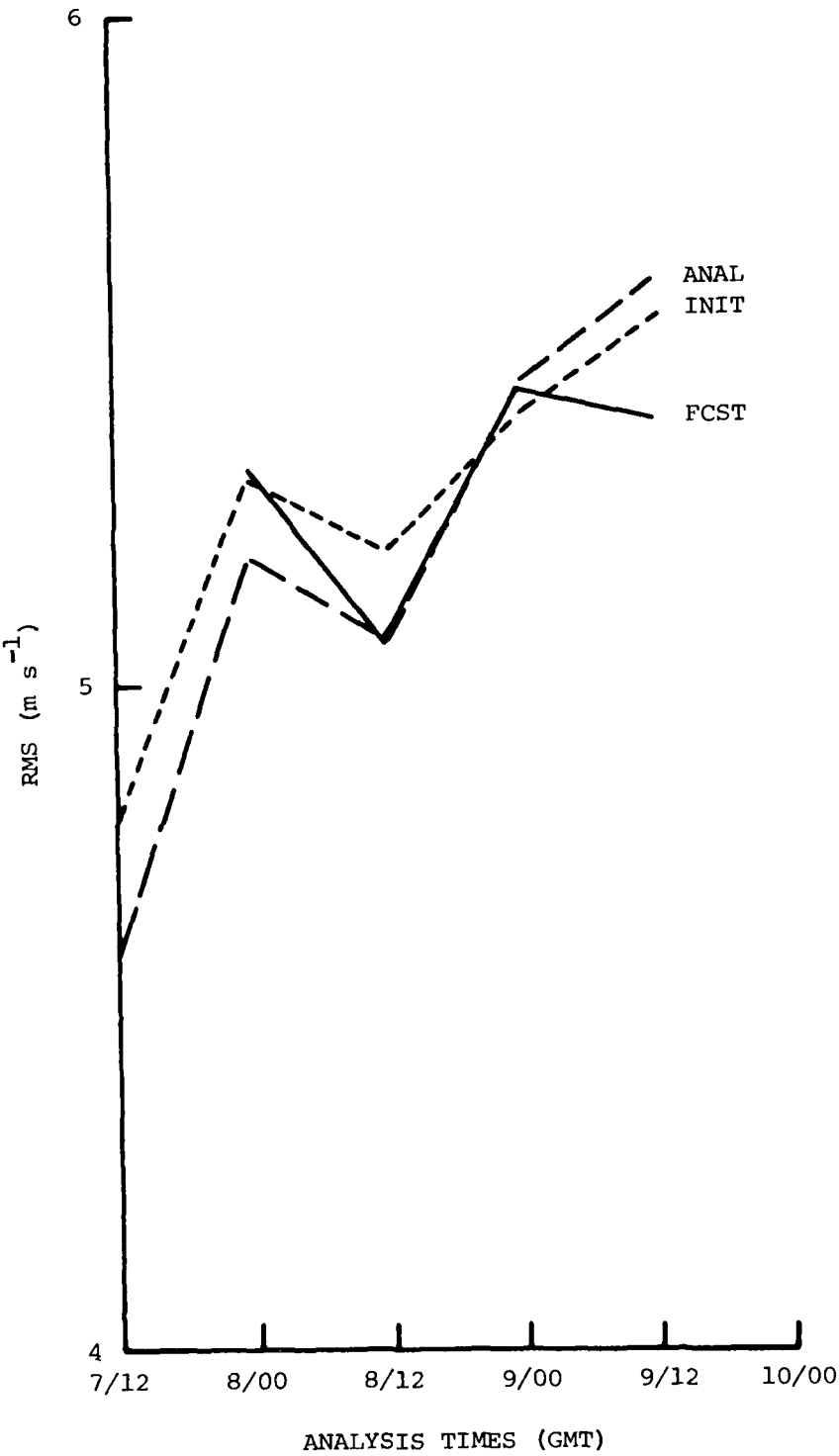

Fig. 5(d). Same as Fig. 4(d) except the Analysis Is Used as the Basis for Retention of Observations

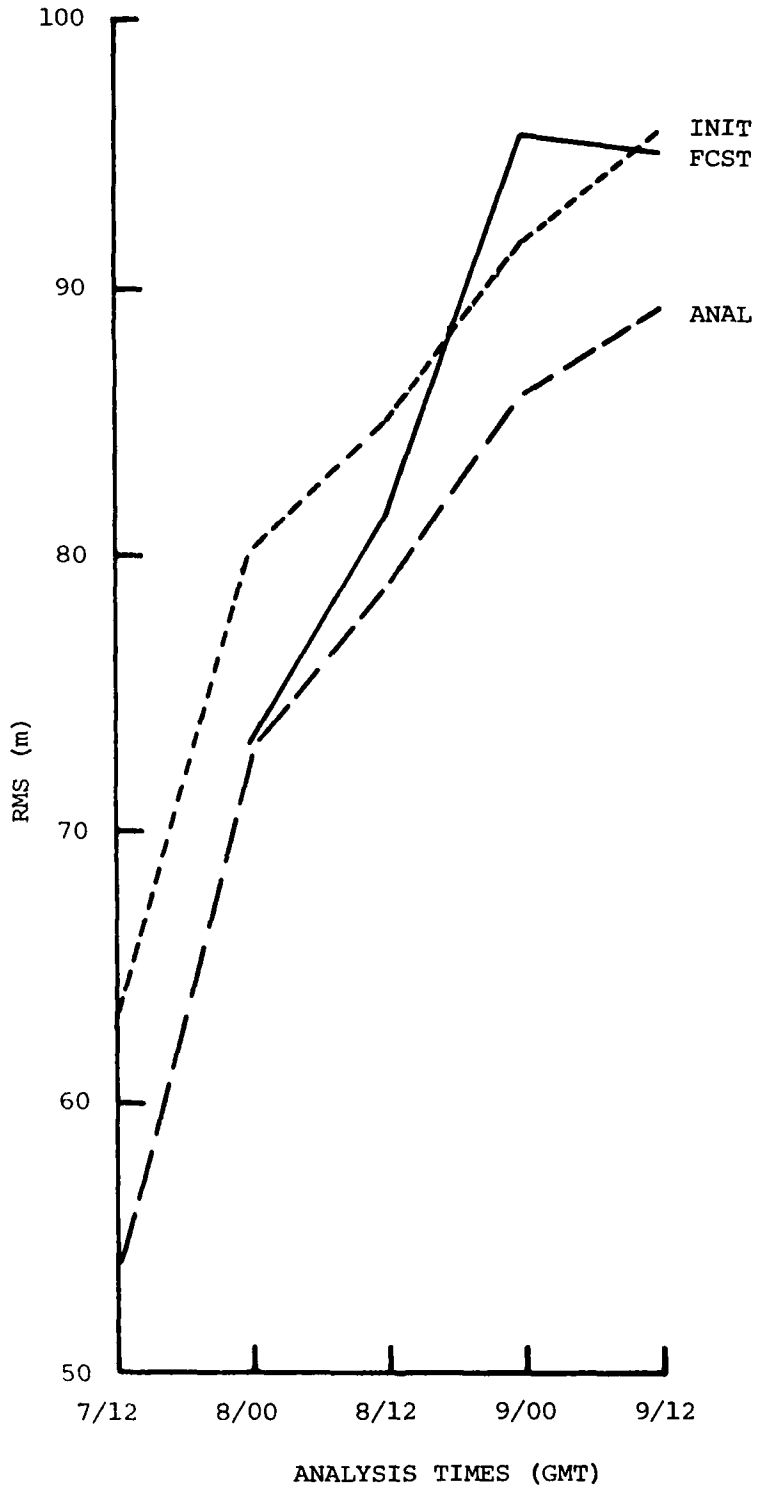

Fig. 5(c). Same as Fig. 4(c) except the Analysis Is Used as the Basis for Retention of Observations

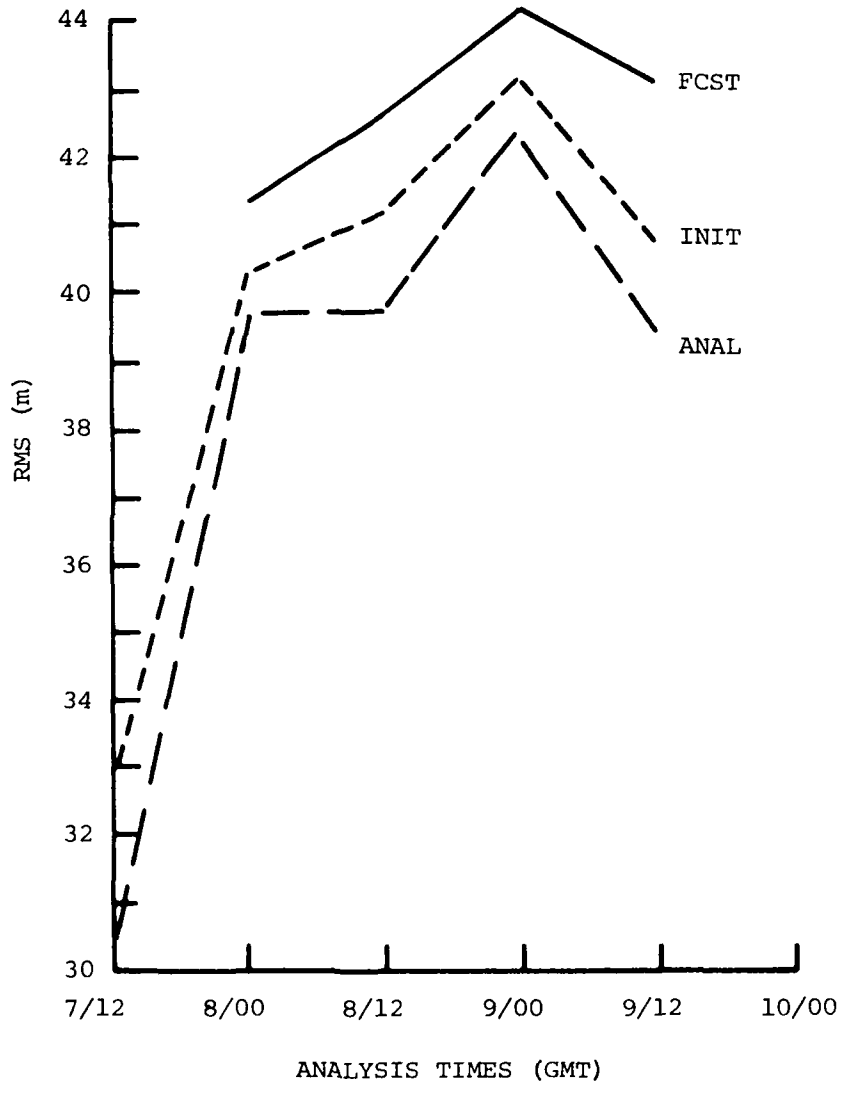

Fig. 5(b). Same as Fig. 4(b) except the Analysis Is Used as the Basis for Retention of Observations

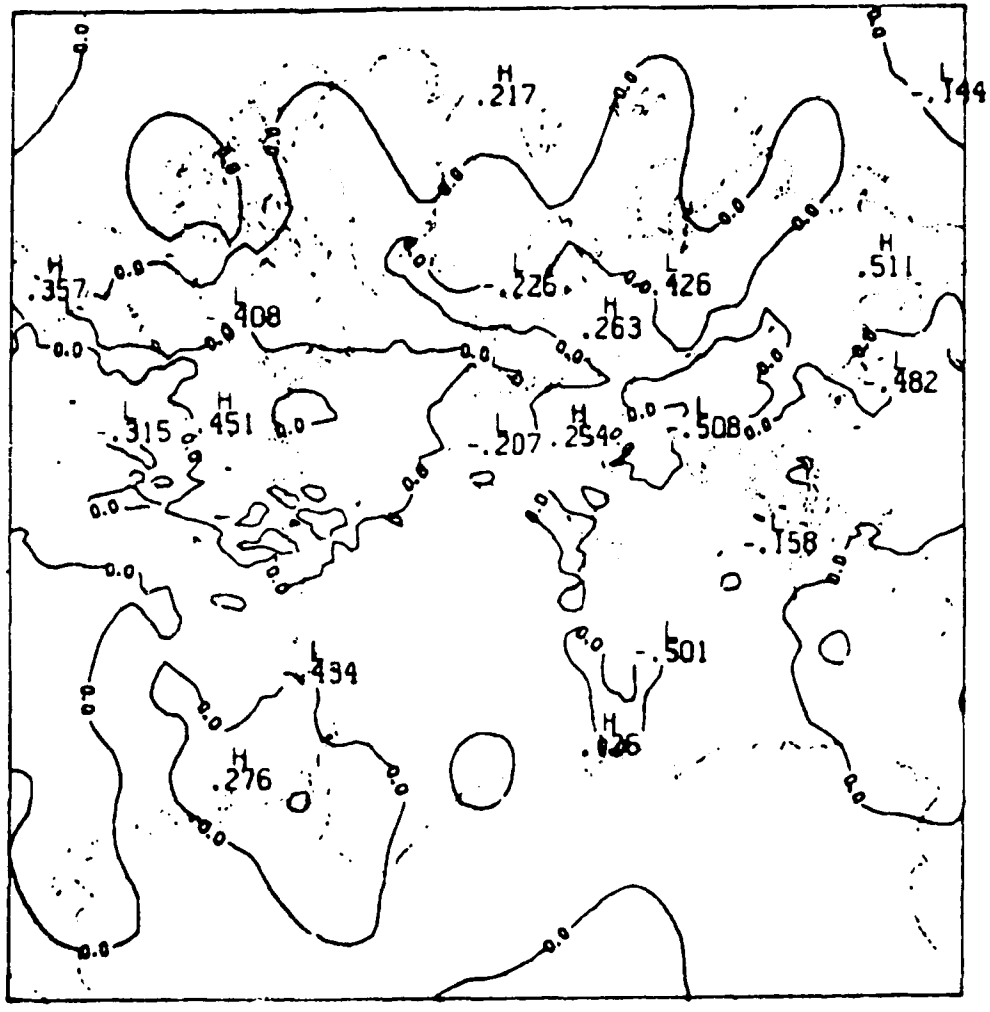

Fig. 7(b). Difference Contours between the Forecast and Analyzed Height Field for 1/8/79 12Z at Level 4 (Contour Interval is 60 m, Labels Are in Hectameters)

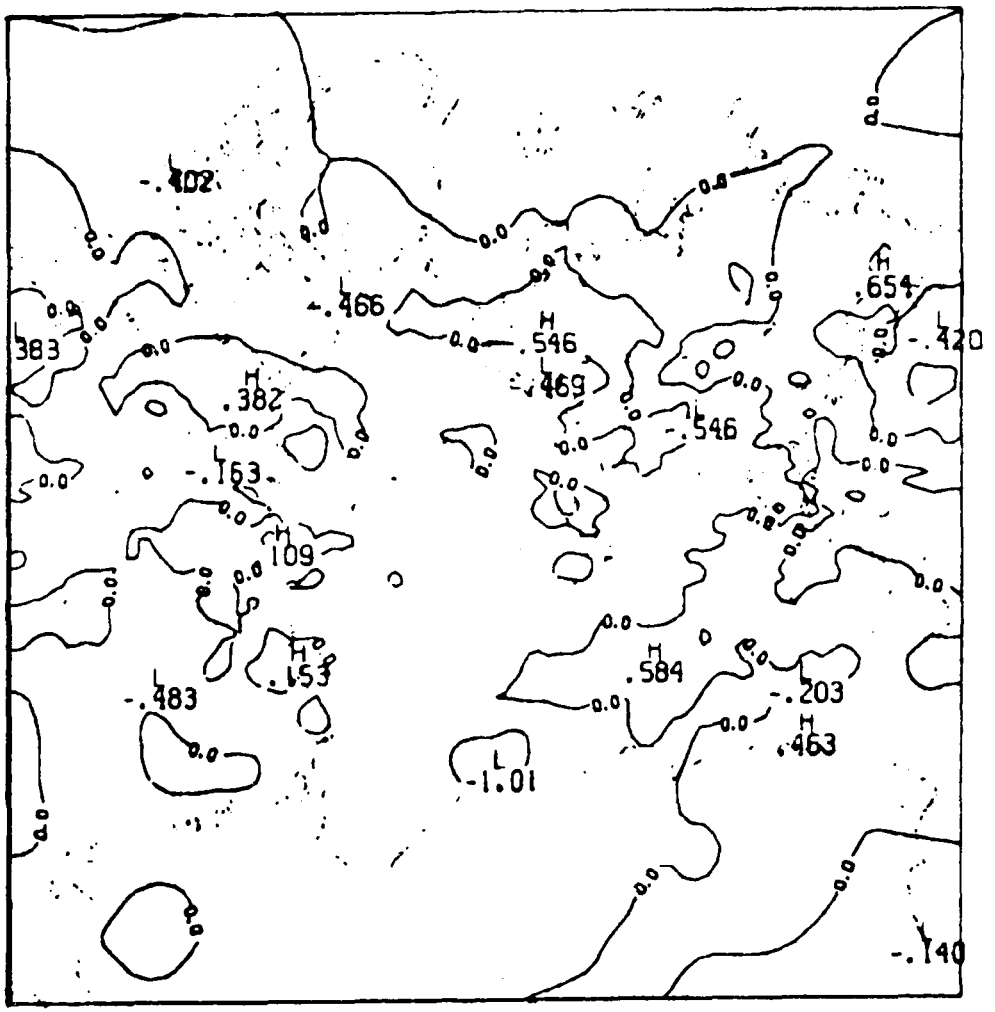

Fig. 7(c). Difference Contours between the Forecast and Analyzed Height Field for 1/9/79 00Z at Level 4 (Contour Interval is 60 m, Labels Are in Hectameters)

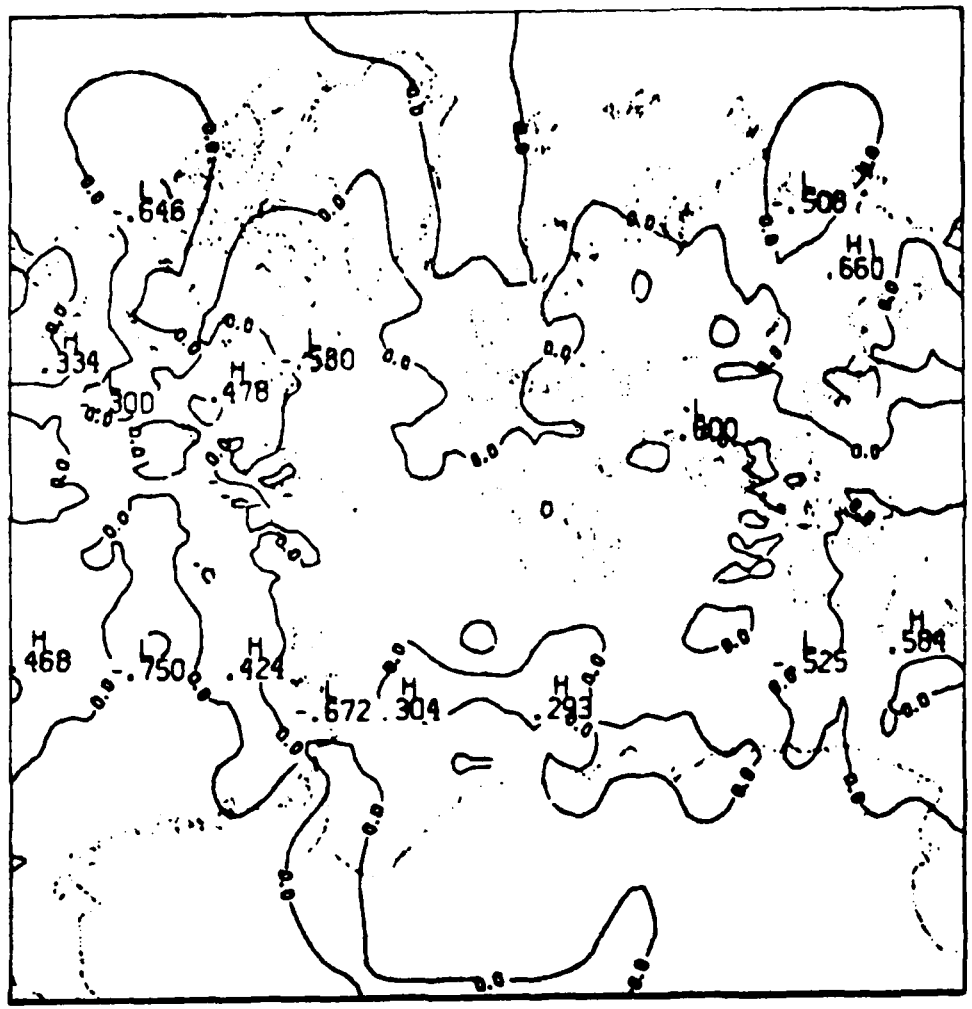

Fig. 7(d). Difference Contours between the Forecast and Analyzed Height Field for 1/9/79 12Z at Level 4 (Contour Interval is 60 m, Labels Are in Hectameters)

of the forecast. As such, one would have hoped that the largest differences would occur in areas where the forecast and FGGE III-A differ most, as depicted in Figs. 6 (a-e), assuming that FGGE III-A fields are sensitive to observations. Unfortunately, the adjustments depicted by Figs. 7 (a-d) are not major at any time, even at the final period (1/9/79 12Z, Fig. 6d), compared with the large differences that appear between FGGE III-A and the forecast at that time. In Eastern US, for instance, where the forecast has heights well below the FGGE III-A analysis with a maximum difference of 238 m, the analysis scheme only slightly increases the forecast heights by a maximum of 47.8 m. Areas such as Eastern Siberia or Antarctica are also slightly adjusted despite the large differences present between the forecast and FGGE III-A data. Whether this pattern would continue indefinitely is unknown, but as residuals increase, the adjustments to the first guess field should increase as well, perhaps halting the present pattern of insensitivity to observations and increasing forecast errors.

G. Conclusions

The current study is not yet complete. Not enough cycles have been generated to test the effects of the analysis and forecast cycle over the long term. Nor has there been *enough* testing to fully determine whether even the complex computer codes are genuinely error free. There are some identifiable sources of error that should be addressed. They are: 1. error due to the analysis procedure, 2. vertical and horizontal interpolation error, and 3. the Flattery scheme.

1. The analysis scheme employs an approximation that does not guarantee a minimum error. As mentioned by HT, the error depends on data distribution and cannot be easily determined a priori, at present. Whether an efficient mathematical evaluation of the error can be produced can only be determined after extensive research into linear algebra and statistics. The sequential procedure also tends to oversmooth the analyzed fields, as does the introduction of first guess information (zero residuals) in areas that lack data. In contrast to a least-squares fit where ill-conditioning creates large uncontrolled errors in data void areas, the sequential method is apparently insensitive to data even in areas of plentiful observations. Figs. 6 and 7, in fact, indicate that the analysis scheme has very little effect on the first guess field, even in the presence of large observation-

forecast differences, assuming that FGGE III-A analyses are sensitive to observations. This seems to be the case even in areas of considerable data such as North America, where one would not expect zero residuals to be retained at the grid corners as is done in the data poor regions. One possible remedy for this, as already mentioned by HT, is the introduction of weights in the analysis procedure. These weights would be based on statistical estimates of error similar to OI procedures. However, because nmf are involved in estimating the observed data, the weights would have to be functions of zonal wavelength and frequency. To amass error statistics in terms of wavelength and frequency would require reducing forecast, analyses, and verifications into expansions of nmf and calculating the necessary means, variances, etc., necessary for statistical weights. This could become a formidable undertaking unless some prior assumptions are made regarding the nature of the error. The weights could then be modeled, as they are for OI techniques, based on the many assumptions and limited available data.

2. Errors due to interpolation are unavoidable in any analysis scheme. For our analysis, the chief sources of these errors are the vertical interpolation with the OI scheme and the interpolation of the nmf to the observation locations in the horizontal. If economy is sought, interpolation may be substituted in the calculation of residuals at the observation points, instead of the current practice of computing first guess fields directly from the spectral expansions. The errors inherent in the vertical interpolation are discussed in the literature and in the first part of this report, relevant to OI errors. The interpolation of the nmf to latitudes of the observations does not necessarily engender large errors, except for the highest wavenumbers. It may be possible to store nmf values for the fixed locations of upper air observations and interpolate only to the variable location sites such as ship reports and satellite data. This would necessarily bias the Northern Hemisphere because of its preponderance of dry land and developed nations where most fixed observing stations are located. In any analysis scheme, however, the Southern Hemisphere always suffers because of the dearth of verifiable data there, and there is no way to judge whether any further lack of accuracy will be produced by this shortcut.

3. The Flattery scheme, as implemented in our analysis, has a fatal flaw which wreaks havoc with the uppermost level. This is due primarily to the lapse rate in the stratosphere which, when extrapolated, results in very high temperature or height values for the top level. Corrections to the Flattery scheme were made by substituting first guess temperature at the highest level. Results showed a slight improvement of the analysis at upper levels but no significant change in lower levels.

Results from the iterative scheme have proved disappointing because the procedure diverged, producing analyses that were apparently farther from the data and requiring greater adjustments during initialization. A recommended remedy could be iterating the analysis scheme before initializing, which would draw the fields closer to observations but forfeit the benefits of bringing the analysis closer to the "slow" manifold by virtue of the initialization.

In general, a full evaluation of our analysis procedure is impossible until further testing and experimentation can be completed. To make the scheme viable greater efficiencies have to be implemented. If vector processing machines such as the Cray are to be assigned the task of producing the analysis, the code must be modified to allow full vectorization. It may also be possible to economize by sticking to spectral expansions. The nmf are determined by expanding their spectral coefficients. It may be possible to rewrite the analysis in terms of expansions in Legendre functions directly rather than in nmf followed by re-expansion on a physical grid in order to define the proper spectral coefficients. Also, it would probably be beneficial to go directly from the analysis procedure to the initialization without involving a physical grid. This would avoid the problem of determining surface pressure residuals from the analysis by separation from the compound variable. This can only be accomplished, however, if the first guess field is expanded in nmf, and the velocity nmf transformed to vorticity and divergence nmf to be compatible with the initialization. Despite the apparent magnitude of the challenge, a scheme that can combine objective analysis with initialization while offering computational economy is a goal worthy of pursuing.

APPENDIX A. FLATTERY ALGORITHM

Given the system of linear constraints imposed on the interface temperatures $\{\hat{T}_k\}$, $k = 1, \ldots, K+1$ and the layer temperatures $\{T_k\}$, $k = 1, \ldots, K$. We assume:

(1) that the layer temperature T_k is the arithmetic average of the bounding interface temperatures $\hat{T}_k$, $\hat{T}_{k+1}$

$$T_k = \frac{1}{2}(\hat{T}_k + \hat{T}_{k+1}), \quad k = 1, \ldots, K; \tag{A-1}$$

(2) that temperature in the layer bounded by two pressure levels $\bar{p}_k$, $\bar{p}_{k+1}$ is linear in $\ln p$, so that the interface temperature $\hat{T}_{k+1}$ is given in terms of the layer temperatures T_k and T_{k+1} as

$$\hat{T}_{k+1} = T_k W_{L,\,k+1} + T_{k+1} W_{U,\,k+1}$$

where

$$W_{L,k+1} = \frac{\ln(\hat{p}_{k+1}/\bar{p}_{k+1})}{\ln(\bar{p}_k/\bar{p}_{k+1})}, \quad W_{U,k+1} = \frac{\ln(\bar{p}_k/\hat{p}_{k+1})}{\ln(\bar{p}_k/\bar{p}_{k+1})} \tag{A-2}$$

$k = 1, \ldots, K;$

(3) that both Eq. (A-1) and Eq. (A-2) are valid also at the lowest and highest bounding interfaces, i.e., $\hat{p}_1$ and $\hat{p}_{K+1}$. Hence

$$\hat{T}_1 = 2T_1 - \hat{T}_2$$

$$= 2T_1 - (T_1 W_{L,2} + T_2 W_{U,2})$$

or

$$\hat{T}_1 = (2 - W_{L,2})T_1 - W_{U,2}T_2 \tag{A-3}$$

$$\equiv T_L W_{L,1} + T_2 W_{U,1}$$

Similarly

$$\hat{T}_{K+1} = 2T_K - \hat{T}_K$$

$$= 2T_K - (T_{K-1}W_{L,K} + T_K W_{U,K})$$

or

$$\hat{T}_{K+1} = (2 - W_{U,K})\, T_K - W_{L,K}\, T_{K-1} \qquad \text{(A-4)}$$

$$\equiv T_{K-1}W_{L,K+1} + T_K W_{U,K+1}.$$

Here, the subscript k designates level in the vertical and is chosen to increase upward. The geometrical configuration may be depicted as follows:

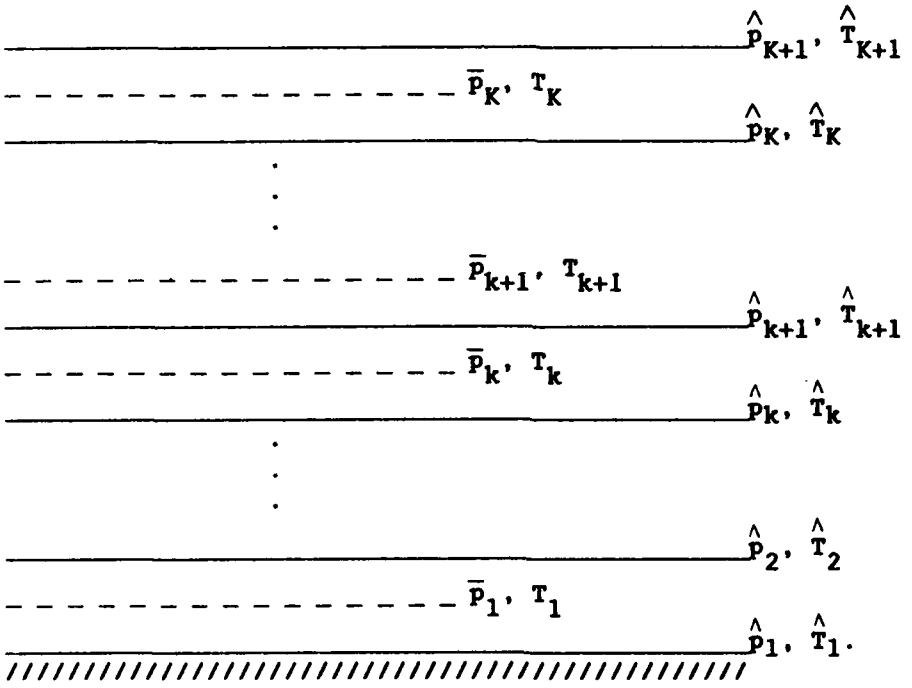

When $\hat{p}_{K+1} = 0$, we cannot employ this method. There are different alternatives here:

(1) Introduce $\hat{p}'_{K+1}$, which is between $\hat{p}_K$ and $\hat{p}_{K+1}$

(2) Assume that the layer above $\hat{p}_K$ is isothermal so that $\hat{T}_{K+1} = T_K$.

The constraints listed above may be put into matrix form given by

$$\hat{A}\hat{T} = BT \qquad \text{(A-5)}$$

where matrices A, B and vectors $\hat{T}$, T are defined as follows:

$$A = \begin{bmatrix} 0.5 & 0.5 & 0 & \cdots & 0 \\ 0 & 0.5 & 0.5 & \cdots & 0 \\ 0 & 0 & 0.5 & \cdots & 0 \\ \cdot & \cdot & \cdot & & \\ & & & 0.5 & 0.5 \\ 1 & 0 & 0 & \cdots & 0 \\ 0 & 1 & 0 & \cdots & 0 \\ \cdot & \cdot & \cdot & & \\ 0 & 0 & 0 & & 1 \end{bmatrix} \begin{matrix} \updownarrow K \\ \\ \updownarrow (K+1) \end{matrix}$$

$$\leftarrow (K+1) \rightarrow$$

$$\hat{T} = \begin{bmatrix} \hat{T}_1 \\ \hat{T}_2 \\ \hat{T}_3 \\ \cdot \\ \cdot \\ \cdot \\ \hat{T}_K \\ \hat{T}_{K+1} \end{bmatrix} \quad \updownarrow (K+1)$$

$$B = \begin{bmatrix} 1 & 0 & 0 & \cdots & 0 \\ 0 & 1 & 0 & \cdots & 0 \\ 0 & 0 & 1 & \cdots & 0 \\ \cdot & \cdot & \cdot & & \\ 0 & 0 & 0 & \cdots & 1 \\ W_{L,1} & W_{U,1} & 0 & \cdots & 0 \\ W_{L,2} & W_{U,2} & 0 & \cdots & 0 \\ \cdot & \cdot & \cdot & & \\ 0 & 0 & 0 & W_{L,K} & W_{U,K} \\ 0 & 0 & 0 & W_{L,K+1} & W_{U,K+1} \end{bmatrix} \begin{matrix} \updownarrow K \\ \\ \updownarrow (K+1) \end{matrix}$$

$$\leftarrow K \rightarrow$$

$$T = \begin{bmatrix} T_1 \\ T_2 \\ T_3 \\ \cdot \\ \cdot \\ \cdot \\ T_{K-1} \\ T_K \end{bmatrix} \quad \updownarrow K$$

To solve Eq. (A-5) in accordance with the least-squares principle we proceed as follows:

(A) When $\{T_k\}$ is given,

$$\hat{T} = (A^T A)^{-1} A^T B T \tag{A-6}$$

(B) When $\{\hat{T}_k\}$ is given,

$$T = (B^T B)^{-1} B^T A \hat{T} \, . \tag{A-7}$$

END

FILMED

8-85

DTIC